2019-10

Transient Stability Evaluation and Enhancement of the Ethiopian 230 Kv And 400 Kv Transmission Network Using Statcom

Baye, Getnet

BAHIR DAR UNIVERSITY

BAHIR DAR INSTITUTE OF TECHNOLOGY

SCHOOL OF RESEARCH AND POSTGRADUATE STUDIES

FACULTY OF ELECTRICAL AND COMPUTER ENGINEERING

TRANSIENT STABILITY EVALUATION AND ENHANCEMENT OF THE ETHIOPIAN 230 kV AND 400 kV TRANSMISSION NETWORK USING STATCOM

GETNET BAYE DEMEKE

Bahir Dar, Ethiopia

October, 17, 2019

TRANSIENT STABILITY EVALUATION AND ENHANCEMENT OF THE ETHIOPIAN 230 kV AND 400 kV TRANSMISSION NETWORK USING STATCOM

Getnet Baye

A thesis submitted to the school of Research and Graduate Studies of Bahir Dar Institute of Technology, Bahir Dar University, in partial fulfillment of the requirements for the degree of Master of Science in Electrical Engineering with specialization in Power System Engineering in Electrical and Computer Engineering Faculty.

Advisor Name: Dr.-Ing. Belachew Bantyirga

Bahir Dar, Ethiopia
October 17, 2019

DECLARATION

I, the undersigned, declare that the thesis comprises my own work. In compliance with internationally accepted practices, I have acknowledged and refereed all materials used in this work. I understand that non-adherence to the principles of academic honesty and integrity, misrepresentation/ fabrication of any idea/data/fact/source will constitute sufficient ground for disciplinary action by the University and can evoke penal action from the sources, which have not been properly cited or acknowledged.

Name of the student Getnet Baye Signature _____

Date of submission: _____/_____/_____

Place: Bahir Dar

This thesis has been submitted for examination with my approval as a university advisor.

Advisor Name: Dr.-Ing. Belachew Bantyirga

Advisor's Signature: _____

Date _____/_____/_____

BAHIR DAR UNIVERSITY

BAHIR DAR INSTITUTE OF TECHNOLOGY

SCHOOL OF RESEARCH AND GRADUATE STUDIES

FACULTY OF ELECTRICAL AND COMPUTER ENGINEERING

THESIS APPROVAL SHEET

Student:

Getnet Baye	.....	16/10/2019
Name	Signature	Date

The following graduate faculty members certify that this student has successfully presented the necessary written final thesis and oral presentation for partial fulfillment of the thesis requirements for the Degree of Master of Science in Electrical Power System Engineering.

Approved By:

Dr.-Ing. Belachew Bantyirga Advisor:	..... Signature	16/10/2019 Date
Yoseph Tekenen Abebe External Examiner:	..... Signature	16/10/2019 Date
Berhanu Zelalem Internal Examiner:	..... Signature	17/10/2019 Date
Mr. Tewodros Gera Chair Holder:	..... Signature	17/10/2019 Date
Mr. Solomon Lale Faculty Dean:	..... Signature	17/10/2019 Date

ACKNOWLEDGEMENTS

First, I would like to thank the almighty God for his savior, mercy and graces he gave to me. Next I would like to express my sincere thanks to my advisor, Dr.-Ing. Belachew Bantyirga, for his uninterrupted encouragement, guidance and supervision throughout this thesis work.

I would like to thank EEP and respective officials for their sincere cooperation in providing me the necessary data and information.

I am also thankful to Mr. Wubetu, transmission section supervisor of EEP North-West region, for his frank help at providing technical advices.

I would like to express my gratitude the school of Electrical and Computer Engineering at Bahir Dar Institute of Technology for providing excellent working conditions and love.

I would like to thank my family. Specially my wife for her prayers, encouragement, financial support and guidance.

Last, but not the least, a sincere appreciation is given to my friends Yalemsew Y, Asresahegn T, Bewuketu G, Ayalsew A, Yalew G and Marsilas D.

ABSTRACT

In this thesis, transient stability enhancement using Static Synchronous Compensator (STATCOM) is presented. The test system was Ethiopian 230 kV and 400 kV power network. The study focuses on the effect of three phase fault at Gilgel gibe III (the largest generation) bus terminal and Kaliti I (it is far from the generation station). Due to the fast growth of power demand, the power system becomes overloaded and pushed to operate with much closed to its stability limit. In this situation, transient instability is occurred. To solve the problem, installing static synchronous compensator (STATCOM) device at proper place in the power system is a better solution. In this thesis, placement and sizing of STATCOM is done using Digital Simulation and Electrical Network Calculation Program (DIgSILENT) software. To enhance transient stability, increase transfer capability and to reduce overloading, the proper placement and sizing of STATCOM is determined by using PV-curve and power flow analysis respectively. The dynamic model of STATCOM was developed based on DIgSILENT simulation language (DSL). The PI controllers are tuned using Modulus Optimum (MO) and Symmetric Optimum (SO) to make the system faster. The inner current controller transient response specifications are: 75.617 ms, 2.1 ms, 1.6 ms 1.0439 and 4.385 for rise time, settling time, peak time and overshoot respectively. The STATCOM was installed at Combolcha substation. The three-phase fault at Gilgel gibe III and Kaliti I buses. The system response was analyzed with and without the device for the two cases. From the simulation result it is clearly shown that, with STATCOM the steady state voltage profile of some buses enhanced by 6.72% at the point of connection. The steady state active power loss was reduced by 2.067% and the transient state active power loss was reduced by 27.4%. The Available Transfer Capability (ATC) enhanced by (9.377%) with the device. In both cases, the fault occurred at 100 ms. The Critical Clearing Time (CCT) is enhanced from 260.5 ms to 288 ms and from 367.8 ms to 411 ms when the fault occurred at Gilgel gibe III and at Kaliti I respectively. It can be concluded that, the Ethiopian power system can benefit significantly from the utilization of STATCOM technologies to solve some of the problems associated with it.

Key words: Transient Stability, STATCOM, DIgSILENT Power Factory, CCT

TABLE OF CONTENTS

LIST OF ABBREVATIONS

AC	Alternate Current
ATC	Available Transfer Capability
AVR	Automatic Voltage Regulator
BBC	British broadcast Corporation
CCT	Critical Clearing Time
CSC	Current Source Convertor
DC	Direct Current
DIgSILENT	Digital Simulation and Electrical Network Calculation Program
DSL	DIgSILENT Simulation Language
DFC	Dynamic Flow Controller
EEP	Ethiopian Electric Power
EEPCo	Ethiopian Electric Power Corporation
EEU	Ethiopian Electric Utility
FACTS	Flexible AC transmission systems
GTO	Gate Turn Off Thyristor
ICS	Inter- Connected System
IGBT	Insulated Gate Bipolar transistor
IGCT	Insulated Gate Commutated Thyristor
IPFC	Interline Power Flow Controller
kV	Kilo Volt
MVA	Mega Volt Ampere
MW	Mage Watt
PCC	Point of Common Coupling
PSS	Power System Stabilizer
p.u	Per Unit
SCS	Self – Contained System
SSSC	Static Synchronous Series Compensator
STATCOM	Static Synchronous Compensator
SVC	Static VAR Compensator
TCSC	Thyristor Controlled Series Reactor
UPFC	Unified Power Flow Controller
VSC	Voltage Source Converter

LIST OF SYMBOLS

α	Alpha
β	Beta
δ	Phase angle
Ω	Ohm
Λ	Lambda
Z	Damping constant
T	Reactor time constant
μ	Mu
*	Asterisk
M	Inertia constant
V	Bus voltage
Pm	Mechanical input power
Pe	Electrical output power
E	Generator internal voltage
X_T	Total reactance
R	Resistance
L	Inductance
Cdc	DC capacitor
Vdc	DC voltage
K_p	Proportional gain
T_i	Integral time constant
J	Moment of Inertia
M	Angular momentum
Te	Electromagnetic torque
Tm	Mechanical torque
Ωm	Angular speed

LIST OF FIGURES

LIST OF TABLES

CHAPTER ONE

1. INTRODUCTION

1.1. Background

Power system generally have different stages: those are generation, transmission, distribution, and loads. Based on the proper design of those stages electrical power is continuously supply to the load. The proper designs of power system components are maintain the power balance between the generation and the load in order to maintain the power system stability [1].

Today increased energy demands resulted in intensive power system growths. The growth makes power systems to get wider in coverage and get complex in interconnection. This situation gives rise to the complexity of stability problems. Keeping the power system stability and improving the power transfer capability of power systems is an issue that must be dealt at the expansion planning stage of power systems.

The Ethiopian Electric Power (EEP) and Ethiopian Electric Utility (EEU) are engaged in Electric power generation, transmission, distribution and sale of electricity. The EEP specially is concerned with constructing new generation sites and reinforcing the existing power stations to satisfy the growing customer power demand. Most of the existing and currently under construction generation sites in [2]. The EEP operate through two different power supply systems, such as the Inter- Connected System (ICS) and Self – Contained System (SCS). The interconnected system of EEP consists of large interconnected power systems with dispersed and geographically isolated generators and load for ease of management and speedy restoration after disturbance. The Ethiopian power network in general is divided in to nine different sub regions, such as: Addis Ababa, Eastern, Northern, Sothern, North–Western, North-Eastern, Western, Central and South-western of EEP system are important area of the ICS. The main energy source of ICS is hydropower plants, and for the SCS mini-hydro and diesel power generators allocated in various areas of the country.

The ICS consists of twelve hydropower, five wind, one geothermal, and four diesel power plants with a total capacity of 4521.8 MW, of which 82 % is generated from hydropower plants. The SCS consists of three small hydro and many isolated diesel plants, located throughout the country with a capacity of 6.15 MW and 30.06 MW respectively. As part of the government's growth and transformation plan, EEP has launched hydropower, and other renewable projects to meet the extra electric power target in the coming years. Grand Renaissance Dam Project under construction, for example, is the largest hydro power plant in Africa, which will generate 6000 MW. The committed and under construction power plants are found in [2].

The Ethiopian power transmission network, which is considered in this thesis, covers very long distance to supply loads, which are far from the generation centers.

The electric energy generated from the main hydropower plants is transported through high voltage transmission lines rated 45 kV, 66 kV, 132 kV, 230 kV and 400 kV. The 400 kV transmission lines of 1492 km were constructed and commissioned recently while 1240 km of 500 kV and DC lines are being considered and under construction. The total length of the existing transmission lines is about 14510.26 km [2]. Regional interconnections with neighboring countries including Djibouti, Sudan and Kenya are under the construction and procurement phases.

The analysis of power system stability is important to plan, design, operation and control of the power system [3].

The consumption of electric power demand in the present day have been increased to such an extent that it has become essential to expand existing or building new power system network. Nevertheless, the expansion or construction of transmission line is limited by economic and environmental constraints. Consequently, power system components increase dramatically that is numerous generators, transmission lines, variety of loads and transformers. Power demand is increase, power system becomes more complex, and some transmission lines are more loaded than that was planned when they were built [4, 5]. Thus, complexity of the power system, the increasing of the loads, loading of transmission lines, and generator far from the load center are cased to power systems to be stressed which exhibit nonlinear behavior and the interactions among power systems components results in various modes of oscillation. These oscillations if not properly damped, may be

sustained for several minutes affecting power flows and may even increase to cause loss of synchronism between system and ultimately lead to total or partial system outage [5-7]. Maintaining power system stability is crucial in ensuring the safe and secure operation of the electrical power network [8]. Transient stability is the main factor that limits the power transfer capability of long distance transmission lines [8].

FACTS devices have been efficiently utilized to control power flow through the transmission lines and enhance system controllability by mitigating power system stability. However, all the FACTS devices are quite effective for different power system applications. STATCOM has more popularity since it is capable of providing support for voltage regulation, shunt compensation, phase angle regulation, and control of the active or reactive power separately transmitted over the line [9]. Basically, FACTS controllers can be Series Controller, Shunt Controller, Combined series-series Controller, and Combined series-shunt Controller [10]:

The Static Synchronous Compensator (STATCOM) is a shunt device of the Flexible AC Transmission Systems (FACTS) family using power electronics to control power flow and improve transient stability on power grids by regulating the voltage at its terminal by controlling the amount of reactive power injected into the system or absorbed from the power system [5]. System modeling and controller design for fast load voltage regulation and mitigation of voltage flicker using a STATCOM were demonstrated in [11]. The STATCOM has been reported to have the capability to regulate voltage, control power factor, and stabilize power flow [12], hence its choice for this research works. The intention of this study would be transient stability enhancement of the existing transmission network the Ethiopian 230 kV and 400 kV transmission line by using STATCOM devices.

1.2. Problem Statement

Blackout events have been registered in Ethiopian electric power system on May 1, 2018. According to BBC Africa news, "Ethiopia hit by power cut as dam's circuit breaks" on May 1, 2018. State media said that the power went out when circuit breaker tripped at Gilgel gibe III dam in southern Ethiopia. Based on this news circuit breaker was tripped, this is due to transient stability problem.

Based on this situation, Ethiopian electric powers have stability problems due to fast growth in power demand and complexity of the system. Since built of transmission lines and power generations are restricted by economic and environmental constraints. More over long distance AC transmission is often subject to stability problem, which limits transmission capacity.

In this situation, the power networks are overloaded and pushed closer to their stability limits. This leads losing of stability followed by disturbance, such as three phase faults, sudden losing of generation and large loads. Consequently, power interruption, equipment damage, and even wide area blackout are weaken the system security and reliability. One of the factors that determine the level of integrity of a power system is the level of security of the network based on transient stability assessment.

For those solution, EEP used shunt capacitor/reactor, fast-acting exciters, and high-speed recloser of circuit breakers, single pole switching and reduction in system transfer reactance. However, it has some drawbacks like slow operation and poor transient stability enhancements. STATCOM device is an alternative solution, which are found to be very effective in a power system transmission network for better transient stability enhancement and increase power transfer capability without sacrificing the desired stability margin. This research studied and investigated the transient stability improvement capability of STATCOM on Ethiopian 230 kV and 400 kV transmission network. The analysis of power system stability is important to plan, design, operation and control of the power system.

1.3. Objective of the study

1.3.1 General objective

The general objective of this thesis is to evaluate and enhance transient stability of the Ethiopian 230 kV and 400 kV transmission network using STATCOM subject to transient disturbance.

1.3.2. Specific objective

- ✓ To determine the placement of STATCOM using load flow and PV-curve analysis and sizing of STATCOM based on load flow analysis
- ✓ To develop the dynamic modeling of STATCOM.
- ✓ To determine the critical clearing time of the Ethiopian 230 kV and 400 kV transmission system with and without STATCOM.
- ✓ To determine the available transfer capability (ATC) of the Ethiopian 230 kV and 400 kV system during steady state and fault conditions.
- ✓ To investigate the use of STATCOM for the improvement of the 230 kV and 400 kV transmission system and finally, recommended to Ethiopian electric power company to install the device at the required location.

1.4. Scope of the study

The thesis is limited to transient stability analysis and improvement of multi-machine 230 kV and 400 kV transmission network using STATCOM and all the buses in the network would be critically examined and analyzed with regard to transient stability. The available transfer capability was determined based on grid loss and PV-curve analysis in the case of steady state. But in the case of fault condition only using grid loss. All the analysis and modeling of the components on this thesis have no practical implementation and they are done by using Dig silent simulation software.

1.5. Significance of the study

This work provides a significant importance of measuring the existing network performance of transient stability and provides transient stability improvement solutions as well as serving as a benchmark for the prediction of the future Ethiopian power network planning and design. In the recent times, the importance of transient stability analysis has been increasing since the electric power systems are being operated closer to their stability limits. In addition the model of Ethiopian 230 kV and 400 kV transmission lines can be the basis for researchers who will be interested in other or similar studies for the same area in the future. Studying of power system stability is crucial in ensuring the safe operation of the electrical power network

1.6. Thesis Outline

This Thesis has a total number of five chapters and the discussion of the study is organized as follows:

- **Chapter One** provides a brief explanation about back ground, statement of problem, objectives, scope and significance of the thesis.
- **Chapter Two** provides literature review on power system stability performance enhancement with FACTS devices proposed by different researchers. About STATCOM placement and modeling has been reviewed.
- **Chapter Three** discuses about power system stability, model of STATCOM for transient stability, PV-curve analysis for placement of STATCOM devices, and developing a complete control system, and tuning of the controllers using suitable tuning techniques.
- **Chapter Four** discuses about result and the discussion.
- **Chapter Five** discuses about the conclusion for the results obtained during simulation and recommendation about future works.

CHAPTER TWO

2. LITERATURE REVIEW

There are a number of related papers about transient stability evaluation and enhancement using different FACTS controllers that have been published on different journals. Some of them have been reviewed in the following ways.

In 2016, P. Suresh & R. Jegedeesh Kumar [10] Used STATCOM, SVC & UPFC have been investigated for the improvement of transient stability of 3-machine 9 bus system. The dynamic behavior of the power system is compared with the presence of STATCOM, SVC and UPFC in the system in the event of a major disturbance. Then the performance of UPFC for power system stability improvement is compared with the STATCOM and SVC. It is clear from the simulation results showed that there is a considerable improvement in the system performance. So that STATCOM is more effective next to UPFC to improve the settling time of the post fault.

In 2017, G. B. Jadhav et al. [9] have presented the performance of a static var compensator and static synchronous compensator with and without power system stabilizer (PSS). Using MATLAB to test the system that STATCOM showed better improvement in transient stability compare with SVC. The performance was also compared with GPSS (Generic Power system Stabilizer) and MBPSS Multiband Power System Stabilizer) to see the effect of further oscillations created during and after fault in the system with SVC and STATCOM. The MBPSS showed better effect than GPSS to damp the further oscillations created in the system during and after fault with SVC and STATCOM.

In April 20,2014, P. Khalkho and A. K. Singh using both power system stabilizer (PSS) and increasing inertia of synchronous machine are very effective for transient stability enhancement of multimachine system is discussed. But using one method is not effective. So that using both methods have better response for transient stability improvement [13].

In Febrary 2014, M. S. Rao and L. M. Mohan using FACTS devices for transient stability performance analysis is presented. By using well designed FACTS device for the improvement of large electrical system. If a severe three phase to ground fault occur in the midpoint of the system, voltage in area1 and area 2 has dropped to zero and the current has

drastically increased, results in large oscillations in generator real power without any controller. It can be observed with STATCOM, these oscillations in real power during such transients were mitigated. The system regains its normal state after transients die out is due to the action of PSS and AVR. It can be observed that surge currents can be bypassed to STATCOM which helps in maintaining nearly constant voltage and current. Working of STATCOM depends on the impedance of the line, capacitor ratings, voltage that has to compensate, MVA rating of STATCOM transformer and reactive power of the system. Generator stator current has controlled with STATCOM and surge currents are mitigated [14].

In July 2014, Mr. Ketan G. Damor, et al [4] suggested that two-area power system were able to show that the improvement of transient stability using a SVC, STATCOM, UPFC, and TCSC was analyzed. From the simulation results, the performance of UPFC is compared with other FACTS devices such as Thyristor Controlled Series Capacitor (TCSC), (STATCOM) and Static Var Compensator (SVC) are more effective. STATCOM is effective for transient stability next to UPFC. The simulation results demonstrate the effectiveness and robustness of the proposed UPFC on transient stability improvement of the system. But due to cost this research is using STACOM for transient stability. Because from different papers UPFC is high cost.

In [15], transient stability improvement of multi machine power system using static VAR compensator (SVC) and also the optimal location of SVC have been studied. SVC is flexible AC transmission system (FACTS) devices which has been done the power supply is more efficient and reliable. Loss of transient stability is caused by fault on transmission facilities, sudden loss of generation, or loss of a large load. The network is design and model using MATLAB/SIMULNK. The SVC is basically a shunt connected variable Var generator whose output is adjusted to exchange capacitive or inductive current to the system and used for voltage control in the power system. The higher value of the effectiveness factor will give the best location of the SVC.

In [16], and [17] transient stability improvement is carried out with the help of shunt FACTS devices such as SVC and STATCOM are discussed. When compare the two shunt FACTS devices STATCOM has a better performance for transient stability. Fuzzy

controlled STATCOM is designed to further improvement of transient stability through fast damping of rotor angle deviation [16].

In [11], Dynamic Stability Improvement of an Integrated Grid-Connected Offshore Wind Farm and Marine-Current Farm Using a STATCOM is presented. The proposed STATCOM joined with the designed PID damping controller on suppressing voltage fluctuation of the studied system and improving system dynamic stability under different operating conditions is effective. So that for this thesis, transient stability analysis and enhancement with STATCOM is presented.

In [18], LabVIEW based simulation of STATCOM for transient stability analysis of electrical power system is studied. It promises a wide scope in enhancing transient stability limit, by providing better location of the FACTS Controller and also by bringing in the cost-effectiveness for the power system. From the power system dynamic stability viewpoint, the STATCOM provides better damping characteristics than the SVC, as it is able to transiently exchange active power with the system. The simulation results show that, the STATCOM controller improve the stability performance of the power system and power system oscillations are effectively damped out under severe disturbance conditions. Reactive power compensation use of STATCOM is studied. Which uses voltage source converter (VSC) and can act as either a source or sink of reactive power to a power network to control the voltage profile of the buses [1].

In[1], [16], and [9], the importance of STATCOM in improving transient stability in the system have been done. The benefits of STATCOM for transient stability enhancement and the working principle is presented.

P. Bisen and A. Shrivastava [19] have been discused that the comparision between SVC and STATCOM for power system stability enhancement. From this discussion STATCOM has supperier performance than SVC for power system stability enhancement. Such as voltage stability, rotor angle stability and transmission capability is improved in the multimachine system. Due to this STATCOM is selected for this research.

2.1.Power System Transient Stability Improvement

Basically power system stability depends on active and reactive power balance between the load and generation within the network. If there is active and reactive power imbalance

between the generation and loads, there will be losing of stability. This leads to loss of system integrity leading to system collapse which has damaging impact on daily different activities. To avoid such devastating impacts there should be effective mechanism for maintaining this balance [8]. Now a day's there are different mechanisms are continued to be employed by power utilities worldwide for insuring this balance and bring about enhanced power system stability. Those mechanisms are the first one is at generating units through the action of power system stabilizers (PSSs), automatic voltage regulators (AVRs), and other supplementary controllers. The power utilities worldwide are currently implementing PSSs and AVRs as excitation controllers to enhance power system stability. However, due to limited capacity and large system voltage variations introduced during disturbances upon utilizing them, they are getting insufficient to create system wide influences. The second one is through the application of FACTS devices and an HVDC control at the transmission level is applicable.

2.2.Overview of FACTS Controllers

FACTS is defined by the IEEE as a power electronic based system and other static equipment that provide control of one or more AC transmission system parameters to enhance controllability and increase power transfer capability[20]. In general, FACTS devices have the following basic application such as power flow control, increase of transmission capability, voltage control, reactive power compensation, stability improvement, and Power quality enhancement [1]. Basically FACTS controllers are power electronics devices which classified into two; thyristor valve/convertor (Static Var Compensator (SVC), Thyristor Controlled Series Compensator (TCSC), Dynamin flow controller (DFC)) and voltage source convertor (Static Synchronous Compensator (STATCOM), Static Synchronous Series Compensator (SSSC), Unified/Interline Power Flow Controller(UPFC/IPFC)) FACTS devices [1].

FACTS devices have been mainly used for solving various power system steady state control problems such as voltage regulation, power flow control, and transfer capability enhancement [20]. As supplementary functions, damping the inter area modes (transient stability) and enhancing power system stability using FACTS controllers have been

extensively studied and investigated [21]. STATCOM is shunt FACTS device damping power oscillation and controlling bus voltages during system disturbance thus allowing for more power transfer. This makes the STATCOM is important for transient stability enhancement.

Basically, FACTS controllers can be divided into four categories [10]:

- ✓ Series Controller,
- ✓ Shunt Controller,
- ✓ Combined series-series Controller,
- ✓ Combined series-shunt Controller

Table 2.1: Comparison among FACTS controllers.

Name	Type	Controller used	Purpose
SVC	Shunt	Thyristor	Voltage control
SSSC	Series	GTO	Power flow control
STATCOM	Shunt	GTO	Voltage control
UPFC	Shunt and series	GTO	Voltage and Power flow control
TCSC	Series	Thyristor	Power flow control
TCPAR	Shunt and series	Thyristor	Power flow control

Table 2.2: Power System Stability Enhancement Comparison of FACTS Devices [22]

Two-area Power System with	Power System Stability Enhancement	Settling time in post fault period (in seconds)
STATCOM	YES	0.4
SVC	YES	0.7
TCSC	YES	0.5
UPFC	YES	0.3

From the table the post settling time is small in UPFC, but it is cost. STATCOM has best post settling time next to UPFC. Based on this analysis STATCOM is used for this thesis. For thesis research, FACTS devices controllers are applied to the system to improve power system stability, particularly transient stability using STATCOM.

CHAPTER THREE

3. THEORTICAL BACKGROUND AND METHODOLOGY

3.1.Introduction

This chapter discussed about power system stability and research procedures and approaches. The tool used for this research (DIgSILENT PowerFactory version 15.1.7 software to design Ethiopian 230 kV and 400 kV transmission networks) and the methods used to design the system modeling. Such methods are the dynamic modeling of STATCOM and placement of STACOM using load flow calculation and PV-curve analysis respectively, the controller design based on vector current control method and the parameters are tuned using tuning method are presented. The flow chart of the methodology is shown in Figure 3.12 below.

Dynamic models definition of generators for transient stability analysis in DIgSILENT PowerFactory software. The model of STACOM in DIgSILENT PowerFactory software and the dynamic models of STATCOM is modeled using DIgSILENT simulation language (DSL).

3.2.Power system stability

According to the IEEE/CIGRE Joint task Force, power system stability is officially defined as "the ability of the power system, for a given initial operating condition, to regain a state of operating equilibrium after being subjected to a physical disturbance, with most system variables bounded so that practically the entire system remains intact"[8]. As shown in Figure 3.1 below, power system stability is classified into three major categories such as Rotor Angle Stability, Frequency Stability and Voltage Stability [8, 23]. This research focuses on Transient Stability enhancement, because it is the primary limiting factors for the power transfer on many inter area links. Since, with the increased loading of long transmission lines.

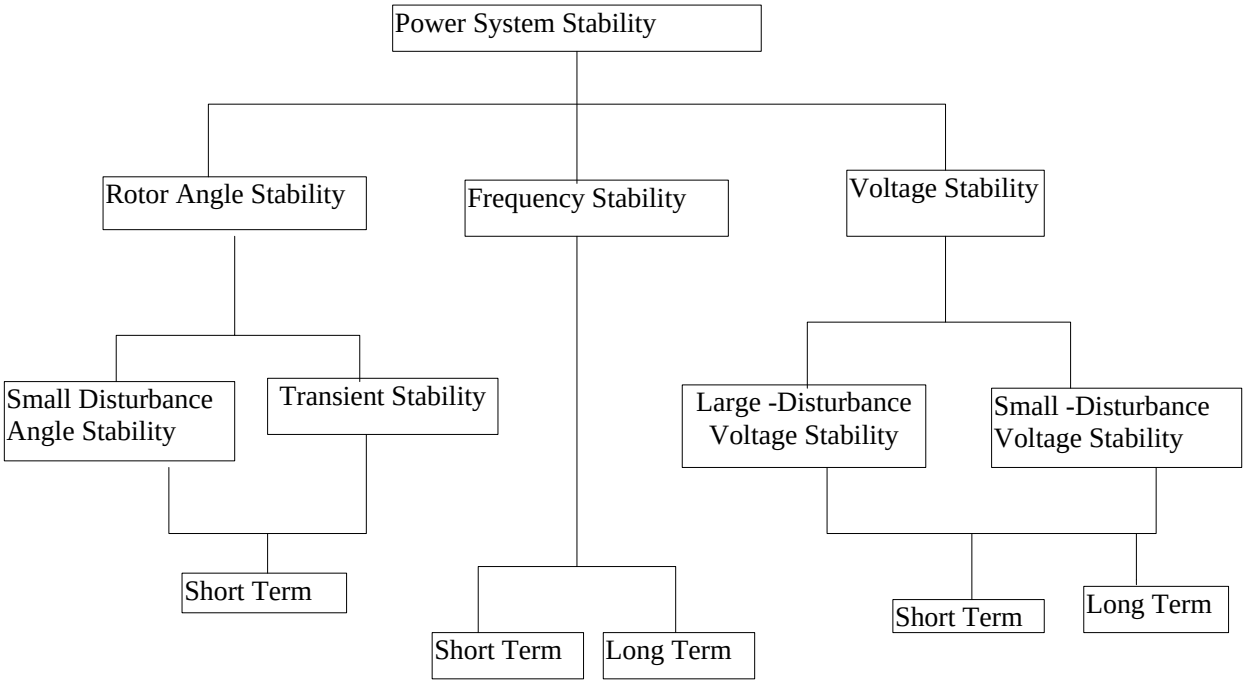

Figure 3.1: Power System Stability Classification

3.2.1. Rotor angle Stability

Rotor angle stability refers to the ability of synchronous machines of an interconnected power system to remain in synchronism after being subjected to a disturbance. It depends on the ability to maintain/restore equilibrium between electromagnetic torque and mechanical torque of each synchronous machine in the system. Instability that may result occurs in the form of increasing angular swings of some generators leading to their loss of synchronism with other generators [8].

Rotor angle stability can be categorized as

- Small-disturbance rotor angle stability
- Large-disturbance rotor angle stability

Small-disturbance (or small signal) rotor angle stability is the ability of power system to maintain synchronism when subjected to small disturbance.

Large disturbance or **transient stability** as it is commonly dealing with the ability of the power system to maintain synchronism when subjected to a severe disturbance. Transient

stability, which is the focus of this study, depends on the initial operating state of the system and the severity of the disturbance. Transient instability is in the form of aperiodic angular separation due to insufficient synchronizing torque, manifesting itself as first swing stability.

3.2.2. Transient Stability

Transient stability is the ability of power system to remain in synchronism when subjected to large disturbance. Such disturbance which could affect the system transient stability include sudden load change, loss of generation, switching operation and faults that result in subsequent circuit operation [5]. These disturbances also result in the oscillations of the rotor and by extension the generated power. Transient stability is a fast phenomenon, usually occurring within one second for a generator close to the cause of disturbance.

3.2.3. Swing equation

The equation governing rotor motion of a synchronous machine is based on the elementary principle in dynamics which states that accelerating torque is the product of the moment of inertia of the rotor times its angular acceleration [24]. This equation can be written for the synchronous generator in the form:

$$J\frac{d^2\theta_m}{dt^2} = T_a = T_m - T_e \qquad (3.1)$$

Where,

J= the total moment of inertia of the rotor masses, in kg-m2

θm= the angular displacement of the rotor, in mechanical radians (rad)

t= time, in seconds (s)

Tm = the mechanical or shaft torque, in N-m

Te = the net electrical or electromagnetic torque, in N-m

Ta = the net accelerating torque, in N-m

In the case of synchronous generator, the electrical and mechanical torque are considered to positive. Which means that T_m is the resultant shaft torque which tends to accelerate the rotor in the positive θ_m direction of rotation, as shown in Figure 3.2 (a) below. The accelerating torque T_a is zero in steady-state operation because T_m and T_e are equal. In this

situation, there is no acceleration or deceleration of the rotor masses and the resultant constant speed is the same as synchronous speed. The rotating masses, which include the rotor of the generator and the prime mover, are said to be in synchronism with the other machines operating at synchronous speed in the power system [2, 24]. The prime mover may be a hydro turbine or a steam turbine, for which models of different levels of complexity exist to represent their effect on T_m.

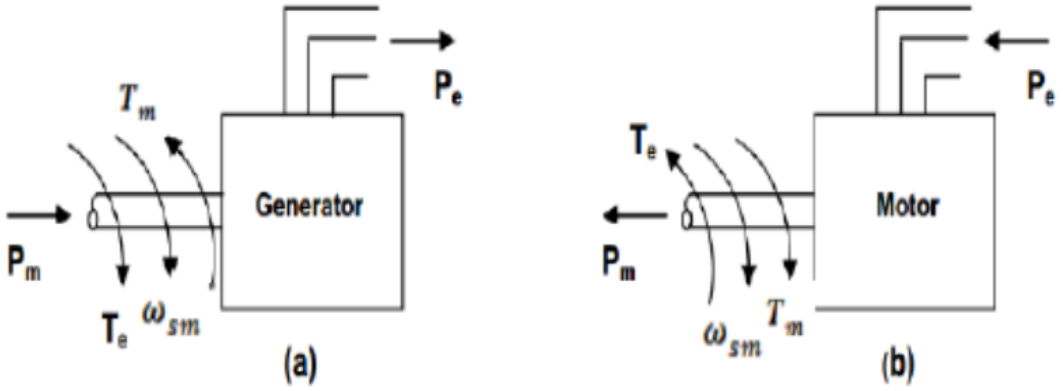

Figure 3.2: Representation of a machine rotor comparing direction of rotation and mechanical and electrical torques for: (a) a generator (b) a motor

T_m is considered constant at any given operating condition for generators even though input from the prime mover is controlled by governors. 1n the synchronous motor the direction of power flow is opposite to that in the generator. Accordingly, for a motor both T_m and T_e in equation (3.1) above are reversed in sign, as shown in Figure 3.2 (b). Te then corresponds to the air-gap power supplied by the electrical system to drive the rotor, whereas Tm represents the counter torque of the load and rotational losses tending to retard the rotor.

Since $\boldsymbol{\theta}$**m** is measured with respect to a stationary reference axis on the stator, it is an absolute measure of rotor angle. Consequently, it continuously increases with time even at constant synchronous speed. Since the rotor speed relative to synchronous speed is of interest, it is more convenient to measure the rotor angular position with respect to a reference axis which rotates at synchronous speed. Therefore, we define

$$\theta_m = \omega_{sm} t + \delta_m \qquad (3.2)$$

Where ω_{sm} is the synchronous speed of the machine in mechanical radians per second and $\boldsymbol{\delta m}$ is the angular displacement of the rotor, in mechanical radians, from the synchronously rotating reference axis. Take the derivatives of equation (3.2) with respect to time the results are obtained:

$$\frac{d\theta_m}{dt} = \omega_{sm} + \frac{d\delta_m}{dt} \tag{3.3}$$

$$\frac{d^2\theta_m}{dt^2} = \frac{d^2\delta_m}{dt^2} \tag{3.4}$$

Equation (3.3) shows that the rotor angle velocity $\omega_m = \frac{d\theta_m}{dt}$ is constant and equals the synchronous speed only when $\frac{d\delta_m}{dt} = 0$. Therefore, $\frac{d\delta_m}{dt}$ represents the deviations of the rotor speed from synchronism and the units are mechanical radians per second. Equation (3.4) represents the angular accelerations measured in (mechanical rad/s^2). Substituting equation (3.4) in equation (3.1),the result obtained:

$$J\frac{d^2\delta_m}{dt^2} = T_a = T_m - T_e \tag{3.5}$$

From elementary dynamics that power is the product of torque and angular velocity (ω_m), and so multiplying equation (3.5) by ω_m the result is.

$$J\omega_m\frac{d^2\delta_m}{dt^2} = P_a = P_m - P_e \tag{3.6}$$

Where

P_m = shaft power

P_e=electrical power transferred

P_a = accelerating power which accounts for any unbalance between Pm and Pe.

Now let us consider the stability of the generator connected to an infinite bus system and an asynchronous motor drawing power from infinite bus as shown in Figure 3.3. We know the apparent power is given by S=P+jQ=VI*=P-jQ=V*I, the real power $P = Re\{V*I\}$.

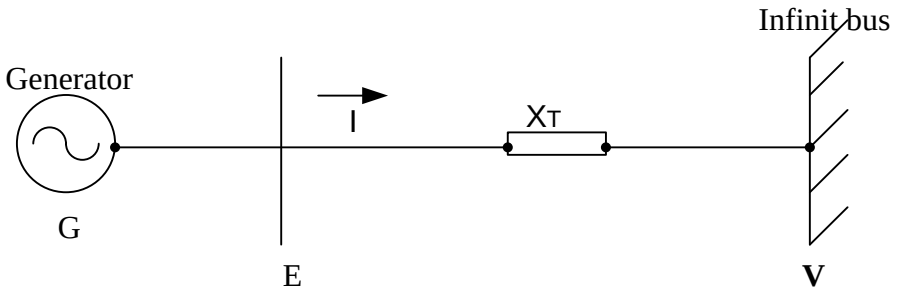

Figure 3.3: Single machine infinite bus system

$$E = V + jXI \tag{3.7}$$

Where, E is the internal voltage of the generator, $E = |E| < \delta$, V is the voltage at infinite bus, taking this as reference i.e. $V = |V| < 0^o$

X is the total reactance. Know solve equation (3.7), the following results are obtained.

$$I = \frac{\left(|E|\cos\delta + j|E|\sin\delta\right) - |V|}{jX} \tag{3.8}$$

$$P_e = \mathrm{Re}|V||I| = \frac{|V||E|}{X}\sin\delta = P_{\max}\sin\delta \tag{3.9}$$

Where, I line current, Pe generated electrical power. Usually, we neglect rotational losses and armature I^2R losses and think of P_m as power supplied by the prime mover and P_e as the electrical power output. Substitute 'M' in to equation (3.6) the result is as follow.

$$M\frac{d^2\delta_m}{dt^2} = P_a = P_m - P_e \tag{3.10}$$

Where, $M=J\omega_{sm}$ is the angular momentum of the rotor. The units of M is joule-seconds per mechanical radian.

In machine data supplied for stability studies another constant related to inertia is often encountered. This is the so-called H constant, which is defined by.

$$H = \frac{\frac{1}{2}J\omega_{sm}^{\ 2}}{S_{mach}} = \frac{\frac{1}{2}M\omega_{sm}}{S_{mach}} \tag{3.11}$$

Where, $\frac{1}{2}J\omega_{sm}^{\ 2}$ stored kinetic energy as synchronous speed in MJ, S_{mach} is the three-phase rating of the machine in mega volt amperes (MVA). Solving M in equation (3.11), the following equation is obtained.

$$M = \frac{2H}{\omega_{sm}} \times S_{mach} \tag{3.12}$$

And substituting for M in equation (3.10), the result obtained the result is as shown:

$$\frac{2H}{\omega_{sm}} \frac{d^2\delta_m}{dt^2} = \frac{P_a}{S_{mach}} = \frac{P_m - P_e}{S_{mach}} \tag{3.13}$$

Note that δm is expressed in mechanical radians in the numerator of equation (3.12) where as ω_{sm} is expressed in mechanical radians per second in the denominator. Therefore, equation (3.13) in per unit as shown equation (3.14).

$$M \frac{d^2\delta_m}{dt^2} = P_a = P_m - P_e \tag{3.14}$$

Equation (3.14), called the swing equation of the machine and the corresponding swing curve is shown in Figure 3.4 below, is the fundamental equation which governs the rotational dynamics of the synchronous machine in stability studies. In a stability study for a large system with many machines geographically dispersed over a wide area. it is desirable to minimize the number of swing equations to be solved. This can be done if the transmission line fault, or other disturbance on the system, affects the machines within a power plant so that their rotors swing together. In such cases the machines within the plant can be combined in to a single equivalent machine just as if their rotors were mechanically coupled and only one swing equation must be written for them. Consider a power plant with two generators connected to the same bus which is electrically remote from the network disturbances. The swing equations on the common system base are:

$$\frac{2H_1}{\omega_s} \frac{d^2\delta_1}{dt^2} = P_{m1} - P_{e1} \tag{3.15}$$

$$\frac{2H_2}{\omega_s} \frac{d^2\delta_2}{dt^2} = P_{m2} - P_{e2} \tag{3.16}$$

Adding the equations together and denoting δ_1 and δ_2 by δ since the rotors swing together, we obtain.

$$\frac{2H}{\omega_s}\frac{d^2\delta}{dt^2} = P_m - P_e \tag{3.17}$$

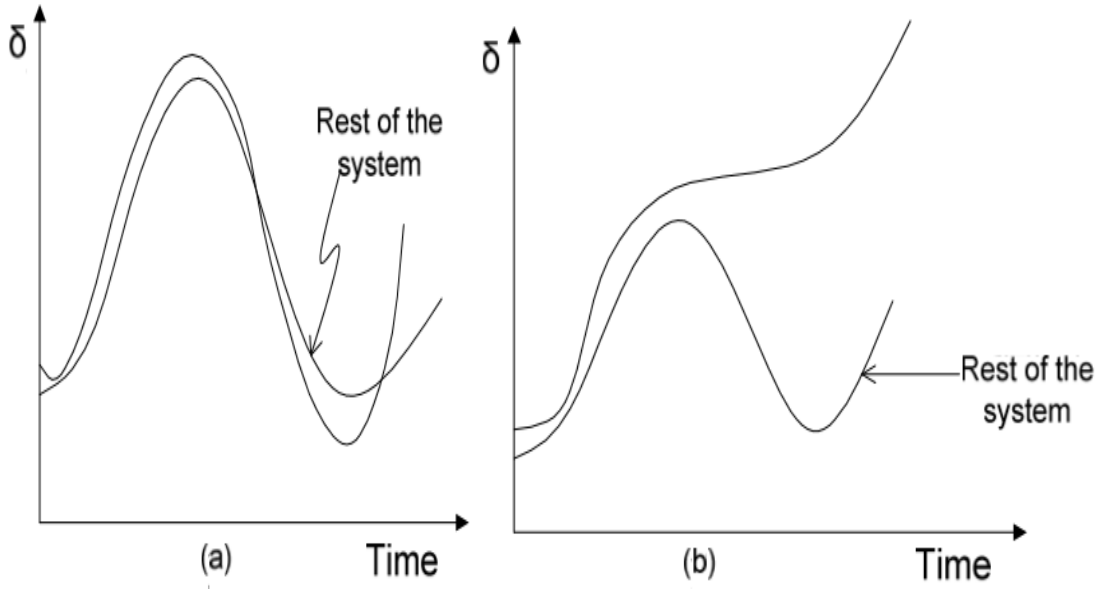

Figure 3.4: Rotor Angle against Time; a) Stable Case b) Unstable Case [23]

where $H = (H_1 + H_2)$, $P_m = (P_{m1} + P_{m2})$, and $P_e = (P_{el} + P_{e2})$. This single equation, which is in the form of equation (3.11) can be solved to represent plant dynamics. For many generators the swing equation will be applied similarly.

which represent the motion of each rotor during the fault and post fault periods. The solutions depend on the location and duration of the fault, and the Ybus resulting when the faulted line/bus is removed. Figure 3.4 shows the plot of the generator rotor angle (δ) against time. For a generator subject to a system disturbance it can either recover and oscillates around a new equilibrium point with the rest of the system or it can pull away from the rest of the system aperiodically. These curves are also known as the "swing curves".

3.2.4. Equal area criterion of stability

The equal area criterion can be used for a quick prediction of stability. This method is based on the graphical interpretation of the energy stored in the rotating mass as an aid to

determine if the machine maintains its stability after a disturbance. The derivation of the equal- area criterion is made for one machine and an infinite bus although the method can be readily adapted to general two-machine systems [23]. Now multiple the swing equation (3.14) by angular volecity of the rotor relative to synchronous speed, which is defined by:

$$\omega_r = \frac{d\delta}{dt} = \omega - \omega_s \tag{3.18}$$

Differentiating equation (3.18) with respect to t and substituting in equation (3.17), we obtain.

$$\frac{2H}{\omega_{sm}} \frac{d\omega_r}{dt} = P_m - P_e = P_a \tag{3.19}$$

When the rotor speed is synchronous, it is clear that $\omega=\omega s$ and ωr is zero. Multiplying both sides of Equation (3.19)by $\omega_r = \frac{d\delta}{dt}$, we have

$$\frac{H}{\omega_{sm}} 2\omega_r \frac{d\omega_r}{dt} = \left(P_m - P_e\right) \frac{d\delta}{dt} \tag{3.20}$$

The left hand side of the equation can be rewritten to give

$$\frac{H}{\omega_{sm}} \frac{d\left(\omega^2{}_r\right)}{dt} = \left(P_m - P_e\right) \frac{d\delta}{dt} \tag{3.21}$$

Multiplying by dt and integrating we obtain

$$\frac{H}{\omega_{sm}} \left(\omega^2{}_{r2} - \omega^2{}_{r1}\right) = \int_{\delta 1}^{\delta 2} \left(P_m - P_e\right) d\delta \tag{3.22}$$

The subscripts for the ωr terms correspond to those for the δ limits. That is, the rotor speed $\omega r1$ corresponds to that at the angle $\delta 1$, and $\omega r2$ corresponds to $\delta 2$.

Since ωr represents the departure of the rotor speed from synchronous speed, we readily see that if the rotor speed is synchronous at $\delta 1$ and $\delta 2$, then correspondingly, $\omega r1 = \omega r2 = 0$. Under this condition, equation (3.22) becomes.

$$\int_{\delta 1}^{\delta 2} \left(P_m - P_e\right) d\delta = 0 \tag{3.23}$$

This equation applies to any two points $\delta 1$and $\delta 2$ on the power-angle diagram, provided they are points at which the rotor speed is synchronous.

In Figure 3.5 two such points are a and e corresponding to $\delta 0$ and δc respectively. If we perform the integration of equation (3.20) in two steps, we can write.

$$\int_{\delta o}^{\delta r}\left(P_m - P_e\right)d\delta + \int_{\delta c}^{\delta r}\left(P_m - P_e\right)d\delta = 0$$
$$\int_{\delta o}^{\delta c}\left(P_m - P_e\right)d\delta = \int_{\delta c}^{\delta r}\left(P_m - P_e\right)d\delta \qquad (3.24)$$
$$\int_{\delta o}^{\delta c}\left(P_m - P_{e2}\right)d\delta + \int_{\delta c}^{\delta r}\left(P_m - P_{e3}\right)d\delta = 0$$

Taking the second term to the right-hand-side:

$$\int_{\delta o}^{\delta c}\left(P_m - P_{e2}\right)d\delta = \int_{\delta c}^{\delta r}\left(P_{e3} - P_m\right)d\delta \qquad (3.25)$$

Observing that these two terms each represent areas on the power-angle curve, we see that we have developed the so-called equal-area criterion for stability. This criterion says that stable performance requires that the accelerating area be equal to the decelerating area, i.e.

$A_1 = A_2$

Where,

$$A1 = \int_{\delta 1}^{\delta cr}\left(P_m - P_{e2}\right)d\delta$$
$$A2 = \int_{\delta cr}^{\delta r}\left(P_{e3} - P_m\right)d\delta$$

,which is illustrated in Figure 3.5, which indicates a way to identify the maximum swing angle, δr. Given a particular clearing angle δc, which in turn fixes A1, the machine angle will continue to increase until it reaches an angle δr such that A2=A1. Stability performance become more severe, or moves closer to instability, when A1 increases, or if available A2 decreases. We consider A2 as being bounded from above by δm, because δ cannot exceed δm. This is because δ>δm results in more accelerating energy, not more decelerating energy. Thus we speak of the "available A2" as being the area within Pe3-Pm bounded on the left by δc and on the right by δm. Contributing factors to increasing A1, and/or decreasing available A2, are summarized in the following four cases and corresponding illustrations.

- ✓ Pm increases: A1 increases, available A2 decreases

- ✓ Pe2 decreases: A1 increases.
- ✓ tc increases: A1increases, available A2 decreases
- ✓ Pe3 decreases: available A2 decreases.

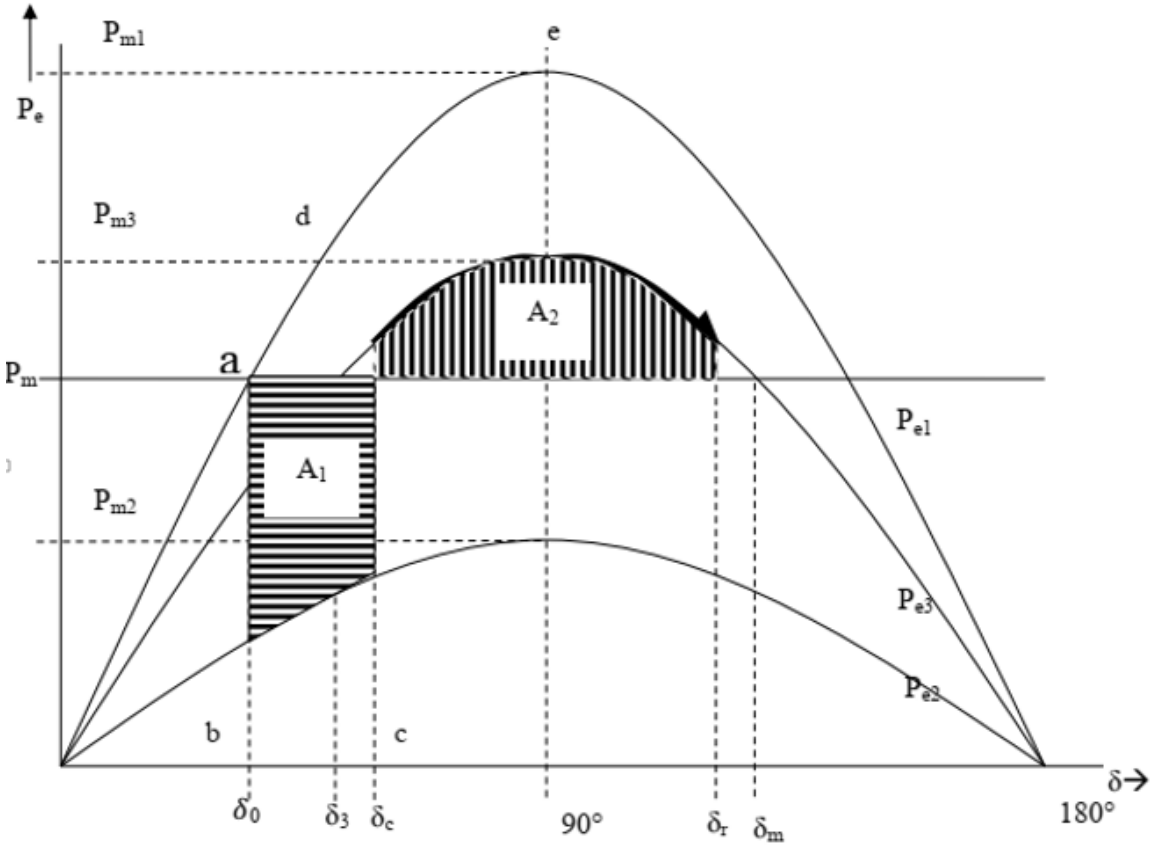

Figure 3.5:Equal Area Criteria [2]

3.2.5. Critical Clearing Angle and Critical Clearing Time

We can express the maximum clearing angle for marginal stability, δcr, as a function of Pm and attributes of the three power angle curves, Pe1, Pe2, and Pe3 by applying the equal area criterion. Let δc=δcr and δr= δm and applying equal area criteria, we have

$$\int_{\delta 1}^{\delta cr}\left(P_m - P_{e2}\right)d\delta = \int_{\delta cr}^{\delta m}\left(P_{e3} - P_m\right)d\delta \qquad (3.26)$$

Define r1=Pm2/Pm1, r2=Pm3/Pm1, Then we obtain:

$$\text{Cos}\,\delta_{cr} = \frac{\frac{P_m}{P_{m1}}\left(\delta_m - \delta_1\right) + r_2 \cos\delta_m - r_1 \cos\delta_1}{r_2 - r_1} \tag{3.27}$$

It is interesting to note that in this particular case, we can also express the clearing time corresponding to any clearing angle δc by performing two integrations of the swing equation.

$$\frac{2H}{\omega_s}\frac{d^2\delta}{dt^2} = P_m - P_e \tag{3.28}$$

For a fault at the machine terminals, Pe=0, so

$$\frac{2H}{\omega_s}\frac{d^2\delta}{dt^2} = P_m \Rightarrow \frac{d^2\delta}{dt^2} = \frac{\omega_s}{2H}P_m \tag{3.29}$$

Thus we see that for the condition of fault at the machine terminals, the acceleration is a constant. This is what allows us to successfully obtain t in closed form, as follows. Integrate (3.29) from t=0 to t=t:

$$\int_0^t \frac{d^2\delta}{dt^2} = \int_0^t \frac{\omega_s}{2H}P_m dt \Rightarrow \frac{d\delta}{dt}\Big|_{t=0}^{t=t} = \frac{\omega_s}{2H}P_m t \tag{3.30}$$

The left-hand-side of (3.30) (3.27)is speed. Speed at t=0 is 0. Therefore

$$\frac{d\delta}{dt} = \frac{\omega_s}{2H}P_m t \tag{3.31}$$

Now perform another integration of (3.31)

$$\int_0^t \frac{d\delta}{dt} = \int_0^t \frac{\omega_s}{2H}P_m t \tag{3.32}$$

The left-hand-side of equation (3.32) is actually an integration with respect to δ, but we need to change the integration limits accordingly, where δ(t=0)=δ1, to get

$$\int_{\delta o}^{\delta(t)} d\delta = \int_0^t \frac{\omega_s}{2H}P_m t dt \tag{3.33}$$

Performing the integration and replacing $\delta(t)$ with δcr and t with tcr results

$$\delta_{cr} = \frac{\omega s}{2H}P_m \frac{t^2_{cr}}{2} + \delta_o \tag{3.34}$$

Solving for t yields:

$$t_{cr} = \sqrt{\frac{2H}{\omega s P_m}\left(\delta_{cr} - \delta_o\right)} \tag{3.35}$$

Where CCT =t_{cr} is critical clearing time, which is the maximum time when the system is stable. So we obtain the time t corresponding to any clearing angle δcr, when fault is temporary (no loss of a component) and fault is at machine terminals, using equation (3.32), by setting δ(t)=δcr=δc. The equal-area criterion is a very useful means for analyzing stability of a system of two machines, or of a single machine supplied from an infinite bus. However, the computer is the only practical way to determine the stability of a large system.

3.2.6. Multi-machine stability studies

The equal-area criterion cannot be used directly in systems where three or more machines are represented. Although the physical phenomena observed in the two-machine problems are basically the same as in the multi-machine case, nonetheless, the complexity of the numerical computations increases with the number of machines considered in a transient stability study. When a multi-machine system operates under electromechanical transient conditions, inter machine oscillations occur through the medium of the transmission system connecting the machines [25]. If anyone machine could be considered to act alone as the single oscillating source, it would send into the interconnected system an elector mechanical oscillation determined by its inertia and synchronizing power. A typical frequency of such an oscillation is of the order of 1-2 Hz, and this is superimposed upon the nominal 60/50-Hz frequency of the system. When many machine rotors are simultaneously undergoing transient oscillation, the swing curves reflect the combined presence of many such oscillations. Therefore, the transmission system frequency is not excessively perturbed from nominal frequency, and the assumption is made that the 60/50 Hz network parameters are still applicable. To ease the complexity of system modeling, and thereby the computational burden, the following additional assumptions are commonly made in transient stability studies:

- ✓ The mechanical power input to each machine remains constant during the entire period of the swing curve computation.
- ✓ Damping power is negligible.

- ✓ Each machine may be represented by a constant transient reactance in series with a constant transient in terminal voltage.
- ✓ The mechanical rotor angle of each machine coincides with δ, the electrical phase angle of the transient internal voltage.
- ✓ All loads may be considered as shunt impedances to ground with values determined by conditions prevailing immediately prior to the transient conditions.

The system stability model based on these assumptions is called the classical stability model, and studies which use this model are called classical stability studies. Throughout this chapter, however, the classical model is used to study system disturbances originating from three-phase faults. The system conditions before the fault occurs, and the network configuration both during and after its occurrence, must be known in any transient stability study. Consequently, in the multimachine case two preliminary steps are required:

- ✓ The steady-state pre-fault conditions for the system are calculated using a production type power-flow program.
- ✓ The pre-fault network representation is determined and then modified to account for the fault and for the post fault conditions.

During and after the fault the power flow into the network from each generator is calculated by the corresponding power-angle equation. The Swing equations, for multi machine power system generally is expressed as:

$$\frac{2H_i}{\omega_s}\frac{d^2\delta i}{dt^2} = P_{mi} - P_{ei} \qquad i = 1,\ 2,\ 3,\ ...N \tag{3.36}$$

Many factors affect the transient stability of a generator in a practical power system can be identified as following [11]:

- ✓ The post-disturbance system reactance as seen from the generator.
- ✓ The duration of the fault-clearing time.
- ✓ The inertia of the generator.
- ✓ The generator internal voltage (determined by excitation system) and infinite bus voltage (system voltage).
- ✓ The generator loading before the disturbance.
- ✓ The generator internal reactance.
- ✓ The generator output during the fault.

- ✓ Short circuit power in substation

3.3. Static Synchronous Compensator (STATCOM)

The Static Synchronous Compensator (STATCOM) is a shunt device of the Flexible AC Transmission Systems (FACTS) family using power electronics to control power flow as well as power system stability on power grids [26].The STATCOM is based on a solid state synchronous voltage source which generates a balanced set of three sinusoidal voltages at the fundamental frequency with rapidly controllable amplitude and phase angle.

The block diagram of STATCOM is shown in Figure 3.6 below, which consists of a voltage source converter (VSC), a coupling transformer and DC voltage source (dc capacitor). Control of reactive current and hence the susceptance presented to power system is possible by variation of the magnitude of output voltage (V_{conv}) with respect to bus voltage (V) and thus operating the STATCOM in inductive region or capacitive region.

The STATCOM regulates voltage at its terminal by controlling the amount of reactive power injected into or absorbed from the power system. The variation of reactive power is performed by means of a Voltage-Sourced Converter (VSC) connected on the secondary side of a coupling transformer. The VSC uses forced-commutated power electronic devices (GTOs, IGBTs or IGCTs) to synthesize a voltage V_{conv} from a DC voltage source. In this Figure 3.6, V represents the system voltage to be controlled and V_{conv} is the voltage generated by the VSC.

$$\begin{aligned} V &= |V| \angle 0° \\ V_{conv} &= |V_{conv}| \angle \delta_{conv} \end{aligned} \tag{3.37}$$

The operation principle of STATCOM as follow:

- ✓ In steady state operation, the voltage V_{conv} is in phase with V (δ=0), so that only reactive power is flowing and active power is zero (P=0).
- ✓ If V_{conv} is lower than V, Q is absorbed from system (V) to V_{conv} (STATCOM is absorbing reactive power), which is inductive operation mode.
- ✓ In contrast, if V_{conv} is higher than V, Q is supplied from V_{conv} to V (STATCOM is generating reactive power), which is capacitive mode.

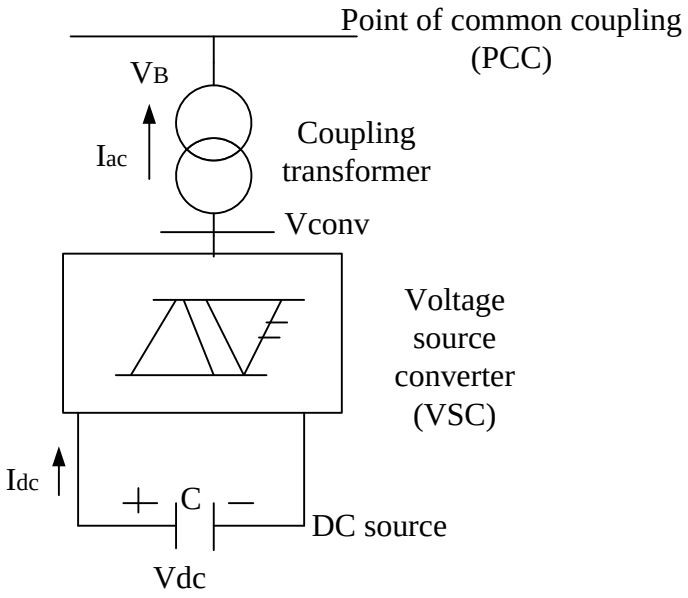

Figure 3.6: STATCOM block diagram

Hence, the amount of reactive power is given by

$$Q = \frac{|V|^2}{X} - \frac{|V||V_{conv}|}{X}\cos(\delta) \tag{3.38}$$

Where: V Line to line voltage of system voltage at PCC, V_{conv} Line to line voltage of generated by VSC, X Reactance of interconnection transformer and filters, δ Phase angle between V with respect to $V_{conv.}$

The STATCOM can supply real power to the ac system from its dc energy storage if the converter-output voltage is made to lead the ac-system voltage. On the other hand, it can absorb real power from the ac system for the dc system if its voltage lags behind the ac-system voltage[27]. Because it compensate transformer and converter losses and keep the capacitor charged.

$$P = \frac{|V||V_{conv}|}{X}\sin\delta \tag{3.39}$$

The STATCOM V-I Characteristics is shown in Figure 3.7 below. It can supply both capacitive and inductive compensation and is able to independently control its output current over the rated maximum capacitive or inductive range irrespective of the amount of ac system voltage. That is, the STATCOM can provide full capacitive reactive power at

any system voltage, even as low as 0.15 p.u. The characteristic of a STATCOM reveals strength of this technology: that it is capable of yielding the full output of capacitive generation almost independently of the system voltage (constant-current output at lower voltages).

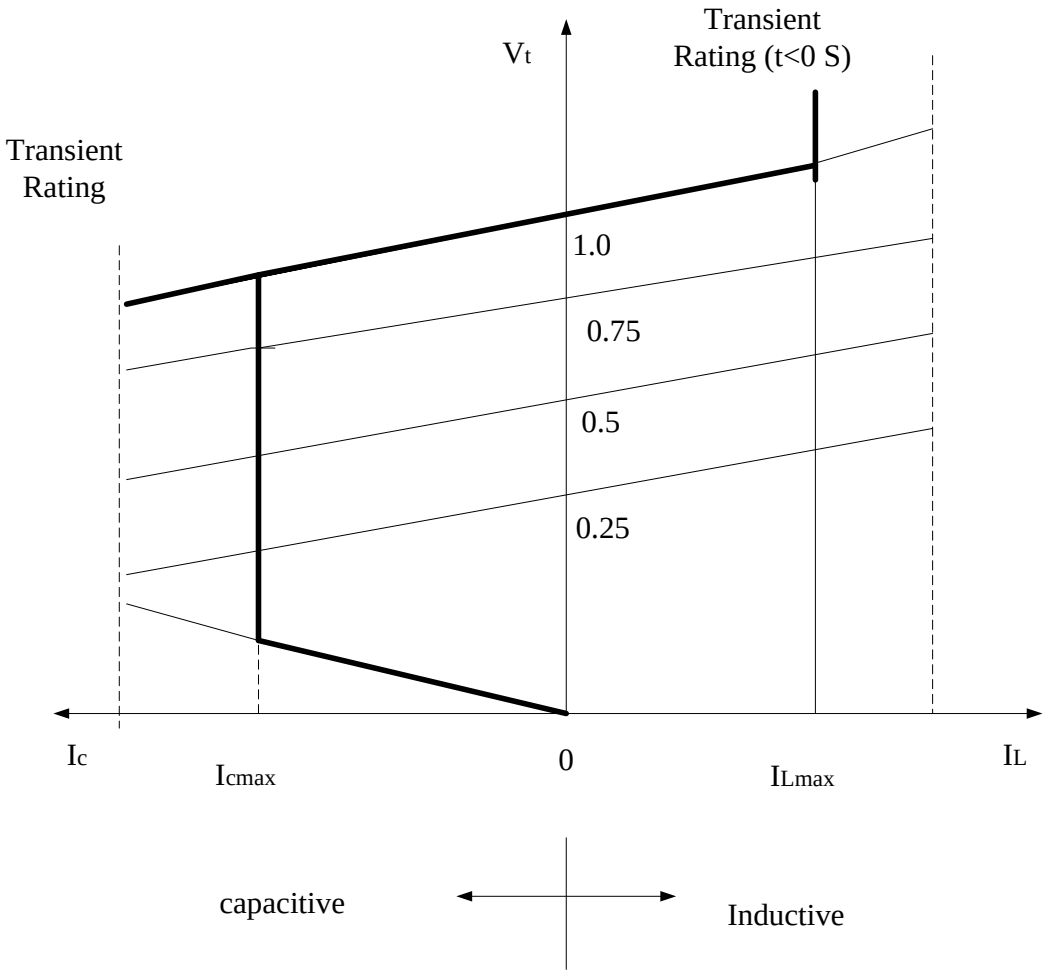

Figure 3.7: V-I Characteristics of STATCOM

This capability is particularly useful for situations in which the STATCOM is needed to support the system voltage during and after faults where voltage collapse would otherwise be a limiting factor [27].

In Figure 3.6 above, the main function of the converter is to produce an AC output waveform from a DC power supply. Based on the DC sources two types of converters are presented. Voltage source converter (VSC) and current source converter (CSC). These

converters are constructed using power switches, like GTO, IGBTs, etc. There is different converter topology in converter valves. These are classified into two: two level topology and multilevel topology. The objective of these topology are [28]:

- ✓ To minimize the switching losses of the semiconductors switches inside the VSC.
- ✓ To produce a high-quality sinusoidal voltage waveform with minimum or no filtering requirements.

The PWM converter model represents a self-commutated, voltage source converter (with a capacitive DC-circuit included). The model equations are derived from the equivalent circuit according to Figure 3.10 below. The circuit is composed of valves with turn-off capability (two dashes), which are usually realized by GTOs or IGBTs. The VSC-converter supports sinusoidal and rectangular modulation. The definition of the K0-factor depends on the selected modulation, it can be either rectangular or sinusoidal modulation.

Power Factory offers two different PWM converter models one with two dc-connections (*ElmVsc*) in Figure 3.8 and the other with one dc-connection (*ElmVscmono*) in Figure 3.9. The internal model used in both cases is the same, the only difference is that in the case of *ElmVscmono* the negative dc pole is directly earthed as shown in figure 2.9 below and manual connection cannot be done [29].

This inverter uses pulse-Width Modulation (PWM) technique to synthesize a sinusoidal wave form from a DC voltage sources with a typical chopping frequency of a few kilohertz. Basic purpose of PWM technique is to reduce inverter output harmonic level, to increase voltage magnitude and to reduce switching losses [30]. The PWM technique can be realized in variety of ways. Among these sinusoidal PWM, space vector PWM, optimized PWM, and sinusoidal PWM with third harmonics elimination are the most common.

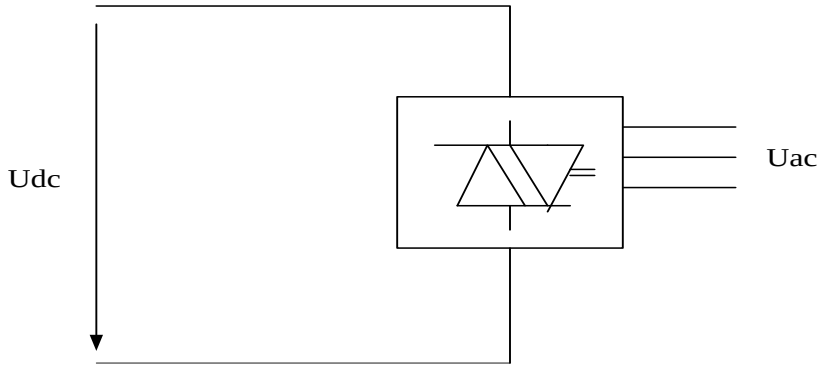

Figure 3.8: PWM-Converter with two dc-connections (*ElmVsc*)

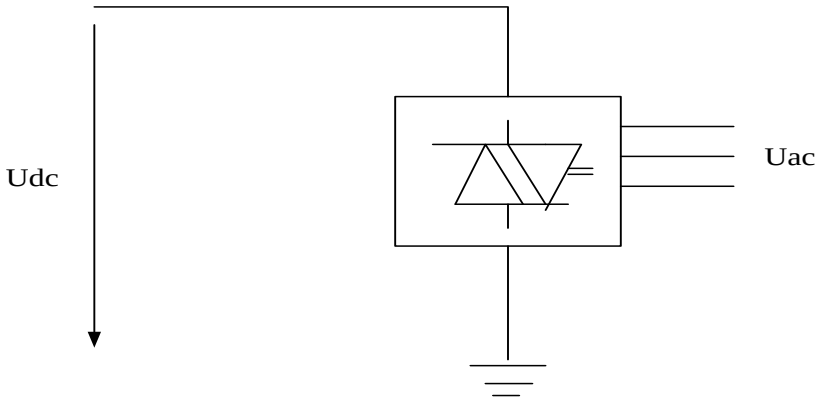

Figure 3.9: PWM-Converter with one dc-connection (*ElmVscmono*)

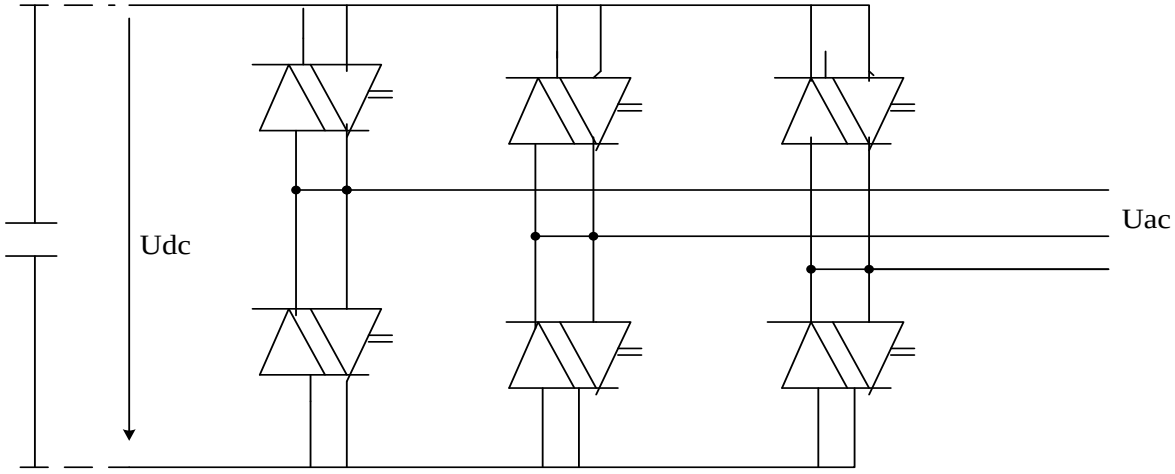

Figure 3.10: Equivalent Circuit, with DC-Capacitance

In sinusoidal PWM scheme converter firing pulse signals are generated by comparing a fundamental frequency sinusoidal wave form with a triangular carrier signal as shown in Figure 3.11 below. The relative level of the two waves is used to control the switching of devices in each phase leg of the inverter. The frequency of the triangular carrier signal determines the switching frequency of the converters.

The PWM is the ratio of triangular wave amplitude and reference sinusoidal wave amplitude and given by equation (3.40):

$$M = \frac{u_{triangular}}{u_{ref}} \tag{3.40}$$

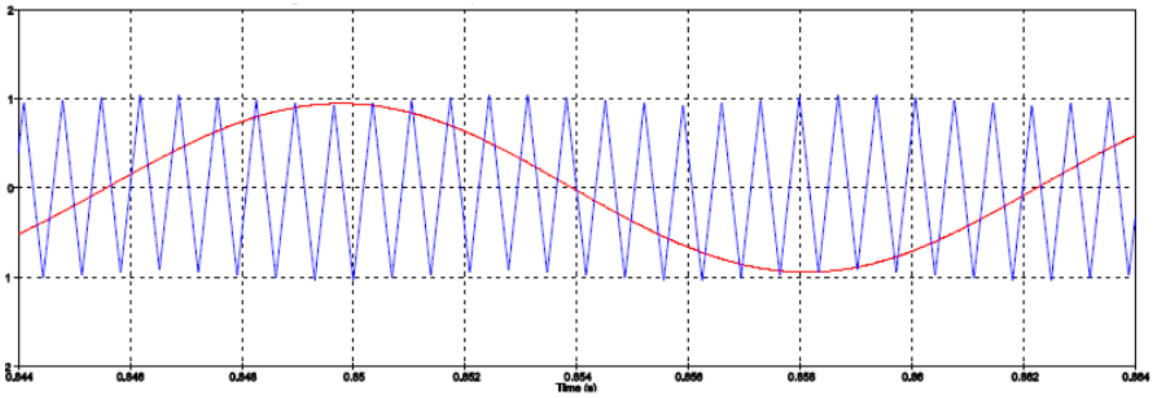

a) **PWM signal for one of the phase leg of VSC**

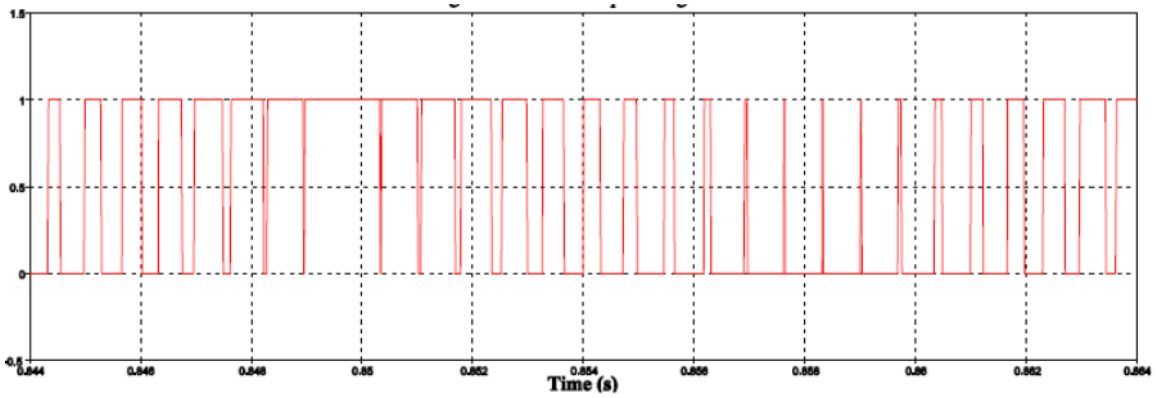

b) **Generated PWM**

Figure 3.11: Sinusoidal PWM based on triangular carrier signal [31].

In the STATCOM modeling, star-delta (Y-Δ) transformer is usually used in STATCOM to prevent the zero sequence components from the network to be transmitted into the STATCOM as well as the primary side of the transformer is required to be grounded. In star-delta connection, the phase shift between the STATCOM and the grid voltage is + 30◦ *or* - 30◦. In case of positive sequence, the primary voltage (star configuration) leads the secondary voltage (delta configuration) by +30. The primary voltage (grid voltage) lag the secondary voltage (STATCOM voltage) in the negative sequence [29].

3.4.Data collection

The transmission line include in this research is 132 kV,230 kV, and 400 kV and at the generation buses terminal the voltages are 10.5 kV, 13.8 kV, and 15 kV. Based on the

existing network data the stability of the power system operating condition such as steady state and transient stability are studied. For this research, load, transmission lines, and generator data are collected from EEP transmission line planning and strategy office as shown in appendix 4, 5, and 6 respectively.

3.5.Data analysis

In the Figure 3.13 below, the study area consists of totally 85 buses. Among those buses, it has one reference/slack bus, 41 load buses, 43 generator buses and 12 hydro power plant, and 5 wind generators. Using DIgSILENT software the single diagram is designed as shown in Figure 3.13.

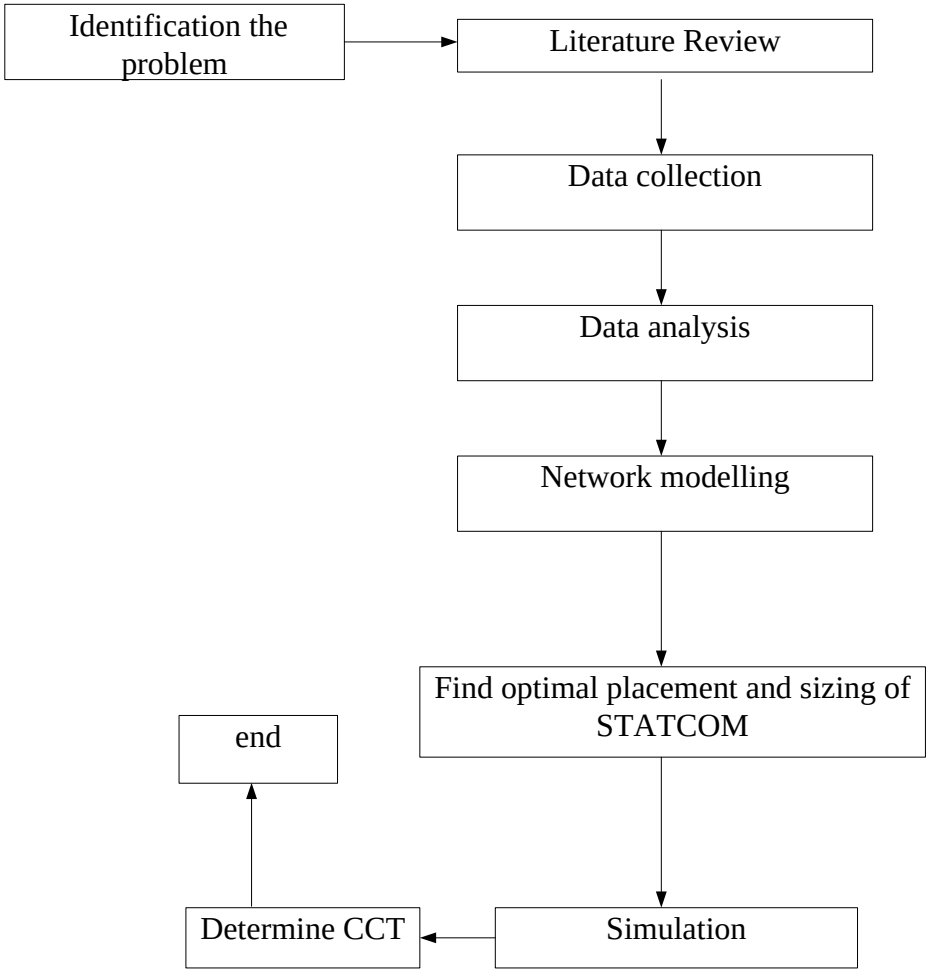

Figure 3.12: Methodology flow chart

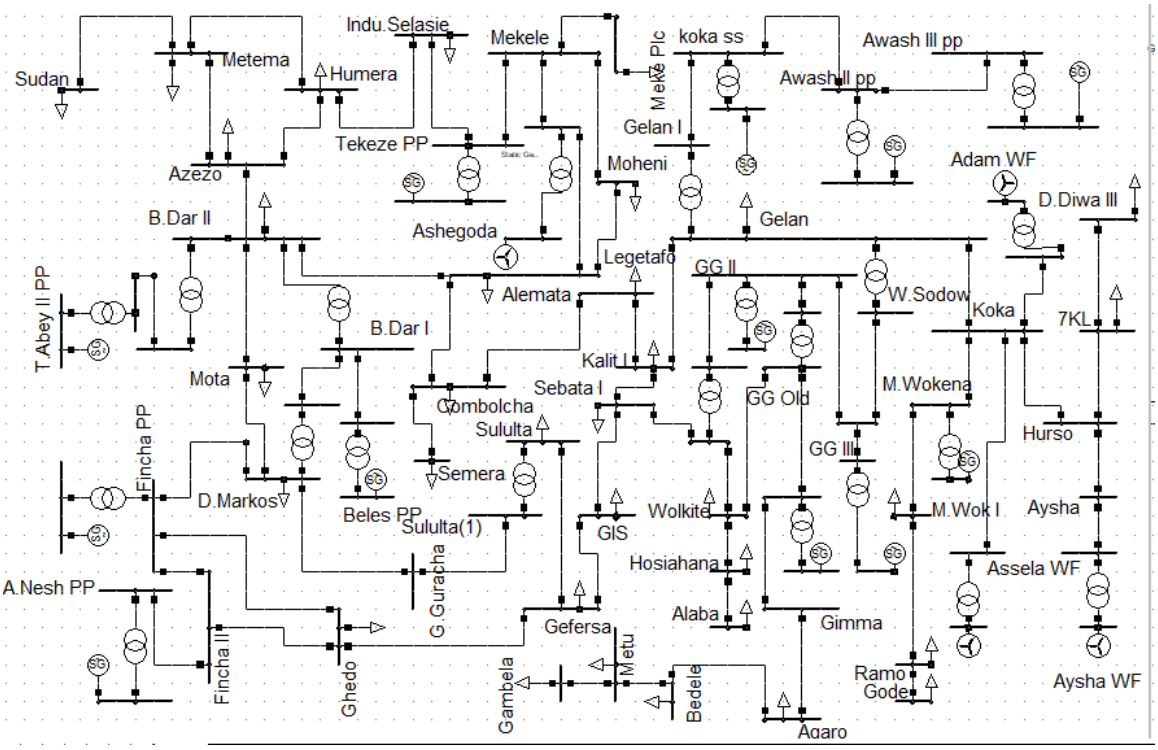

Figure 3.13: single line diagram of Ethiopian 230 kV/400 kV transmission networks

The PowerFactory implementation of STATCOM as shown Figure 3.14 below, which consists of the PWM converter used as voltage source converter (VSC), coupling transformer, and DC capacitor used as energy storage device.

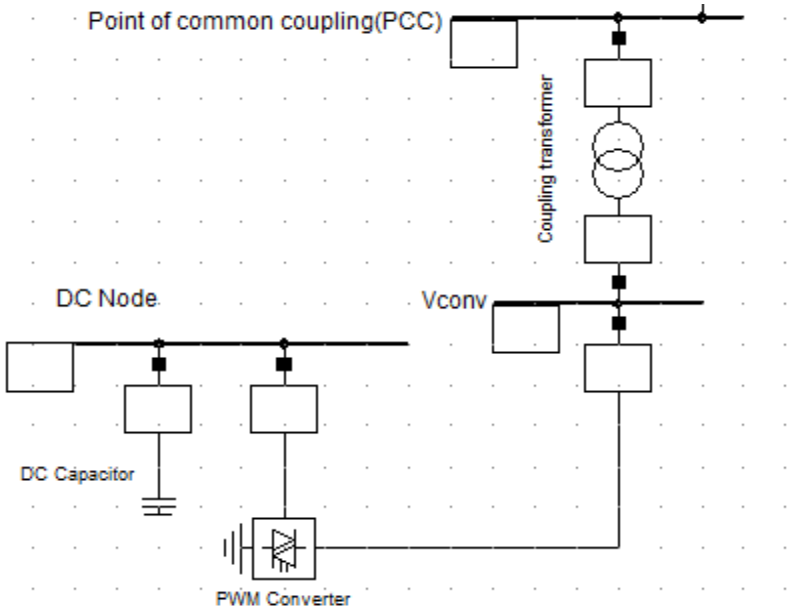

Figure 3.14: PowerFactory model of STATCOM

3.6.Placement of STATCOM using PV-curve

PV-curve technique is used for carrying out voltage stability performance analysis of the system under study. It is used to obtain P-V curve of power system for each bus. In P-V curve starting with initial operating point and increasing load to the maximum loading point as shown in Figure 3.15 below. The PV-curve scripts are developed in DIgSILENT programing language (DPL) in DIgSILENT PowerFactory version 15.1.7 software.

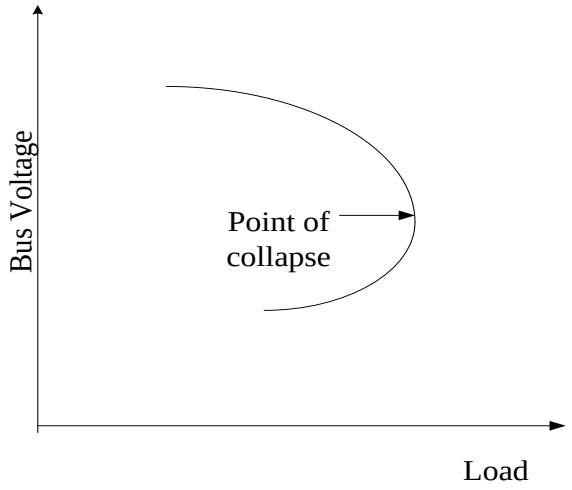

Figure 3.15: PV-curve

3.7.Modeling of STATCOM

The IEEE definition of STATCOM is "a self-commutated switching power converter supplied from an appropriate electric energy source and operated to reproduction set of adjustable multiphase voltage, which may be coupled to an AC power system with objective of exchanging independently controllable real and reactive power"[32].

Generally STACOM consists of the following components.

- Voltage Source Converter (VSC)
- DC energy storage device (capacitor)
- Coupling transformer
- System controller

Before going to study the modeling and control of STATCOM components. It is better to realize about its components before going to the design aspects of STATCOM components are important parts for economic and technical analysis.

For this thesis, VSC using IGBT based PWM inverter is used. PWM has different modulation technique. The PWM technique chosen on DIgSILENT power factory for this work is sinusoidal PWM. Fundamental frequency component voltage output of the converter can be related to the DC operating voltage by the following equation.

$$V_{conv} = K_0 MUdc \tag{3.41}$$

Where, K_0 is constant factor depends on modulation for this work K_0=0.612, due to sinusoidal modulation. M is the modulation index, The output voltage of STATCOM is obtained in linear operating mode ($0 < M \leq 1$) [33]. 'M' for this is 0.8 is chosen to calculate DC voltage.

Transformers are used for converting the system voltage to a value suitable for the converter. For STATCOM application standard transformers are used. The leakage reactance of the transformer is usually in the range of 0.1-0.2 p.u [28].

For this thesis coupling transformer converts 230 kV to 30 kV that is suitable for the converter and the reactance is chosen 0.2 p.u.

$$L = \frac{V^2_{conv}}{Snom} * \frac{X_l}{2\pi f} \tag{3.42}$$

Where, *V* stand for the secondary voltage, 30 kV, Snom stand for STATCOM rated apparent power, Snom=200 MVA is the rated (base) power of the converter, *f* stand for the system frequency, which is 50 *Hz*, X_L stands for inductive reactance, equal to 0.2 *p.u, L* strand for inductance, By solving the equation (3.42) above, the transformer has inductance, L=2.866 mH and resistance, R=0.0045 Ω.

Capacitor sizing

DC capacitor is used to maintain constant DC voltage which is important parts of the converter. Hence, the design of DC capacitor is the primary importance. The advantage of its design is to achieve a small ripple in DC voltage. The capacitor sizing is characterized

by the time constant τ defined as the ratio between the DC power stored at the DC side of the converter to the converter rated MVA power [34].

$$\tau = \frac{C_{dc}U_{dc}}{2S_{nom}} \tag{3.43}$$

Usually τ assumes the value between 5 ms-10 ms [35]and for this thesis τ=5 ms is chosen. DC link voltage based on equation (3.41) above become: Udc=61 kV. Moreover, solve equation (3.43) above, the capacitor is resulted: Cdc=537.5 μF.

3.7.1. STATCOM controller design

There are different power flow controller strategies. Vector current control and direct power flow control strategies are the two well know [28].

For this research vector current control strategies have been selected because it has excellent dynamic performance and inherent protection against overcurrent than direct power flow control strategies. Due to this reason Vector current control is the most widely utilized. In vector current control method two transformations are performed. The first one Clark's transformation, which is used to convert three phase AC quantities from a-b-c reference frame into α-β stationary reference frame. The second one is park's transformation which converts α-β stationary reference frame into d-q rotating reference frame.

The other important property of vector control strategy is decoupled control ability that makes possible independent control of active and reactive powers. The decoupling of quantities allows the implementation of a cascaded control strategy which has improved dynamic performance. Cascaded control strategy consists of outer controllers and the inner current controllers. The outer controllers consists reactive power controller, active power controller, DC-voltage controller, and frequency controller, while the inner is only inner current controller. For this thesis the cascaded controller consists of the outer controller is DC-voltage controller, while the inner controller is inner current controller.

3.7.2. STATCOM Mathematical modeling

For balanced three phase voltage equivalent circuit of VSC based STACOM is shown in Figure 3.16 below.

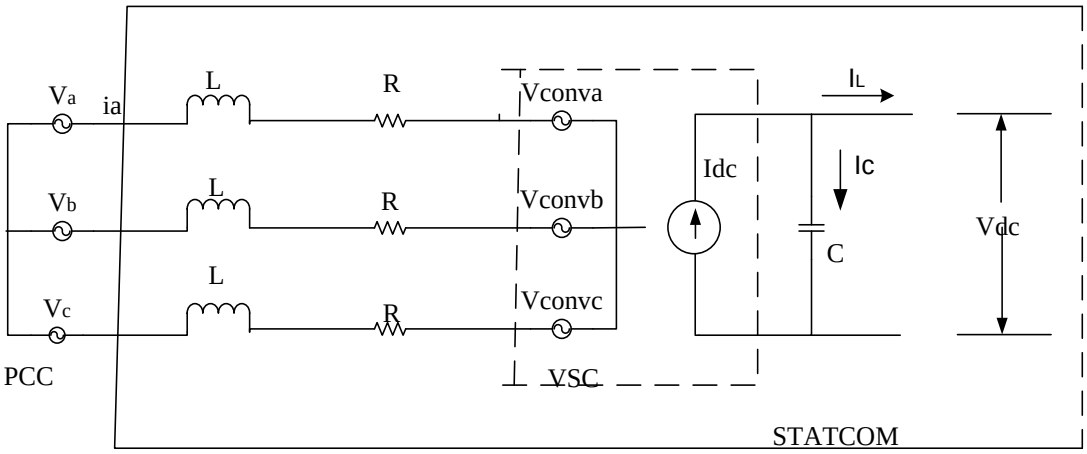

Figure 3.16: Equivalent circuit of VSC based STATCOM

From the equivalent circuit the following equation is developed by applying Kirchhoff voltage law in the AC source circuit.

$$V_{convabc} = R\,\mathrm{i}_{abc} + L\frac{di_{abc}}{dt} + V_{abc} \tag{3.44}$$

Where, i_{abc} =AC current of voltage source converter, $V_{convabc}$ = Converter ac side output voltage, Vabc = Grid voltage in abc reference frame, R =Reactor resistance, L =Reactor inductance. The space vector definition of voltage and current [36]:

$$\begin{aligned} \vec{U}_{\alpha\beta} &= \frac{2}{3}\left(V_{an} + V_{bn}e^{j\frac{2\pi}{3}} + V_{cn}e^{j\frac{-2\pi}{3}} \right) \\ \vec{I}_{\alpha\beta} &= \frac{2}{3}\left(i_{an} + i_{bn}e^{j\frac{2\pi}{3}} + i_{cn}e^{j\frac{-2\pi}{3}} \right) \end{aligned} \tag{3.45}$$

Now, apply Clark's transformation to equation (3.44), and equation (3.45), the result is.

$$\begin{vmatrix} V_\alpha \\ V_\beta \end{vmatrix} = \frac{2}{3}\begin{vmatrix} 1 & -\frac{1}{2} & -\frac{1}{2} \\ 0 & \frac{\sqrt{3}}{2} & -\frac{\sqrt{3}}{2} \end{vmatrix} * \begin{vmatrix} V_a \\ V_b \\ V_c \end{vmatrix} \tag{3.46}$$

$$\vec{V}_{\alpha\beta} = V\vec{conv}_{\alpha\beta} - R\vec{I}_{\alpha\beta} - L\frac{d\vec{I}_{\alpha\beta}}{dt} \tag{3.47}$$

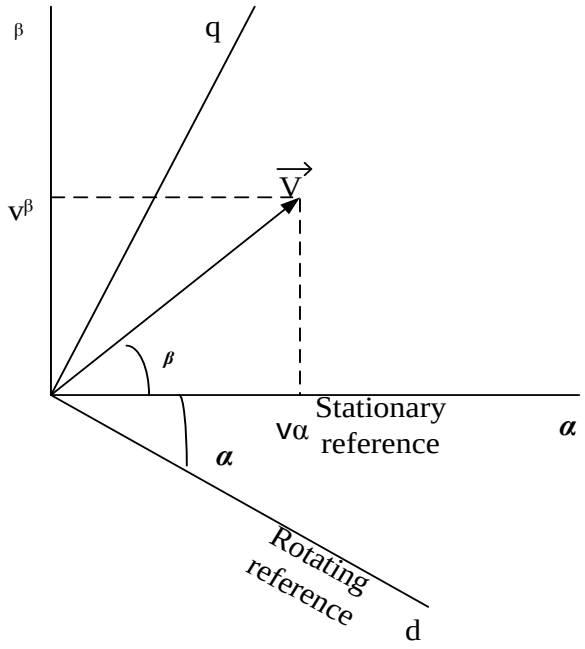

Figure 3.17**: Voltage phasor referred to stationary and moving reference frames**

Equation (3.47) above, represents the space vector expression of αβ stationary reference frames. If the reference system is moving with the angular velocity, ω_k, then the angle is formed by the moving reference frame and the stationary reference frame, angle 'α' is variable.

Hence, as is shown in Figure 3.17 above and phasor for example, $\vec{V}$ forms an angle (α+β) with respect to the new rotating reference frame.

In consequence, to express the space phasor in this new moving reference frame, it is necessary to add the angle alpha, 'α'. By using the Euler formulation to do this, the following equation is obtained:

$$\vec{V}_{\alpha\beta}e^{j\alpha} = V\vec{conv}_{\alpha\beta}e^{j\alpha} - R\vec{I}_{\alpha\beta}e^{j\alpha} - L\frac{d\vec{I}_{\alpha\beta}}{dt}e^{j\alpha} \tag{3.48}$$

Now, simplifying equation (3.48) above, the following result is obtained:

$$\vec{V}_{\alpha\beta}e^{j\alpha} = V\vec{conv}_{\alpha\beta}e^{j\alpha} - R\vec{I}_{\alpha\beta}e^{j\alpha} - e^{j\alpha}L\frac{d\vec{I}_{\alpha\beta}}{dt} - j\frac{d\alpha}{dt}L\vec{I}_{\alpha\beta}e^{j\alpha} \tag{3.49}$$

And finally, the stationary reference frame is as follows:

$$\vec{V}_{\alpha\beta} = \vec{Vconv} - R\vec{I} - L\frac{d\vec{I}}{dt} - j\omega_k L\vec{I} \tag{3.50}$$

Since, $\frac{d\alpha}{dt} = \omega_k$

Where, ω_k is the angular speed of the grid voltage vector. This equation is usually broken down into its two orthogonal projections, over the direct and quadrature axes (dq reference frame):

$$V_d = Vconv_d - RI_d - L\frac{dI_d}{dt} + \omega_k LI_q \tag{3.51}$$

$$V_q = Vconv_q - RI_q - L\frac{dI_q}{dt} - \omega_k LI_d \tag{3.52}$$

In equation (3.51) above all the terms projection on the d-axis except the last term, $\omega_k LI_q$ which is align in the d-axis. In the same way equation (3.52) the last term, $\omega_k LI_d$ is aligned q-axis. Both terms are called decoupling terms and add an extra difficulty to carrying out the control system, since any change in one of the axes changes the decoupling term in the other one.

By applying Kirchhoff's current low at the node of the DC side of the converter in Figure 3.16 above, the following equation is obtained:

$$C_{dc}\frac{du_{dc}}{dt} = i_{dc} - i_L \tag{3.53}$$

i_{dc} is DC current, i_L is DC link current, and $C_{dc}\frac{du_{dc}}{dt}$ is the current which pass through the capacitor.

3.7.3. Power delivered by the STATCOM to the grid

According to the Theory of circuit which the total apparent power (S) in the three phase circuit, either balanced or not can be calculated as the sum of symmetrical components in to which decomposed. So that the balanced three phase apparent power is expressed as follows:

$$\vec{S} = P + jQ = \vec{V}_a\vec{I}^*_a + \vec{V}_b\vec{I}^*_b + \vec{V}_c\vec{I}^*_c \tag{3.54}$$

In the equation (3.54), asterisk * represents the complex conjugate of the phasor in polar notation. When the apparent power expressed in terms of symmetrical components:

$$\vec{S} = 3\vec{V}_{a0}\,\vec{I}^{*}_{a0} + 3\vec{V}_{a1}\,\vec{I}^{*}_{a1} + 3\vec{V}_{a2}\,\vec{I}^{*}_{a2} \tag{3.55}$$

When the converter is connected with the grid, there is no neutral wire. As a result there is no zero component and also due to balanced system no negative component. Hence equation (3.55) become:

$$\vec{S} = 3\vec{V}_{a1}\,\vec{I}^{*}_{a1} \tag{3.56}$$

Now, using space phasor referred to the moving reference frame

$$\begin{aligned}\vec{V} &= \frac{2}{3}\left(v_{an} + v_{bn}e^{j\frac{2\pi}{3}} + v_{cn}e^{-j\frac{2\pi}{3}}\right)e^{j\alpha} = V_d + jV_q \\ \vec{I} &= \frac{2}{3}\left(i_a + i_b e^{j\frac{2\pi}{3}} + i_c e^{-j\frac{2\pi}{3}}\right)e^{j\alpha} = I_d + jI_q\end{aligned} \tag{3.57}$$

Then, the apparent power is expressed as follow:

$$\vec{S} = \frac{3}{2}\vec{V}\,\vec{I}^{*} = \frac{3}{2}\left[\left(V_d + jV_q\right)\left(I_d + jI_q\right)^{*}\right] \tag{3.58}$$

Now, separate equation (3.58), into it real and imaginary components and d-axis component of the grid voltage $V_d = \vec{V}_d$ and q-axis component grid voltage Vq=0. Then, the apparent power is reduced to:

$$\vec{S} = \frac{3}{2}\left(V_d I_d\right) + j\frac{3}{2}\left(-V_d I_q\right) \tag{3.59}$$

Therefore, the apparent power split into real power (P) and imaginary power (Q):

$$\begin{aligned}P &= \frac{3}{2}V_d I_d \\ Q &= -\frac{3}{2}V_d I_q\end{aligned} \tag{3.60}$$

Equation (3.60) above, indicates that active power is dependent on the d-axis current, while reactive power is dependent on q-axis current. Hence, active and reactive powers are decoupled and independent control is possible by independently controlling i_d and i_q.

On the other hand, the DC side power equation is:

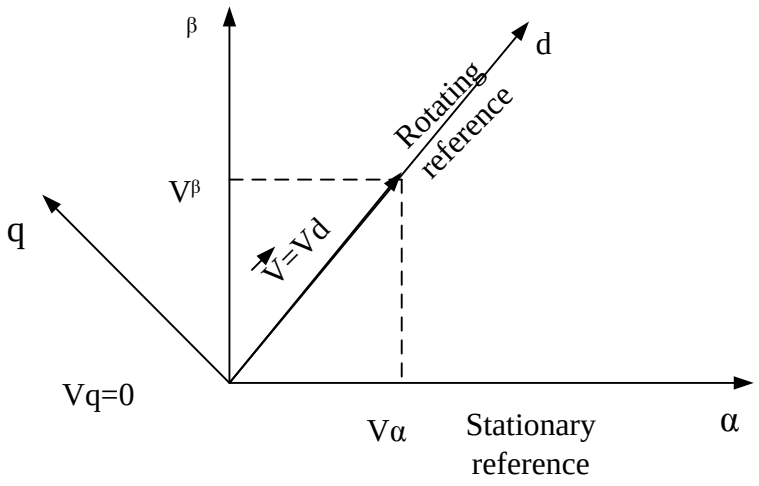

Figure 3.18: Voltage phasor aligned with the d axis of the moving reference frame.

$$P_{dc} = v_{dc} i_{dc} \tag{3.61}$$

3.7.4. Control strategy of STATCOM

The key objective of STATCOM controller is to control the real and reactive powers supplied to the grid independently as shown

Figure 3.19 below. The d-axis grid voltage, V_d, remains constant, the grid voltage, V_q=0, and the real and reactive power is regulated by means of, I_d and I_q, of the current injected into the network respectively. By analyzing the terminal equations, the dq components depends on the voltage generated by the converter, the resistance, reactance of the filter and on the decoupled terms since V_d is constant.

$$\begin{aligned} V_{convd} &= V_d + RI_d + L\frac{dI_d}{dt} - \omega_k LI_q \\ V_{convq} &= RI_q + L\frac{dI_q}{dt} - \omega_k LI_d \end{aligned} \tag{3.62}$$

From equation (3.62) above, it is possible to control I_d and I_q, independently by means of inverter voltage V_d and V_q, with a dynamic that depends on the R and L value of the filtering inductance. The active power supplied into the grid is zero, because the STATCOM is not required to generate or absorb active power (in ideal case).

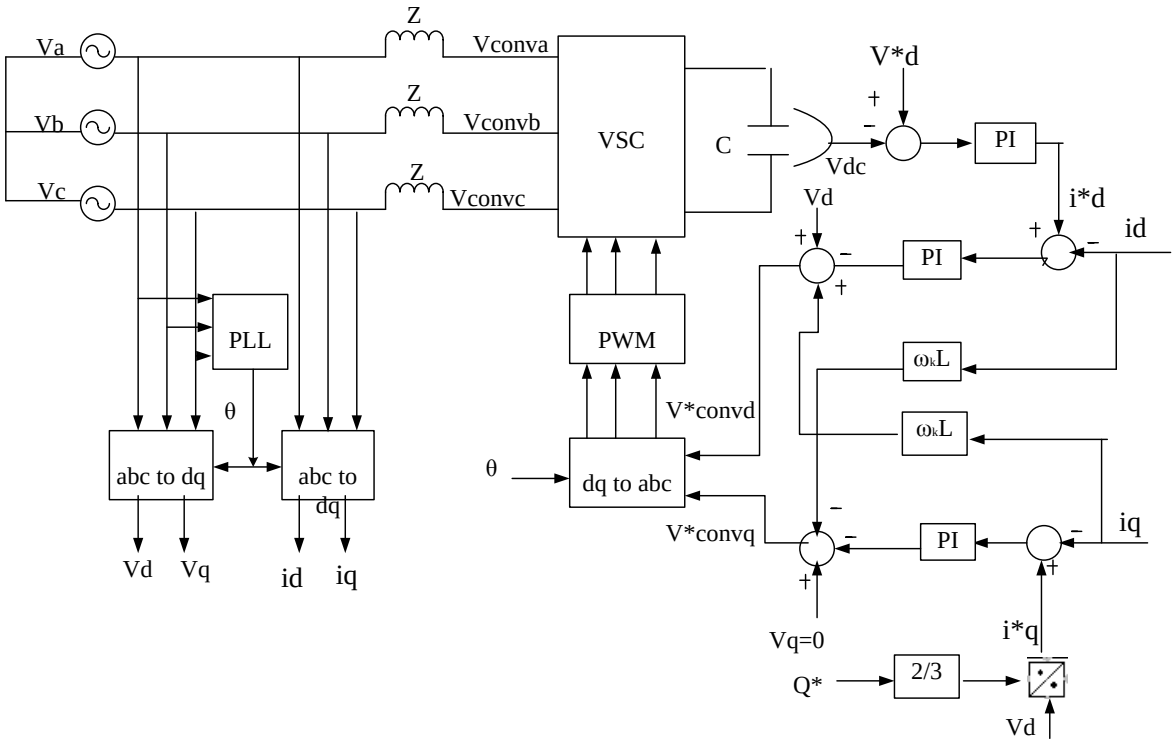

Figure 3.19: Proposed control schematic for STATCOM

3.7.5. Inner current control loop

The current controller loop is the inner part of the cascaded control strategy. It needs to be very fast as compared to the outer controllers so as to achieve control system stability. This is provided current reference values from the outer controllers and dq transformed currents from the grid. The block diagram of inner current control loop shown in Figure 3.20 below. The asterisk '*', indicates the reference value. In the current control loop, there are two PI regulators each for d and q axis currents components.

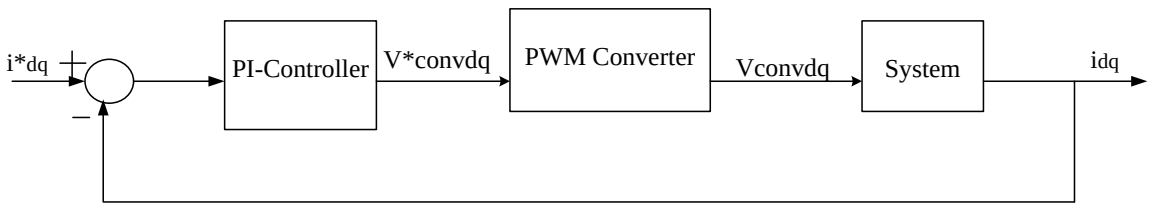

Figure 3.20: Block-diagram of the inner current control loop

This controller transforms the error current from the comparison to a voltage signal, which is used by pulse width modulation index (PWM) generator for switching the converter.

PI regulator, which is defined by the following equation:

$$K_p\left(1+\frac{1}{T_i s}\right) \tag{3.63}$$

Where, K_p is proportional gain and T_i is integral time constant.

PWM converter, which is approximation by first order equation. It produces output voltage, which is the converter side voltage as shown in Figure 3.20 above.

$$U^{ref}{}_{dq}\left(\frac{1}{1+T_{conv}s}\right)=U_{dq} \tag{3.64}$$

Where, $T_{conv}=\left(\frac{T_{switch}}{2}\right)$ and $T_{switch}=\frac{1}{f_{switch}}$, Hence this approximation shows that the converter is an ideal power transformer with time delay 'T_{conv}'. The switching frequency of PWM is very large compared to the supply frequency. For this design the switching frequency of IGBT is 2000 Hz is selected.

$$T_{conv}=\left(\frac{T_{switch}}{2}\right)=0.00025\ second \tag{3.65}$$

Plant transfer function, which is the transfer function of the system that developed after some mathematical manipulation the following equation, is obtained.

$$\begin{aligned} V_d &= L\frac{di_d}{dt}+Ri_d \\ V_q &= L\frac{di_q}{dt}+Ri_q \end{aligned} \tag{3.66}$$

In equation (3.66) above, the cross-coupling terms are eliminated and hence it is possible to have independent control of the d and q component currents. Now apply Laplace transformation in equation (3.66) above, the following transfer function is obtained.

$$G(s)=\frac{1}{R+Ls}=\frac{1}{R}\left(\frac{1}{1+\tau s}\right) \tag{3.67}$$

Where, $\tau = \frac{L}{R}$ which is reactor time constant. After simplify current control loop, converter and system transfer function the following reduced form is developed in Figure 3.21 below.

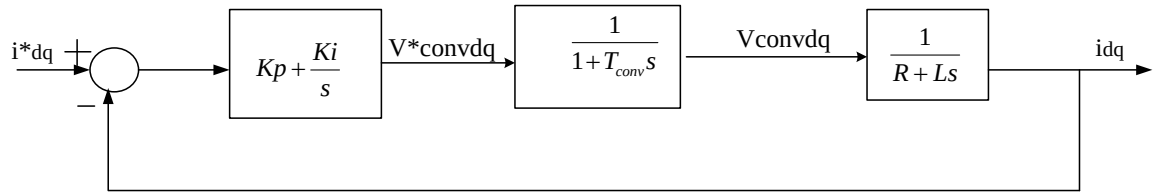

Figure 3.21:The reduced form of inner current controller loop

3.7.6. DC voltage control loop

DC voltage control is important for controlling the power exchange between the converters. The DC voltage control aimed at keeping the DC voltage at a defined value using the converter current as a control variable. Assuming the converter is ideal or lossless the active power in the ac side is equal to the DC power in the DC side. Then equating the AC active power equation in equation (3.60) and the DC power equation (3.61) above leads to:

$$\frac{3}{2}V_d I_d = V_{dc} I_{dc} \tag{3.68}$$

And solve equation (3.68), i_{dc}, is become:

$$i_{dc} = i_L + C_{dc}\frac{du_{dc}}{dt} \tag{3.69}$$

Substitute equation (3.69) into equation (3.68), gets the relation between DC voltage and direct current.

$$\frac{3}{2}V_d I_d = V_{dc}\left(i_L + C_{dc}\frac{du_{dc}}{dt}\right) \tag{3.70}$$

Laplace transformation and solving for Udc leads us to the following important result.

$$U_{dc} = \frac{1}{Cs}\left(\frac{3}{2}\frac{V_d I_d}{v_{dc}} - i_L\right) \tag{3.71}$$

To make more illustrative lets show the relationship using block diagram. Here to avoid the effect of the disturbance from i_L, compensation term, which have the value $\frac{3}{2}\frac{v_{dc}}{v_d}i_L$ can

be added before the converter. The inner current loop is approximated by first order equation shown

Figure **3.22**.

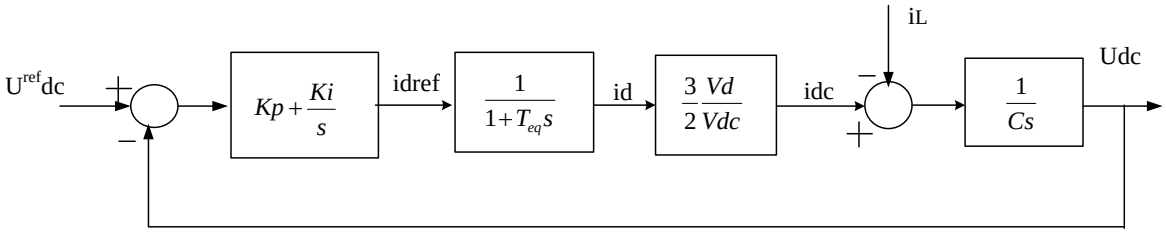

Figure 3.22: DC voltage controller block diagram

3.7.7. Tuning of inner current controller

There are different methods to tune controllers. The advantage of tuning is to make the current control loop work faster response of the system and the plant output is oscillation free. The tuning of the controllers for VSC here is based on the principle adopted for the basic electrical derives [37].

Accordingly, the speed of the controllers increases towards the inner loop. The inner loop is tuned according to the Optimum Modulus (MO) criterion [28]. This method is implemented when the controlled system has one dominant time constant and the other minor time constant. The dominant pole is canceled by the controller zero to arrive at a standard transfer function.

The open-loop transfer function for the inner current control loop in Figure 3.21 is given as follow:

$$G,\mathrm{ol(s)} = \frac{\mathrm{i_{dq}}}{\mathrm{i^{*}_{dq}}} = K_p\left(1+\frac{1}{T_i s}\right)\left(\frac{1}{1+T_{conv}s}\right)\left(\frac{1}{R+Ls}\right) \qquad (3.72)$$

Where, $T_i = \frac{K_p}{K_i}$ and $T_i = \tau = \frac{L}{R}$, hence $\mathrm{T_i}$ is equal to the reactor time constant τ.

Substituting the reactor values L=2.866mH, R=0.0045 Ω:

$T_i = \tau = \frac{L}{R}$ =0.637 second

As a result pole zero cancellation take place. The zero of the controller cancels the dominant pole. After applying the MO tuning criterion, the second order closed-loop transfer function of the current control loop is found to be as:

$$G,\mathrm{cl(s)} = \frac{\frac{K_p}{T_i T_{conv} R}}{s^2 + \frac{s}{T_{conv}} + \frac{K_p}{T_i T_{conv} R}} \tag{3.73}$$

It can easily be deduced from the transfer function mentioned above that the damping ratio is $\xi = 0.707$ [38]. The estimated values of the proportional and integral gains of the current PI controller are:

$K_p = \frac{T_i R}{2T_{conv}}$ and $T_i = \tau = \frac{L}{R}$. The value of T_{conv} from equation (3.65) above.

$$K_p = \frac{T_i R}{2T_{conv}} = 5.76 \tag{3.74}$$

Finally, the closed loop transfer function becomes:

$$G,\mathrm{cl(s)} = \frac{8.038\times10^6}{s^2 + 4\times10^3 s + 8.038\times10^6} \tag{3.75}$$

Based on the closed loop transfer function equation (3.75) above, the following step response specification was developed. These are rise time is 75.617 ms, settling time= is 0.0021 s, peak time is 0.0016 s, peak amplitude is 1.0439, and maximum over shoot is 4.3858%. the graphical step response is shown in Figure 3.23.

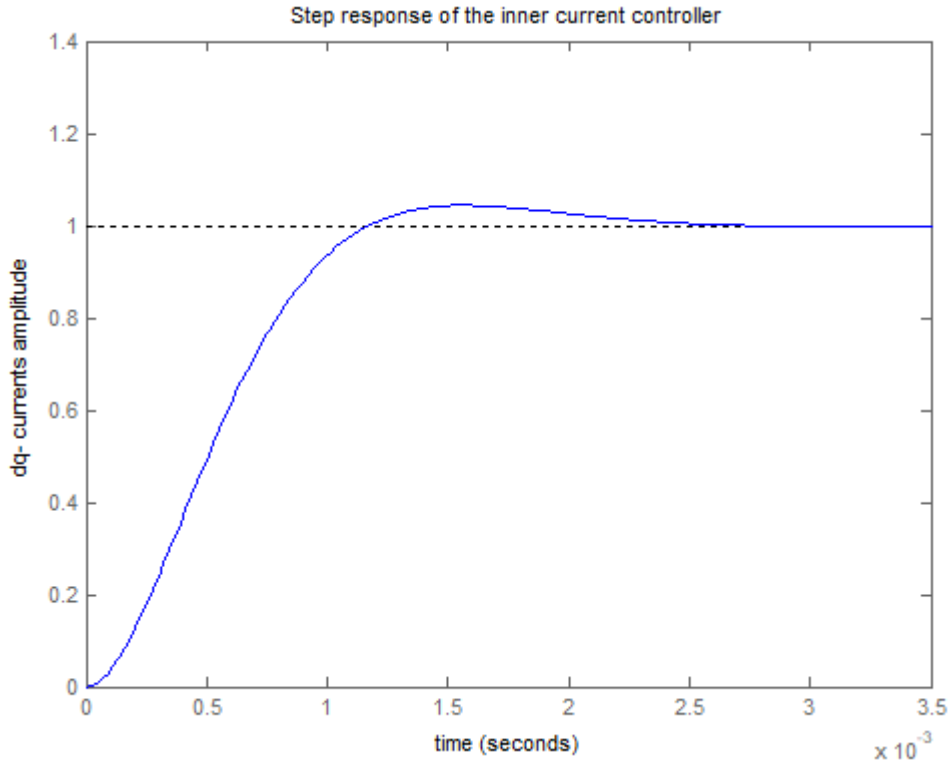

Figure 3.23: Inner current controller step response with the design current controller

3.7.8. Tuning DC voltage controller

From the DC voltage control loop block diagram as shown in the Figure 3.22. The open loop transfer function result is shown equation (3.76) below:

$$G,ol(s) = K_p\left(\frac{T_i s+1}{T_i s}\right)\left(\frac{1}{T_{eq}s+1}\right)\frac{3}{2}\frac{V_d}{v_{dc}}\frac{1}{Cs} \tag{3.76}$$

The DC voltage control loop parameter is tuned based on Symmetrical Optimum (SO) criterion [38]. Because the open loop transfer function of the DC voltage controller loop has a pole at the origin as shown in the Figure 3.22

After using symmetrical optimum (SO) tuning criterion, the closed loop transfer function of DC voltage controller loop is achieved:

$$G,cl(s) = \frac{K_c T_i s + K_c}{T_i T_{eq} C s^3 + T_i C s^2 + K_c T_i\ s + K_c} \tag{3.77}$$

Accordingly, the parameters are tuned by symmetrical optimum method. Proportional time constant T_i is [35].

$$T_i = \alpha^2 T_{eq} \tag{3.78}$$

Where, the value of parameter ' α ' is vary from 2 to 4 [35, 38]. The current control loop the equivalent time delay is calculated as shown:

$$T_{eq} = 2T_{conv} = 0.0005\text{second} \tag{3.79}$$

T_i=0.0045 second, when α =3.

Based on symmetrical optimum tuning method the proportional gain (Kp) is determined using the following data Vdc=61 kV, Vd=V=30 kV, and C=537.5 μF .

$$K_p = \frac{2}{3}\frac{V_{dc}C}{V_d \alpha T_{eq}} = 0.5 \tag{3.80}$$

Where, constant Kc is defined by:

$$K_c = \frac{3}{2}\frac{K_p V_d}{V_{dc}} = 0.37 \tag{3.81}$$

Finally, the overall transfer function becomes:

$$G, cl(s) = \frac{1.665*10^{-4}S + 0.37}{1.21*10^{-9}s^3 + 2.42*10^{-6}s^2 + 1.665*10^{-4}S + 0.37} \tag{3.82}$$

The step response of designed DC voltage controller is obtained using Matlab. These are rise time is 1.6 ms, peaking time is 1.4 ms, peak amplitude is 1.2476, and settling time is 11.7 ms. The controller step response is shown in Figure 3.24.

The time response of the inner current controller is around three times lower than the time response of DC voltage controller and has lower over shoot. The implication is that the slow response is important in cascaded control system stability. The higher peak value is indicating the system oscillation exhibit a large overshoot in its transient response.

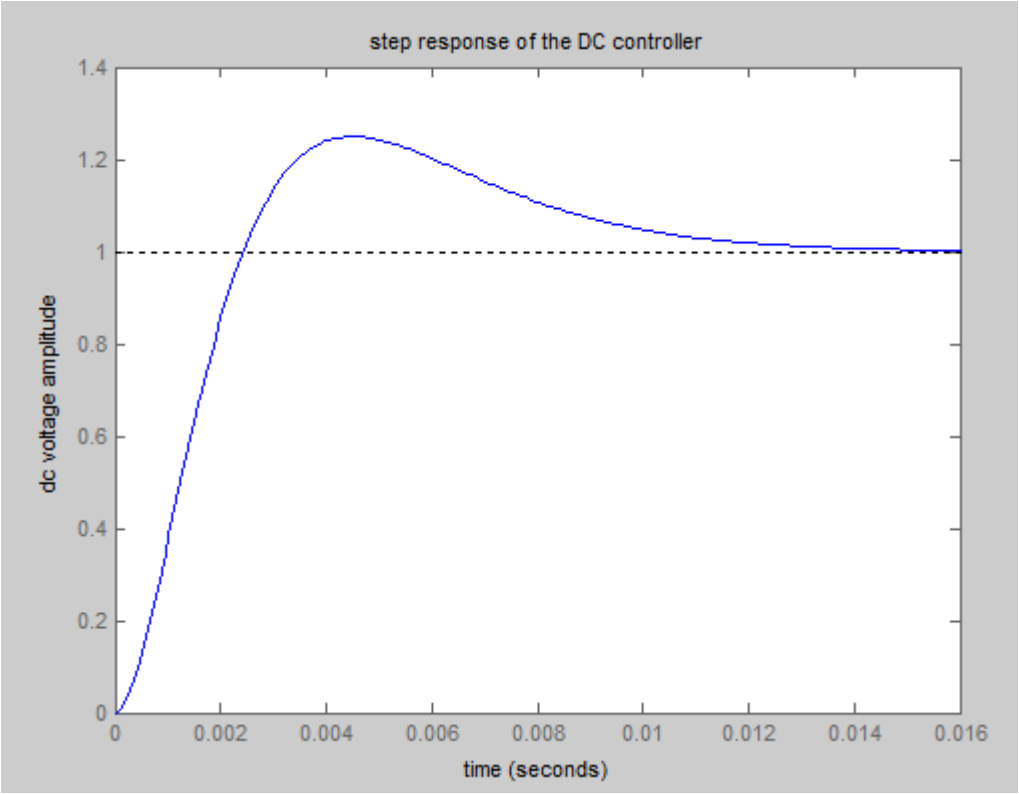

Figure 3.24:Step response of the designed DC voltage control loop

3.8.Stability model analysis

Stability analysis calculations are typically based on predefined system models. In the majority of cases the standard IEEE definitions for controllers, prime movers and other associated devices and functions are used [29]. For this case study, the synchronous generator additional parameters such as ***dynamic model type GENROU, different exciter type for instance EXST1***, and ***governor type HYGOV*** are implemented by using built in models. In DIgSILENT PowerFactory has several dynamic models to represent to a number of power system components, but its model library does not include dynamic model of FACTS devices. However, in addition to typical functions for power system analysis, DIgSILENT PowerFactory offers versatility to model new components using its programming language DIgSILENT simulation language (DSL).

DIgSILENT Simulation Language (DSL) allows programming control models of any power system element, including protection devices, as well as it permits developing other

components or routines oriented to run together with the time domain simulations. DSL language uses the modeling of block diagrams

(Transfer functions in terms of Laplace or frequency domain) in order to develop a DSL model, since this is the most common way to find information regarding control devices. There are two ways of developing a DSL model [29]:

- ✓ Through DSL simulation language code.
- ✓ Via graphical interface using predefined blocks in the program.

The basic difference between them is that in the second case, there is no direct contact with the DSL language, since the equations and language are immersed in the predefined blocks in the program library.

Composite Model is a "mask" used to administrate the models associated to a machine or a system which selects all of the models and elements wanting to be related. The Composite Model is represented by means of a Composite Frame, which is a block diagram that interrelate the distinct objects of the control system defined by the composite model. On the other hand, the composite model can be formed by a "Common Model", measuring devices and the network objects requiring control.

Common Model combines general models in the time domain or equations with a set of parameters and creates an integrated model in the time domain. The Common Model is graphically represented by means of a "Block Diagram" that includes the transfer functions and control system equations to be implemented.

Block Diagram must also be composed by "**Macros**" representing the distinct control system transfer functions. These Macros allow for definition of: input signals, output signals, parameters, internal variables, state equations, state variables, and minimum/maximum limits [39].

In the Macros, contrary to the Composite Block Diagram, the initial conditions remain undefined.

This case study consists of the dynamic model definition of the generators. In Figure 3.25, Figure 3.26, and Figure 3.27 below, shows the composite model AVR and common model

HYGOV, which is how the controller dynamics are defined in PowerFactory. These models are considered in the simulation. For instance, generator Tana Beles. We can view the difference dynamics controllers that are defined. Here AVR, and Governor.

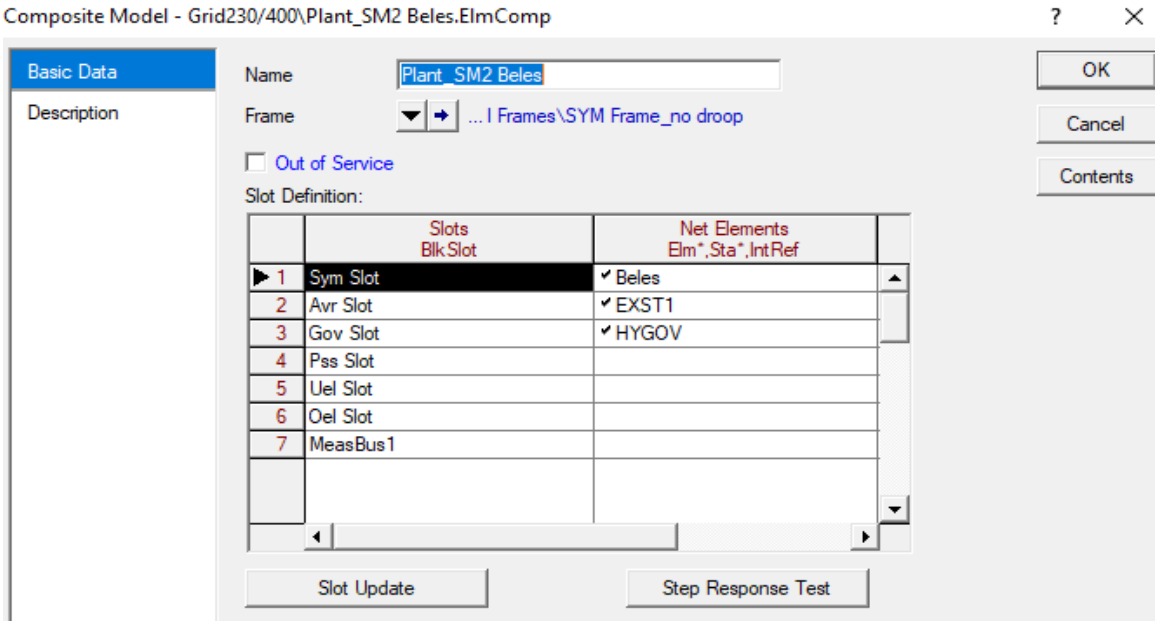

Figure 3.25: Composite model of Tana Beles

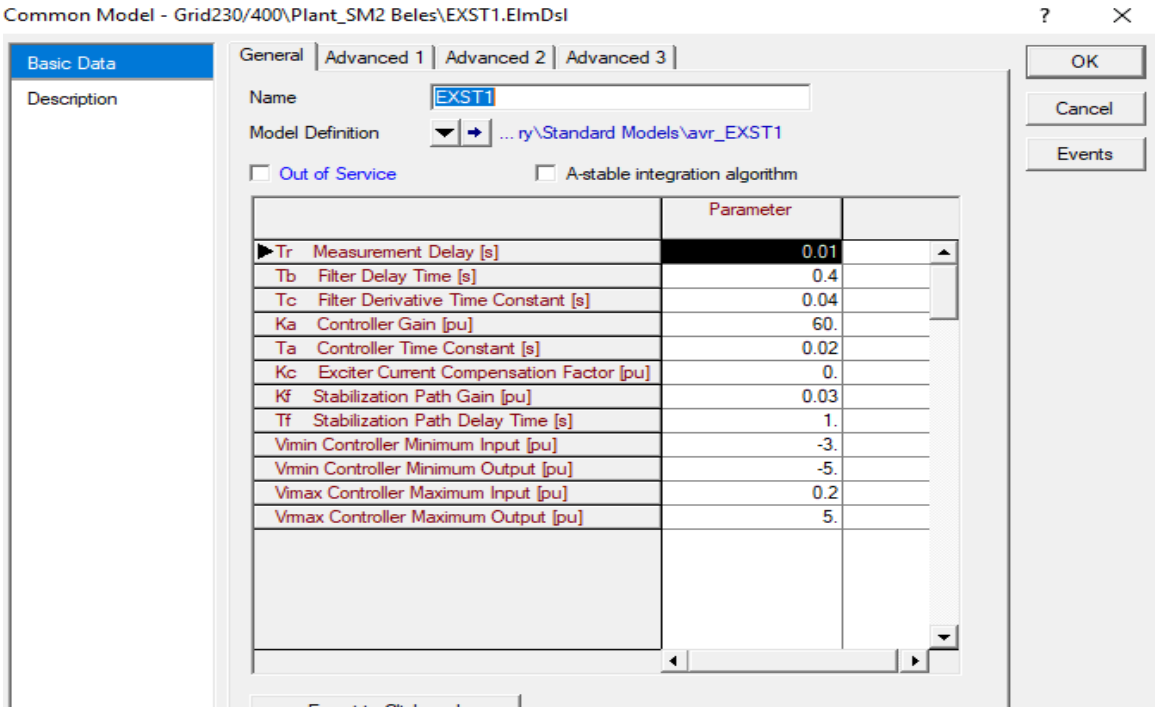

Figure 3.26: Common model Tana Beles AVR types EXST1

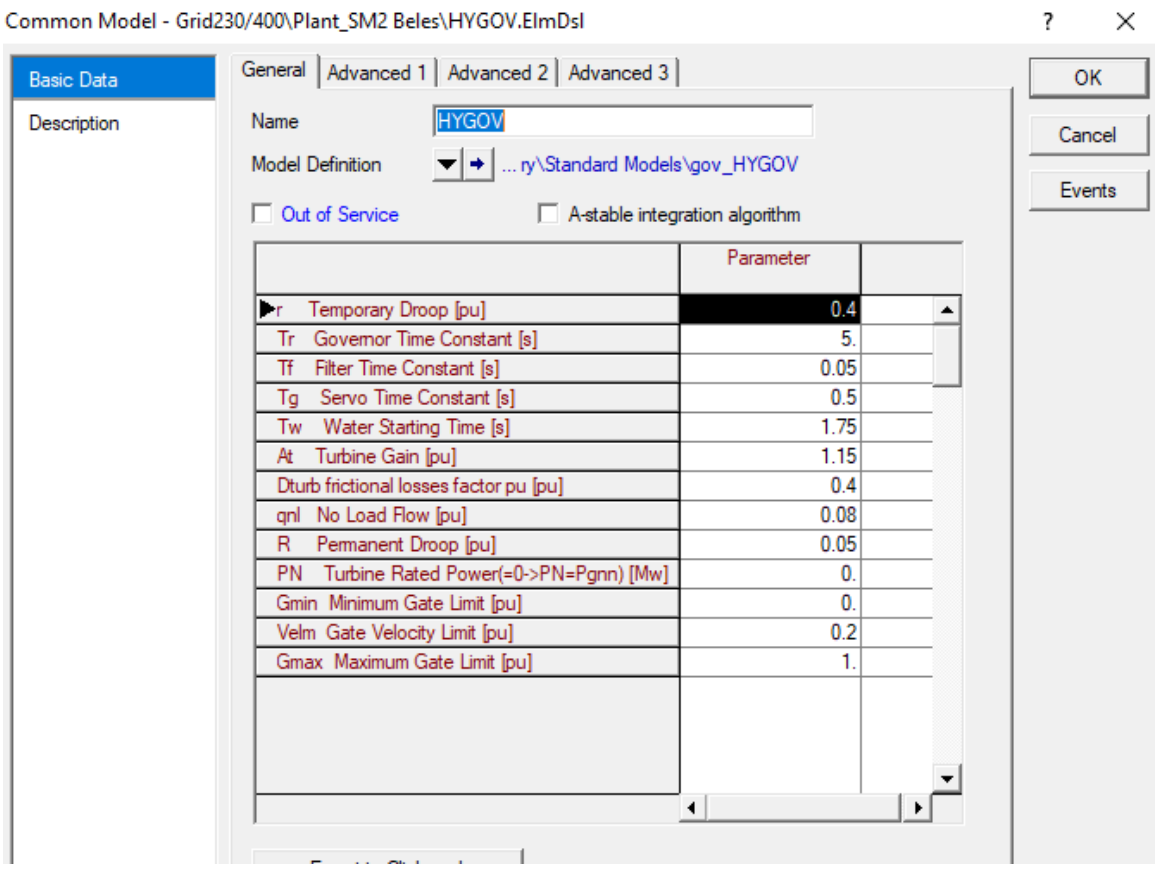

Figure 3.27: Common model Tana Beles governor type HYGOV

3.9.Dynamic model of STATCOM in DIgSILENT simulation language (DSL)

STATCOM application has two control modes such as Vdc-Q and Vac-Vdc.

Vdc-Q: Implies specifies DC-voltage and reactive power output/flow.

Vac-Vdc: Implies specifies DC-voltage and AC-voltage.

For this work Vdc-Q, control mode is selected because the parameters are mathematically determined. But in the case of Vac-Vdc controller, Vac PI-controller parameters are determined by using try and error method. There are no any mathematical manipulations to calculate Vac PI-controller parameters. The composite model frame, User defined model of inner current controller and User defined DC voltage PI-controller are shown in appendix 2.

CHAPTER FOUR

4. RESULTS AND DISCUSSION

This chapter studies, the results and discussion of Ethiopian 230 kV/400 kV transmission network. The study focuses on the optimal location of STATCOM by using PV curve method and the size is determined by load flow analysis used Newton-Raphson method. Transfer capability in steady and transient state operation is analyzed with and without the device by studying the losses of the grid and PV-curve. Transient stability simulation with and without the device was discussed, when the three-phase fault was applied. The transient stability was simulated, using RMS simulation in DIgSILENT PowerFactory version 15.1.7 software with and without STATCOM. In transient stability analysis, the basic parameters to be analyzed bus voltage, rotor angle, power oscillation damping, post settling time, and critical clearing time (CCT).

4.1.Load flow calculation

The significance of load flow calculation was to obtain the magnitude and phase angle of the bus voltage as well as the grid power in the system. The load flow calculation results are shown in appendix 2 and some selected buses shown in figure 4.1 and figure 4.3 below without and with STATCOM respectively. And also table 4.1 below shows the load flow calculation results some selected buses voltage profile without STACOM, but in the case of table 4.2 below shows the voltage profile with and without STATCOM.

As shown in the figure 4.1 below the STATCOM was inactive and the voltage profile was low. But in figure 4.3 the STATCOM was active the voltage profile was enhanced.

The size of STATCOM was determined based on the load flow calculation as shown figure 4.2. Table 4.1 shown some buses stead state voltage profile, which is the more illustrative of the system. From table 4.1 below displays load flow calculation simulation result demonstrate buses Semera and Combolcha had the lowest voltage magnitude of 0.937 p.u and 0.936 p.u, respectively. As a result, the lowest bus is Semera. The next step was to

simulate and plot the P-V curves for the weakest bus voltage. The result shown in figure 4.2 below, which is more clear the load flow result.

Table 4.1: Steady state Voltage profile without STATCOM

Bus Name	Voltage magnitude (p.u)	Bus Name	Voltage magnitude (p.u)
Bahr Dar	0.987	Sululta	0.979
Azezo	0.967	Alaba	0.952
Metema	0.954	Sebeta I	0.973
Sudan	0.948	Welayta sodo	0.994
Humera	0.968	Hurso	0.983
Mekele	0.973	Kaliti I	0.987
Combolcha	**0.937**	Legetafo	0.972
Semera	**0.936**	Alemata	0.972

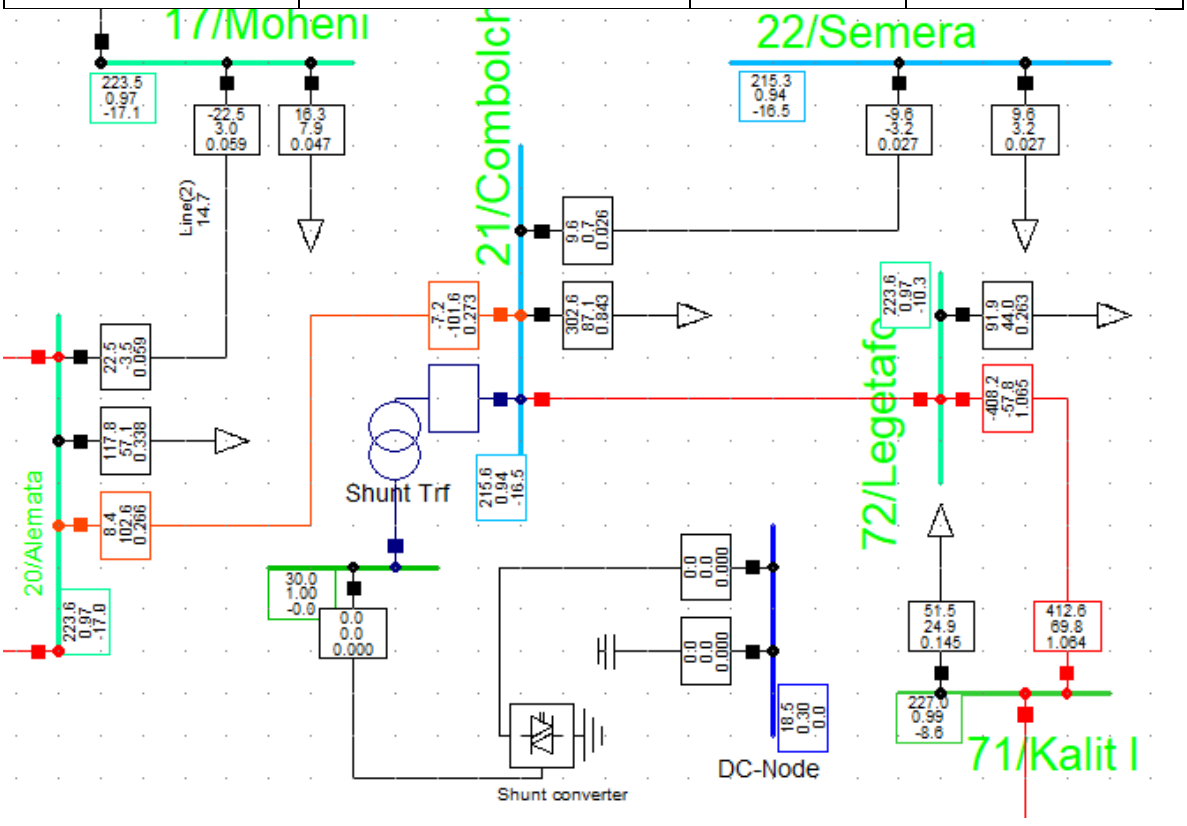

Figure 4.1: Load flow calculation without STATCOM at the point of connection and near to the point of connection.

4.2.Simulation result of STATCOM Placement using P-V curve

P-V curve was done in DIgSILENT PowerFactory software using DPL script, which was developed in the software and the result is shown in figure 4.2. It realized that bus Combolcha and Semera were the weakest bus and had almost same point of collapse. However, Combolcha has large load, due to this reason. Combolcha was the optimal placement in 230 kV and 400 kV Ethiopian transmission network. So that the PV-curve method has been used to successfully identify the weakest bus in the network to place the STATCOM. Thus, STATCOM was installed at Combolcha bus.

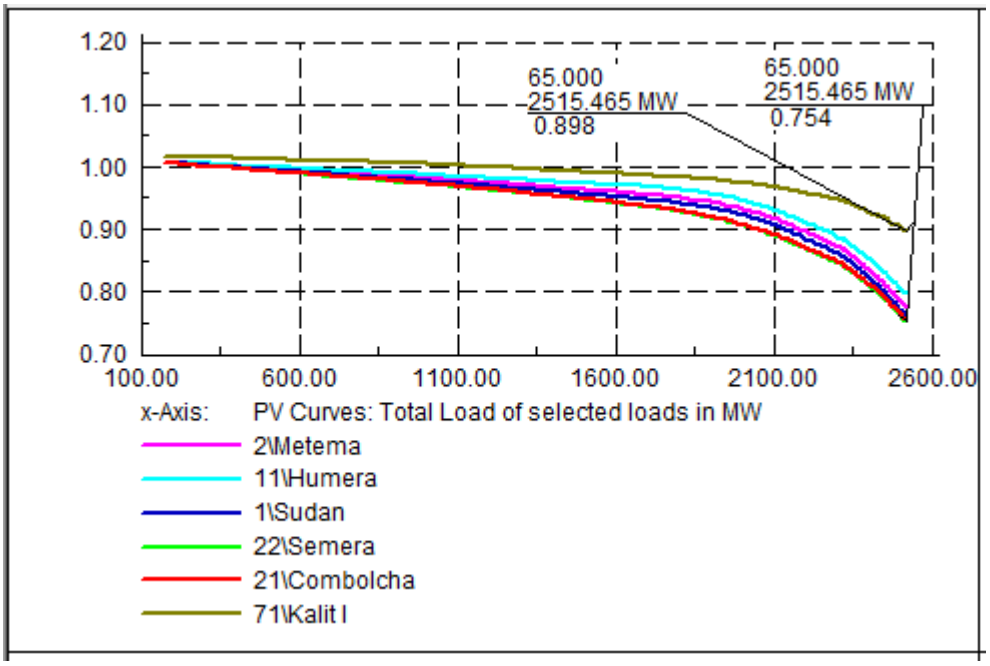

Figure 4.2: PV-curve without STATCOM

The load flow calculation results of some selected buses voltage profile are shown in table 4.2 below with and without STATCOM.

As shown the table 4.2 above the improvement was greatest at the point where the STATCOM was installed. The bus voltages at Combolcha and Semera have improved from 0.937 p.u and 0.936 p.u to 1 p.u, and 0.999 p.u respectively. Buses where near to the point of connection have been better improvement. Legetafo and Alemata have been enhanced next to Combolcha and Semera. However, the buses far from the point of connection, there

had a small significance effect for the voltage profile. In the table 4.2 illustrates, bus Alaba, Sebeta I, Welayta sodo, and Hurso have been a little improvement. Because they are far from the point of connection.

Table 4.2: Comparison of voltage profile

Bus Name	Without STATCOM (p.u)	With STATCOM (p.u)	Improved (p.u)
Bahr Dar II	0.987	0.992	0.005
Azezo	0.967	0.973	0.006
Metema	*0.954*	0.962	0.008
Sudan	0.948	0.953	0.005
Humera	0.968	0.974	0.006
Mekele	0.973	0.982	0.009
Combolcha	**0.937**	**1.00**	0.064
Semera	**0.936**	**0.999**	0.063
Sululta	0.977	0.983	0.006
Alaba	0.952	0.953	0.001
Sebeta I	0.973	0.975	0.002
Welayta sodo	0.994	0.995	0.001
Hurso	0.983	0.984	0.001
Kaliti I	0.987	0.995	0.008
Legetafo	0.972	0.99	0.018
Alemata	0.972	0.984	0.012

Semera has better improvement than Alemata even though bus Semera is further away. This is due to the impedance value. The impedance value between Combolcha and Semera are 0.03503 p.u, while between Combolcha and Alemata are 0.1053 p.u.

The same is true for other buses. Those results shown in appendix 2, STATCOM could be influenced by the electrical distance, which is also a function of line impedance.

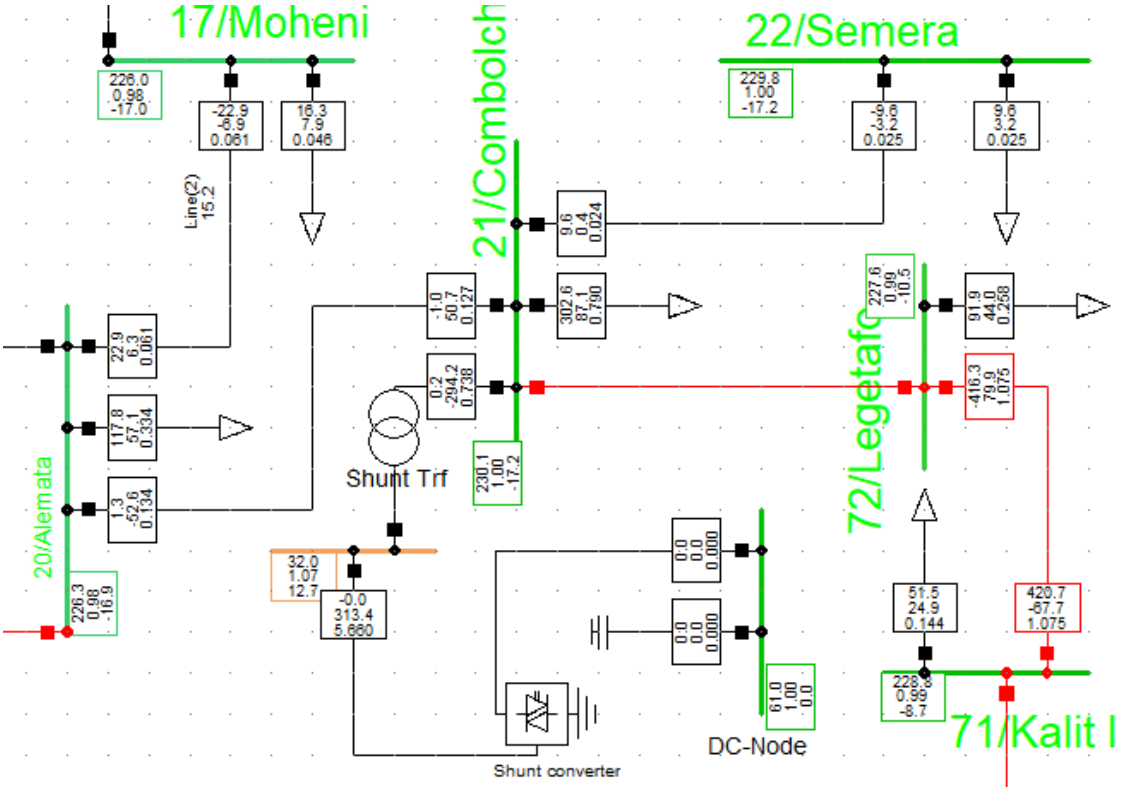

Figure 4.3: Load flow calculation with STATCOM at the point of connection and near to the point of connection.

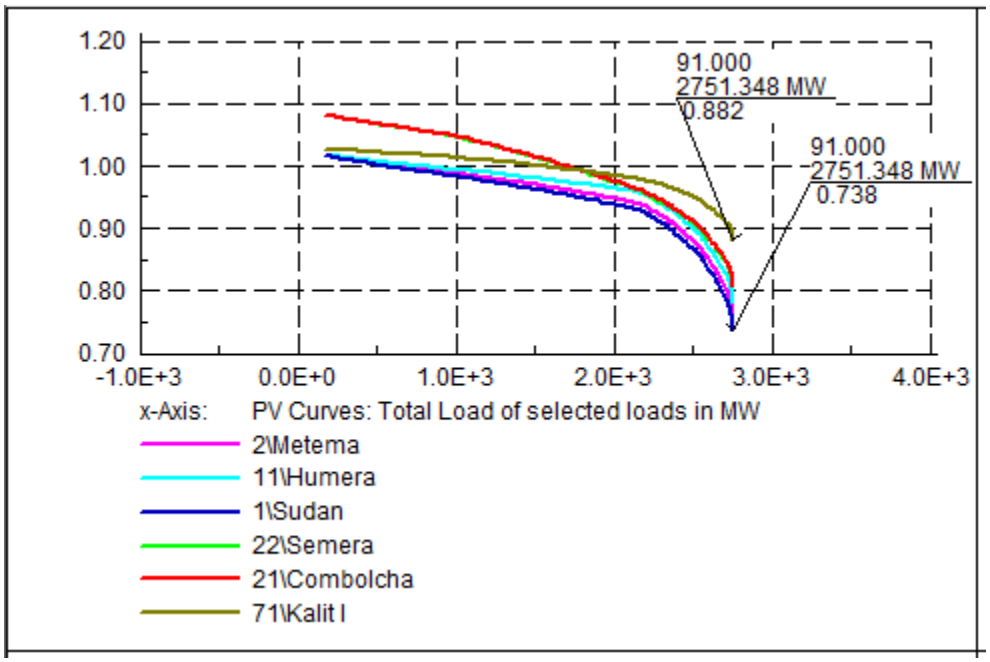

Figure 4.4: PV-curve with STATCOM

The point of collapse of figure 4.2 above compare to with figure 4.4 was poor. From figure 4.2 and 4.4 displays the active power was increased from 2515.465 MW to 2751.348 MW. Hence, the available transfer capability was increased to 235.883 MW (9.377%). Which implies that, the performance of the system increased by 235.883 MW power. The power system stability and security were maintained by this amount of power.

4.3.Available Transfer capability

From the load flow result shown table 4.3 A) below the active and reactive power loss were reduced to 2.04 MW and 225.26 MVAr in percentage 2.067% and 84.31% respectively in table 4.3 A), when STATCOM is connected. In table 4.3 B) below in transient stability three phase fault at Gilgel gibe III bus terminal was occurred at fault clearing time was 260.8 ms The real and reactive power losses are reduced to 25.8 MW (27.48%) and 160.64 MVAr (79.84%) respectively, when STATCOM is connected at the weakest bus. Consequently, the transfer capability was increased.

Table 4.3: Grid summery load flow results

A) At steady stability

Components		Without STATCOM	With STATCOM
Generation	Active power (MW)	2983.33	2981.28
	Reactive power (MVAr)	1364.92	1055.27
Load	Active power (MW)	2884.17	2884.17
	Reactive power (MVAr)	1116.73	1116.73
Grid Loss	Active power (MW)	99.16	97.11
	Reactive power (MVAr)	267.17	41.91

a) At transient stability

Components		Without STATCOM	With STATCOM
Generation	Active power (MW)	3781.35	2906.67
	Reactive power (MVAr)	1617.16	1039.30
Load	Active power (MW)	368747	2838.65
	Reactive power (MVAr)	1440.37	1099.05
Grid Loss	Active power (MW)	93.88	68.08
	Reactive power (MVAr)	201.18	40.54

4.4.Simulation and analysis of transient stability

Transient stability simulations were carried out in RMS tool in DISILENT PowerFactory software. The simulations have been done without and with STATCOM. The results were recorded. There are different parameters in transient stability assessment in this thesis. The parameters are: bus voltage magnitude, generator apparent power (MVA) and rotor angle (swing curve) shown below in the subsequent figures. Three phase fault were considered at the terminal of the generator at Gilgel gibe III and Kaliti I. The response of the network was considered to evaluate transient stability and power oscillation damping capability of STATCOM.

Transient stability is the main measure of power system stability. Due to this point of view the analysis and evaluation of transient stability is necessary. To simulate and analysis transient stability with three phase fault was occurred at 100 ms and at different fault clearing time. The fault was cleared by the removal of the fault. The fault impedance was (0+j0) Ω.

- Scenario one: fault at Gilgel gibe III bus terminal (the largest generation)
- Scenario two: fault at Kaliti (relative which links most of the system)

4.4.1. Three phase fault at Gilgel gibe III bus terminal

The response of the network, when three phase fault was occurred at the terminal of Gilgel gibe III generator. The bus voltage was dropped during the fault, but recover quickly to

their steady state value. Figure 4.5 below shows the voltage magnitude response with and without STATCOM at Gilgel gibe III . The voltage profile at bus terminal of Gilgel gibe III generator during the fault was zero p.u, illustrated in figure 4.5. At the fault clearing time was 260.5 ms. As the result, the generator did not generate electrical power. The oscillations rose to 1.15 p.u after the fault clearance without STATCOM. However, with STATCOM the oscillation reduce to 1.09 p.u.

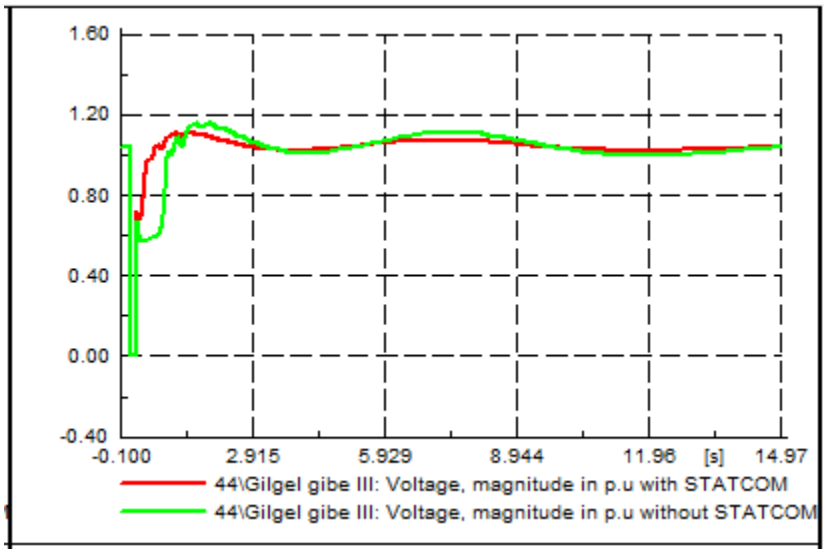

Figure 4.5: Bus voltage response of the Gilgel gibe III generator with and without STATCOM

The other voltage profile also dropped to their minimum allowable value of 0.95 p.u until the fault is cleared. When the fault is sustained for longer time, the network becomes collapse. Figure 4.6 below shows the voltage response with and without STATCOM

Figure 4.6 A) below shows the bus voltage magnitude response with and without STATCOM fault at Gilgel gibe III bus terminal. When bus voltage magnitude at Sudan, Metema, Azezo, and Bahr Dar II dropped to 0.279 p.u, 0.282 p.u, 0.285 p.u, and 0.279 p.u respectively without STATCOM, but when STATCOM was connected the voltage drop was enhanced to 0.571 p.u, 0.546 p.u, 0.55 p.u, and 0.545 p.u during the fault duration. As shown in figure 4.6 A), bus voltage magnitude to regain with their steady stat value with the device was best. STATCOM was in operation the bus voltage response are damped to steady state operation around 9 second at voltage magnitude of Bahr dar, Azezo, Metema and Sudan were 0.992 p.u, 0.973 p.u, 0.962 p.u, and 0.953 p.u respectively.

Figure 4.6 B) below shows the bus voltage magnitude response with and without STATCOM fault at Gilgel gibe III bus terminal. Which displays the bus voltage magnitude at Alemata, Combolcha, Humera, and Geffersa dropped to 0.326 p.u, 0.123 p.u, 0.308 p.u and 0.015 p.u respectively without STATCOM, but when STATCOM was connected the voltage drop was enhanced to 0..6 p.u, 0.579 p.u, 0.565 p.u and 0.381 p.u during the fault duration. STATCOM did not in operation the oscillations were high.

STATCOM was in operation the bus voltage response are damped to steady state operation around 10 second at voltage magnitude of Alemata, Combolcha, Humera, and Geffersa were 0.984 p.u, 1 p.u, 0.974 p.u, and 0.998 p.u respectively.

In figure 4.6 C) below, the bus voltage at Alaba, Gelan, and Koka dropped to 0.269 p.u, 0.11 p.u, and 0.16 p.u respectively without STATCOM, but when STATCOM was connected the voltage drop was enhanced to 0.512 p.u, 0.116 p.u, and 0.18 p.u during the fault duration respectively.

In the case of Welayta sodo during the fault duration almost the same with and without STATCOM. Koka, Alaba, welayta sodo, and Gelan the bus voltage response are damped to steady state operation around 9.5 second at voltage magnitude of 1.012 p.u, 0.953 p.u, and 1.01 p.u respectively. Hence, when the device connected, it regains its steady state operation is better, rather without STATCOM.

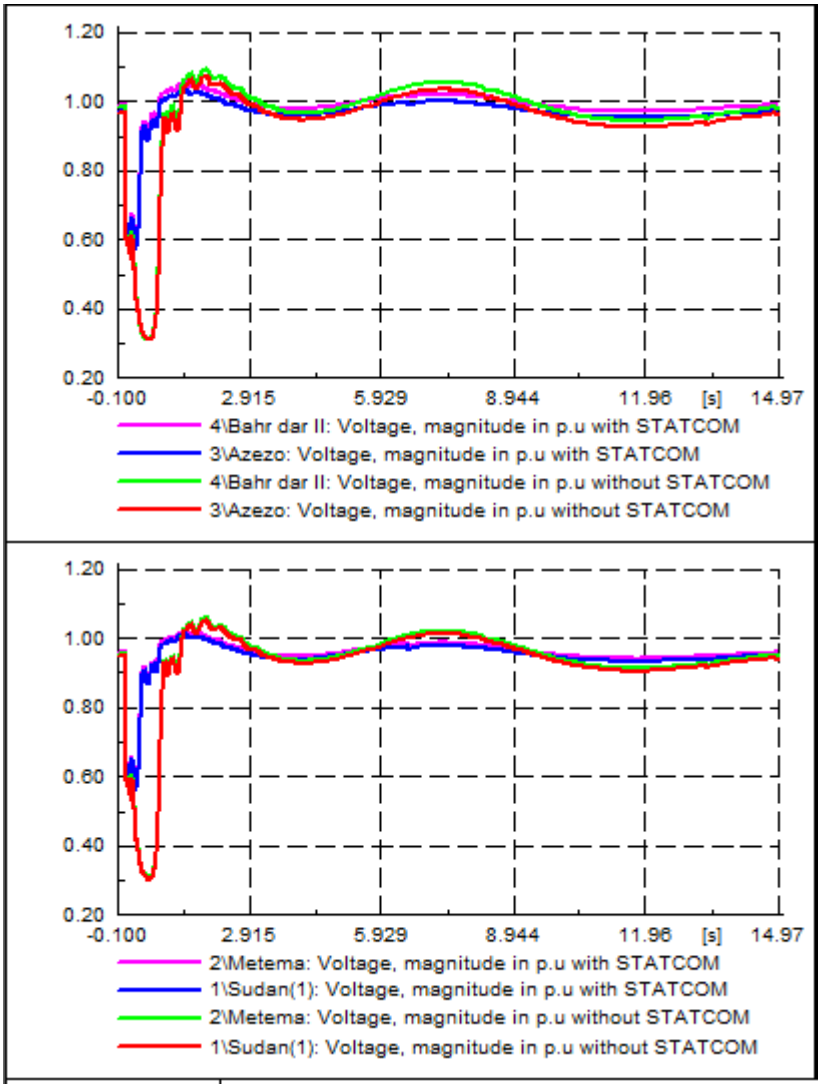

A) Bus at Bahr Dar II, Azezo, Metema, and Sudan with and without STACOM.

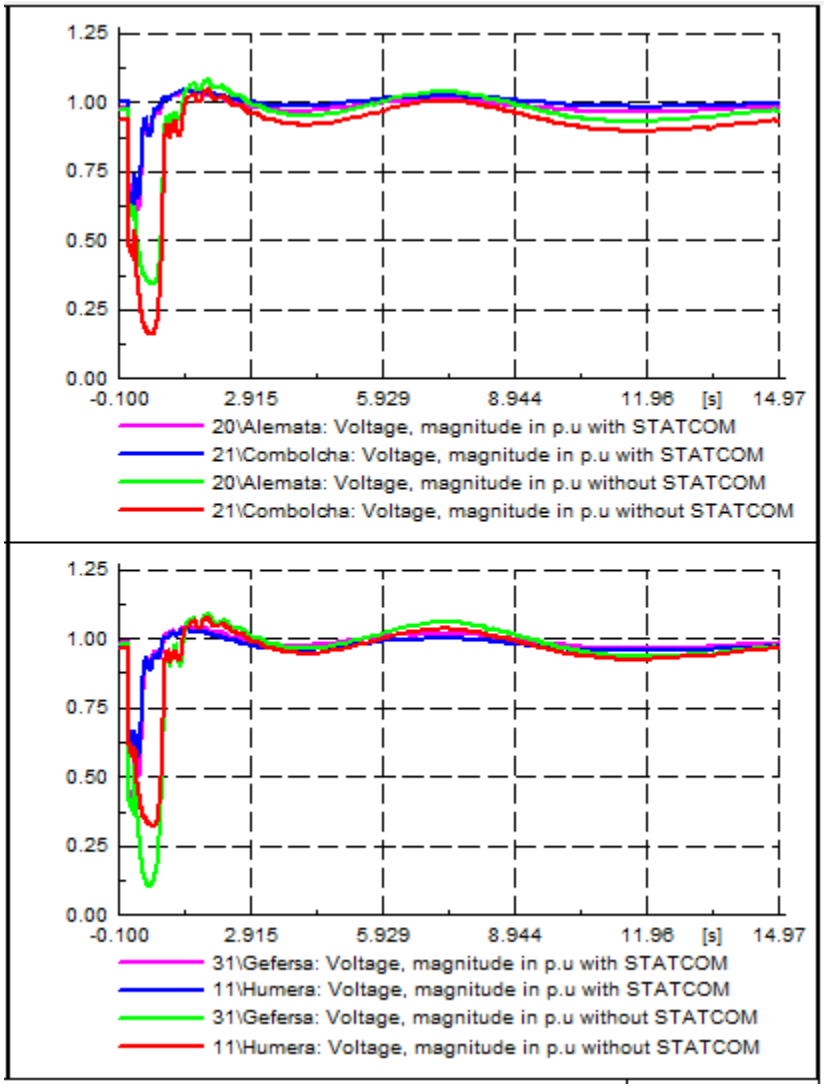

B) Bus at Alemata, Combolcha, Humera, and Geffersa with and without the STACOM.

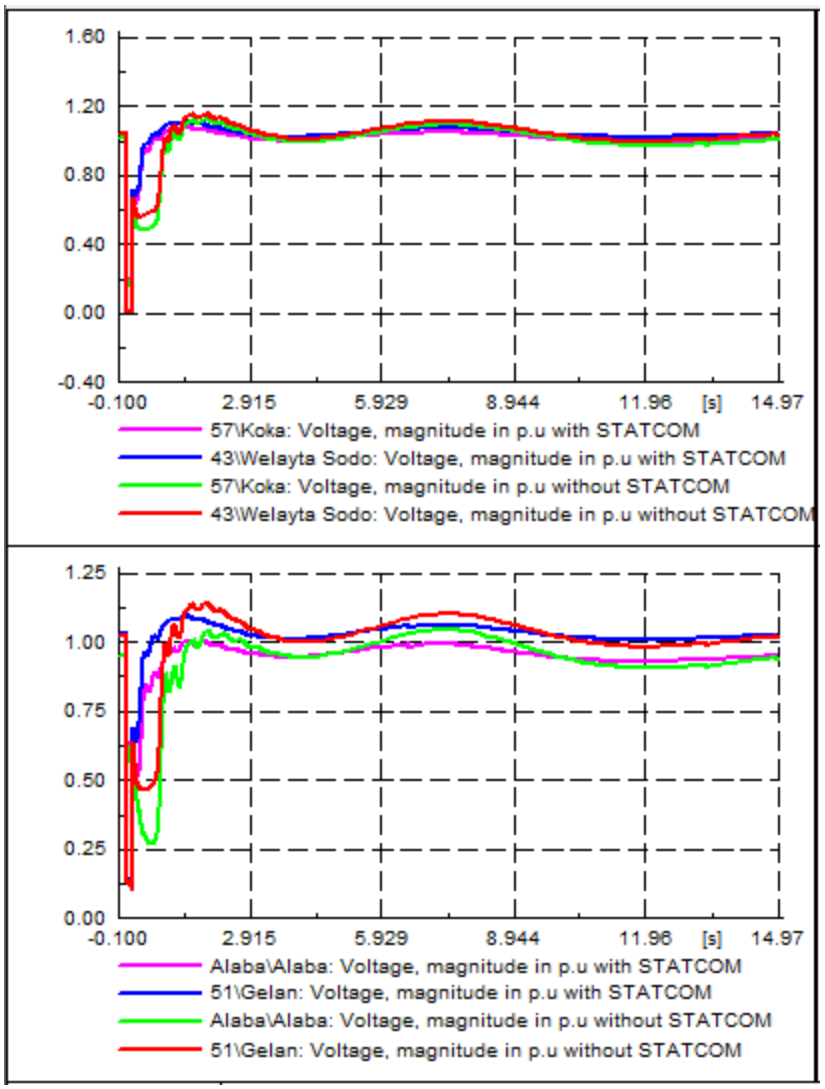

C) Bus at Alaba, Welayta sodo, Gelan, and Koka with and without the STACOM.

Figure 4.6: A-C, bus voltage magnitude in p.u with and without STACOM three phase fault at Gilgel gibe III bus terminal.

The rotor angle response of generators shown figure 4.7 below, which illustrates the rotor angle response simulation result with and without the STATCOM. The fault clearing time was 260.5 ms. The critical clearing time the major index of transient stability, which is determined by varying the fault clearing time. Initially fault clearing time chosen 200 ms and by varying this time and simulate until the critical clearing time was found. The process is shown in table 4.4 below, which determine the critical clearing time without STATCOM. And also the procedure for CCT determination with STATCOM is the same. The process is proceeding before the instability occurred. The network critical clearing time was 260.5 ms without STATCOM. However, when the STATCOM was in operation the critical

clearing time was increased to 288 ms. In the figure 4.7 the rotor angles retains accelerating and go out of synchronism. But when connected STATCOM, the response start decreasing.

Determine CCT by varying fault clearing time shown in table 4.4.

Table 4.4: Determine CCT by varying fault clearing time without STATCOM

Fault clearing time in (ms)	Stability of the network	Fault clearing time in (ms)	Stability of the network
200	Stable	250	Stable
220	Stable	260	Stable
400	Instable	267	Instable
230	Stable	260.9	Instable
240	Stable	260.8	Instable
280	Instable	***260.5***	***Stable***
270	Instable	260.7	Instable

Figure 4.7 shows, the rotor angle response of generators from A-C, when three phase fault occurred at Gilgel gibe III bus terminal with and without STATCOM.

From figure 4.7 A) below displays, the rotor angle response of generator at Beles, Tekeze, Fincha, and Tes Abay II with and without the device. Without the device the oscillations were high, but with the device the oscillations relatively damped. It displays that with the device the rotor angle response of Beles, Tekeze, Fincha, and Tes Abay II regain their steady state operation at around 2.84 second, 2.9 second, 3.2 second, and 4.2 second respectively.

From figure 4.7 B) below displays, the rotor angle response of generator at Gilgel gibe I, Gilgel gibe II, Meka wokena, and Amerti nesh with and without the device. Without the device the oscillations were high, but with the device the oscillations relatively damped. It shows that with the device the rotor angle response of Gilgel gibe I, Gilgel gibe II, Meka wokena, and Amerti nesh regain their steady state operation at around 3.6 second, 37 second, 2.9 second, and 2.92 second respectively.

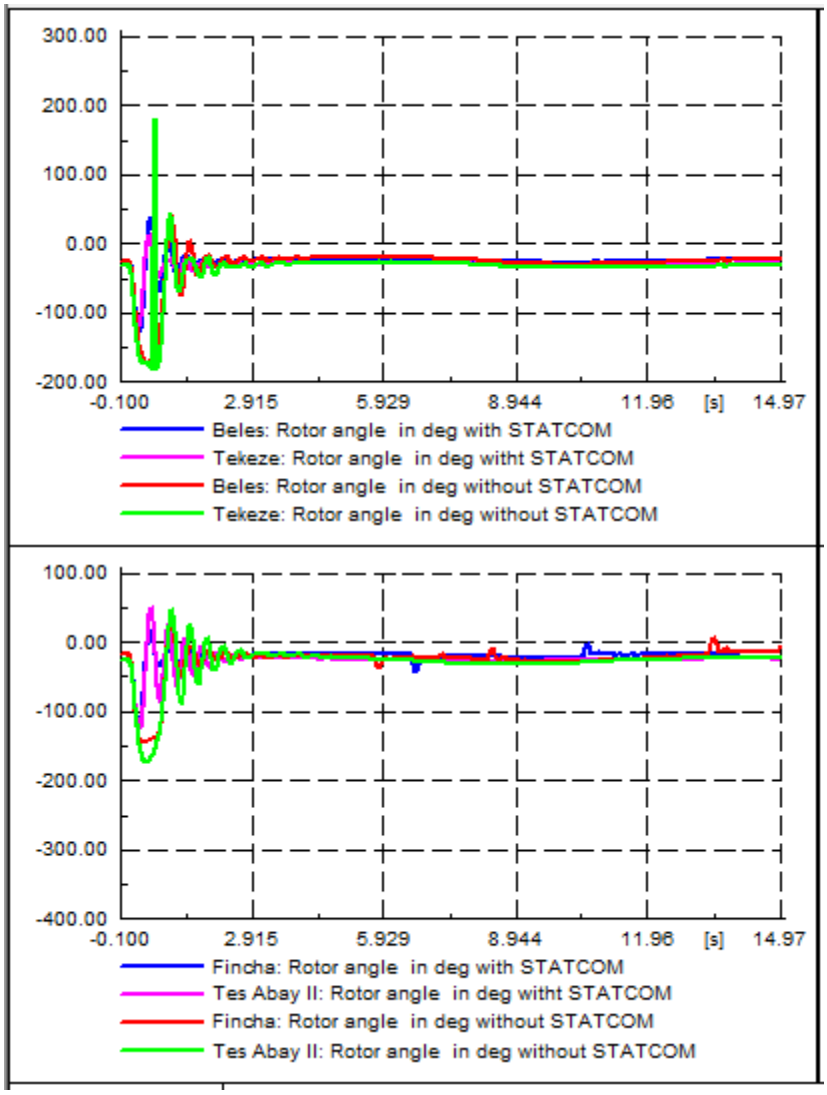

A) Rotor angle response of generator Beles, Tekeze, Tes Abay II, and Fincha

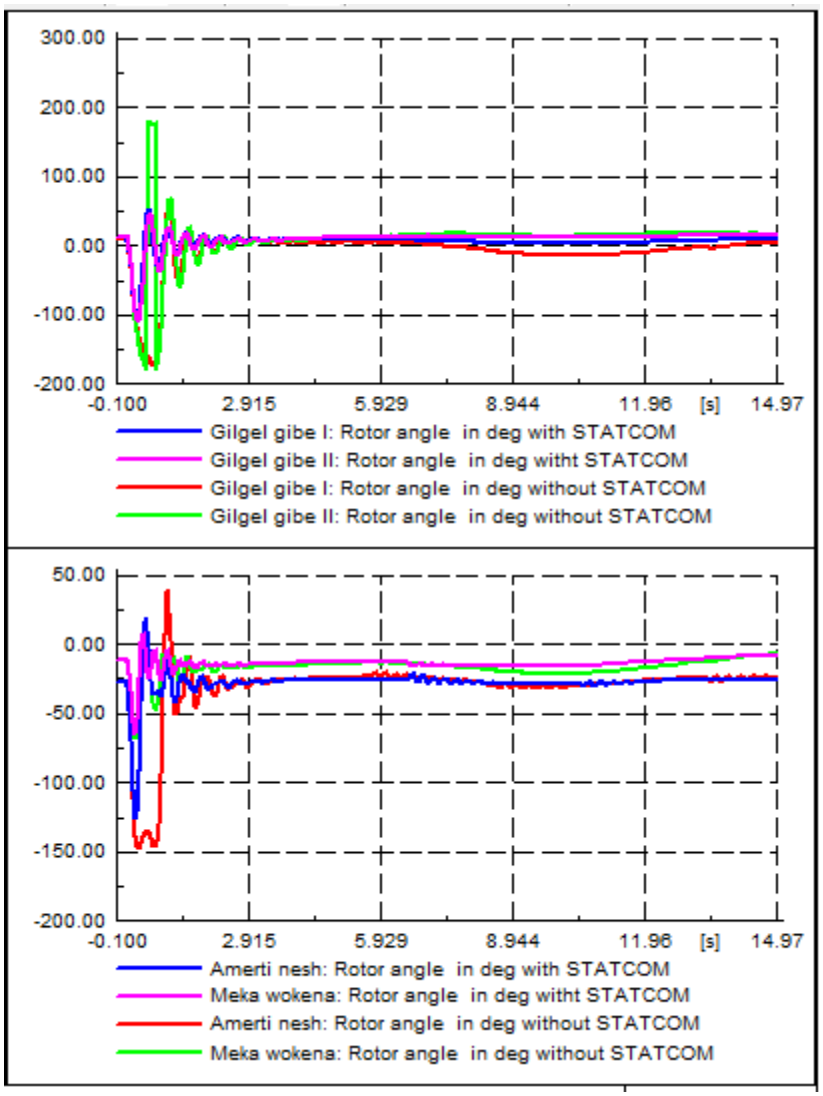

B) Rotor angle response of Gilgel gibe I, Gilgel gibe II, Amerti nesh, and Meka wokena

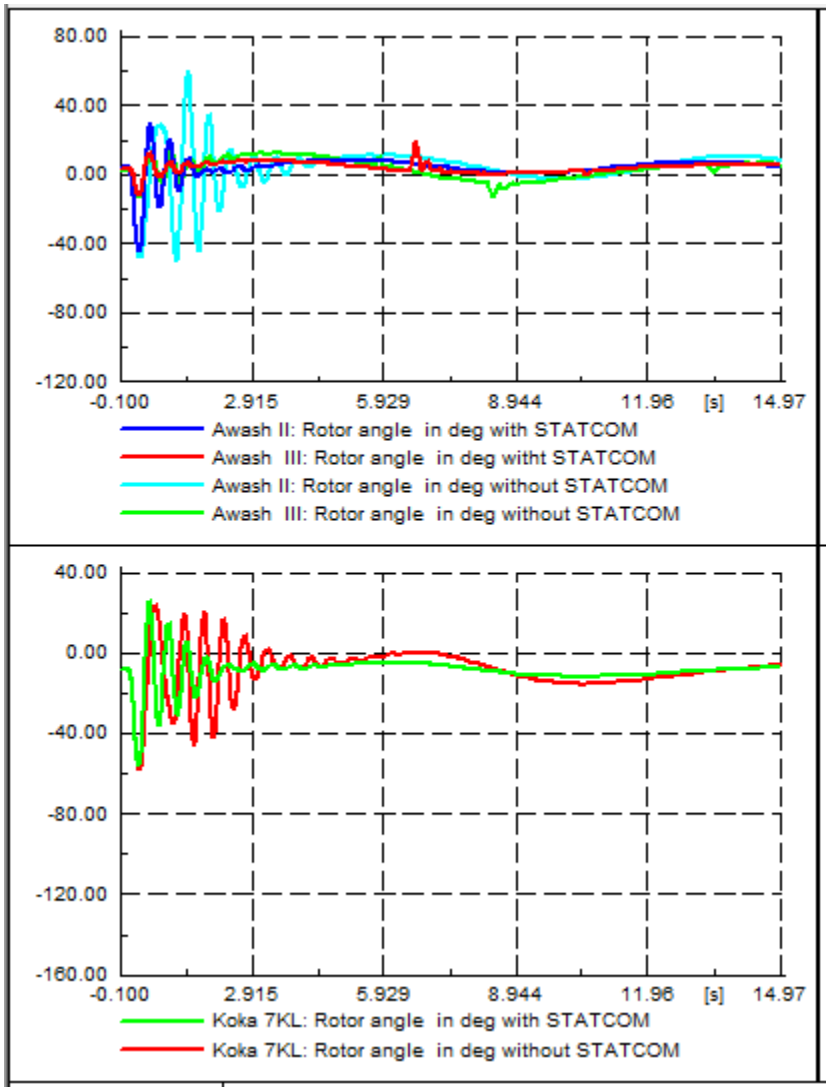

C) Rotor angle response of Koka 7KL, Awash II, and Awash III

Figure 4.7: Rotor angle response of generators from A-C three phase fault at Gilgel gibe III bus terminal with and without STATCOM

From figure 4.7 C) above displays, the rotor angle response of generator at Koka 7KL, Awash II, and Awash III with and without the device. Without the device the oscillations were high, but with the device the oscillations relatively damped. It shows that with the device the rotor angle response of Koka 7KL, Awash II, and Awash regain their steady state operation at around 9.5 second, 11.3 second, and 10.5 second respectively.

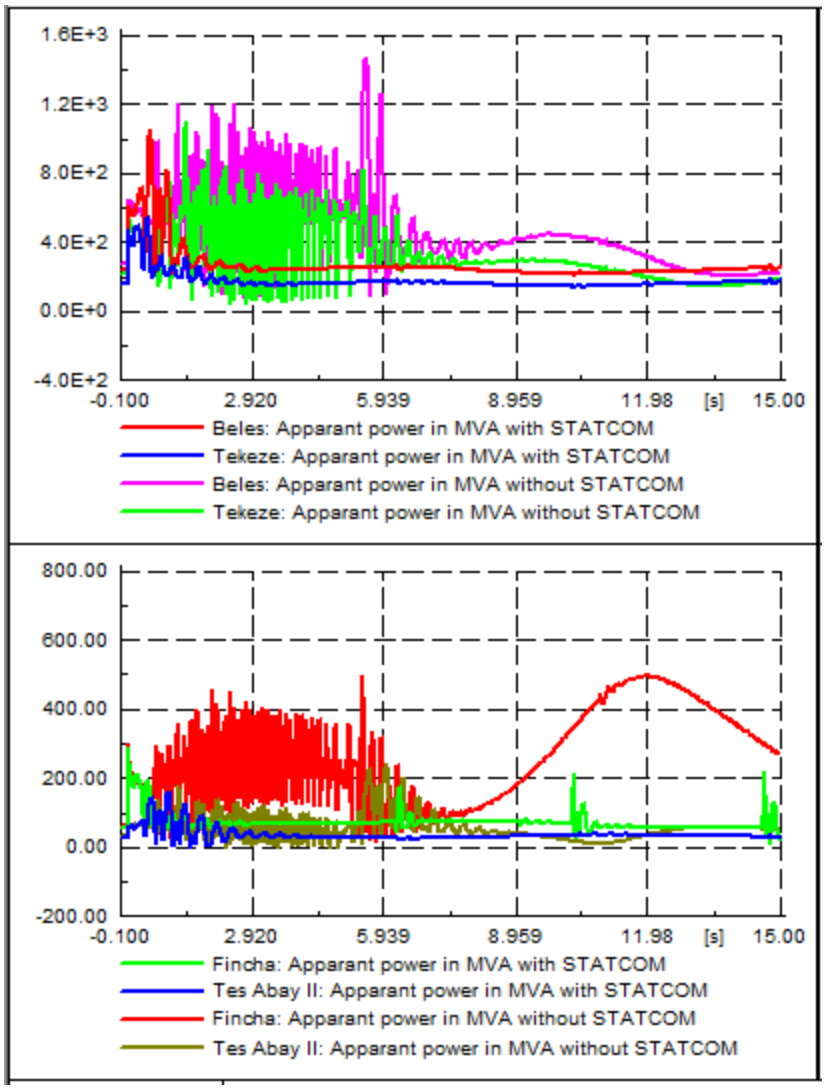

A) Apparent power of generators Beles, Tekeze, Tes Abay II, and Fincha

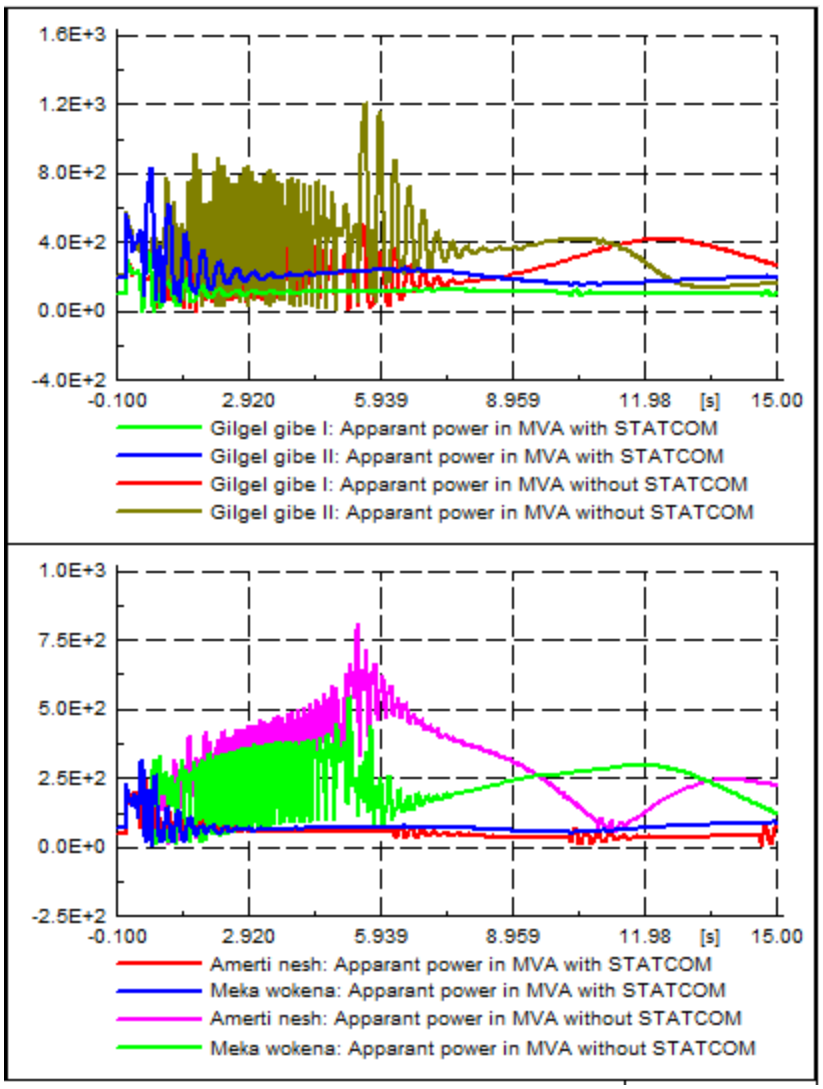

B) Apparent power at Gilgel gibe I, Gilgel gibe II, Amerti nesh, and Meka wokena

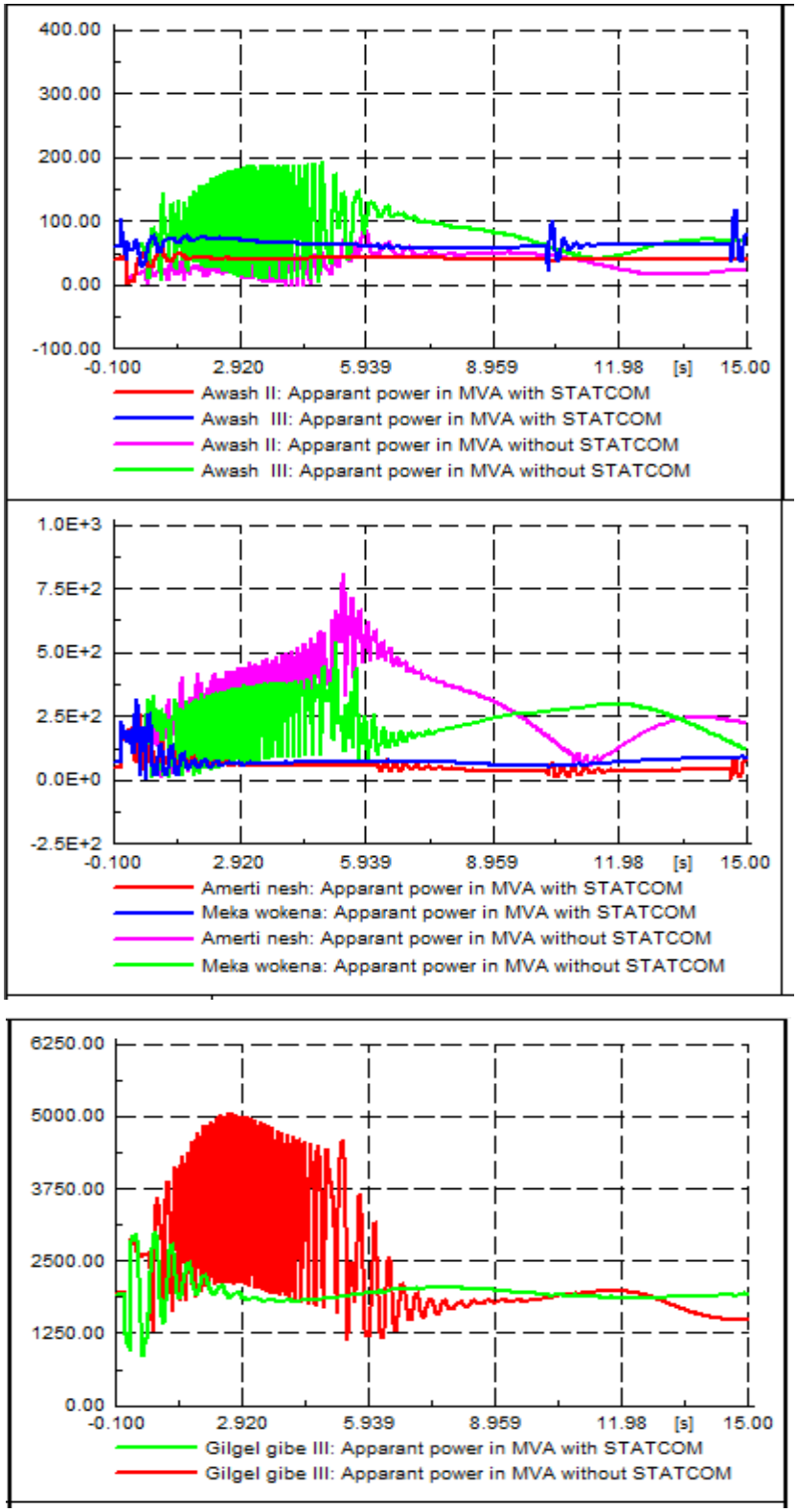

A) Apparent power at Koka 7KL, Awash II, Awash II, Gilgel gibe III

Figure 4.8: Apparent power response of generators A-C fault at Gilgel gibe III bus terminal with and without STATCOM.

Apparent power response of synchronous generators is shown in figure 4.8 above with and without STATCOM. From the figure 4.8 A) above the power oscillation damping after fault clearing time 260.8 ms was instable and high with the simulation time 15 second without the STATCOM. However, when STATCOM was in operation the power oscillations are damped to steady state operation. After the fault removed the steady state operation at Tana Beles, Tekeze, Fincha, and Tes Abay II were around 2.20 second, 2.50 second, 2.60 second, and 3.99 second respectively. See figure 4.8 A) Tana Beles regains its steady state operation at 2.20 second with 214 MVA. Thus, Tana Beles had best post settling time in figure 4.8 A). Which means apparent power response was best.

From the figure 4.8 B) above displays the apparent power response, the power oscillation after fault clearing time 260.8 ms was undamped without STATCOM. And also Gilgel gibe I, Gilgel gibe II, and Meka wokena without STATCOM the power oscillation rose to maximum of 450 MVA, 900 MVA, 375 MVA, and 370 MVA at a time of around 968 ms, 1.8 second, 191.6 and 396 ms respectively. However, when STATCOM was in operation the power oscillations are damped to steady state operation. When fault was cleared the systems regain their steady state operation. From figure 4.8 B) observed that Gilgel gibe I, Gilgel gibe II, Amerti nesh, and Meka wokena regain their stead state value at 296 ms, 394 ms, 291.6 ms, and 298 ms with the corresponding apparent power value at 108 MVA, 210 MVA, 45 MVA, and 70 MVA respectively. Amerti nesh had best apparent power response in figure 4.8 B).

From the figure 4.8 C) the power oscillation damping after fault clearing time 260.8 ms was instable and go beyond the simulation time 10 second without the STATCOM. However, when STATCOM was in operation the power oscillations were damped to steady state operation as shown figure 4.8 C). In figure 4.8 C) observed that Koka, Awash II, Awash III, and Gilgel gibe III had been regain their steady state value at 498 ms, 494ms , 292 ms, and 592 ms respectively.

Gilgel gibe III was poor to regain their steady state operation. Because the post settling time was 592 ms, which is greatest from the other generators.

4.4.2. Three phase fault at Kaliti I

The three-phase fault was happen at Kaliti I bus. The voltage magnitude, rotor angle, and apparent power response with and without the device were plotted in the following subsequent figures.

Figure 4.9 and 4.10 below shows the voltage response with and without STACOM three phase fault at Kaliti I. Which implies that, the voltage response oscillations high, when the faults was cleared at 367.8 ms without STATCOM. However, when STATCOM was in operation, the oscillations were damped to steady state operation.

Figure 4.9 shows the voltage response at Kaliti I with and without STATCOM.
The bus voltage was dropped to zero p.u during the fault, but recovers quickly to their steady state value, when the fault was removed as observed in figure 4.9 below. It regain to steady state operation around 10 second with the voltage magnitude of 0.987 p.u with the STATCOM. With the device, it can be observed that after fault clearance, oscillations of rose to a peak value of 1.062 p.u, while without the device the peak value was around 1.099 p.u.

In figure 4.10 A) below shows the bus voltage magnitude at Alemata, Bahr Dar II, Combolcha, and Geffersa dropped to 0.321 p.u, 0.279 p.u, 0.135 p.u, and 0.096 p.u respectively without STATCOM, but when STATCOM was connected the voltage drop was enhanced to 0.365 p.u, 0.338 p.u, 0.366 p.u, and 0.109 p.u during the fault duration.
In figure 4.10 B) below shows the bus voltage magnitude at Metema, Sudan, Azezo, and Humera dropped to 0.28 p.u, 0.277 p.u, 0.283 p.u, and 0.301 p.u respectively without STATCOM, but when STATCOM was connected the voltage drop was improved to 0.337 p.u, 0.335 p.u, 0.338 p.u, and 0.356 p.u during the fault. Hence, the device was in operation the performance of the system was increased.

In figure 4.10 C) below the bus voltage at **Gilgel gibe old**, **Gilgel gibe I**, **Gilgel gibe II**, and Sebeta II reduced to 0.268 p.u, 0.267 p.u, 0.242 p.u and 0.302 p.u respectively without STATCOM, but when STATCOM was connected the voltage drop was improved to 0.345 p.u, 0.346 p.u, 0.322 p.u and 0.378 p.u during fault duration. This implies STATCOM has best voltage improvement capability.

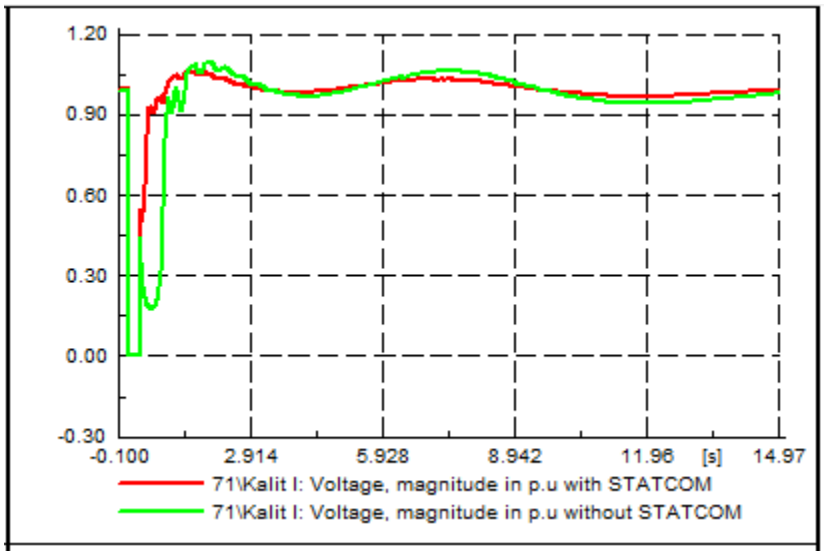

Figure 4.9: Kaliti I bus voltage response with and without STATCOM fault at Kaliti I

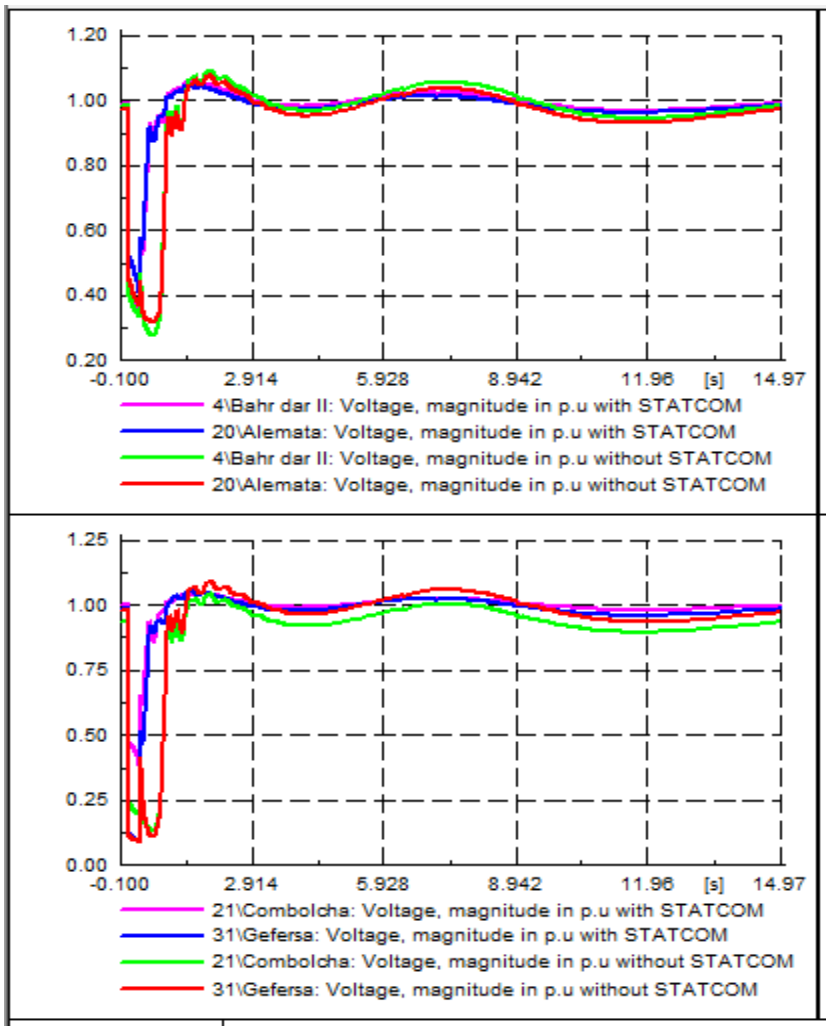

A) Bus voltage response at Bahr dar II, Alemata, Combolcha, and Geffersa

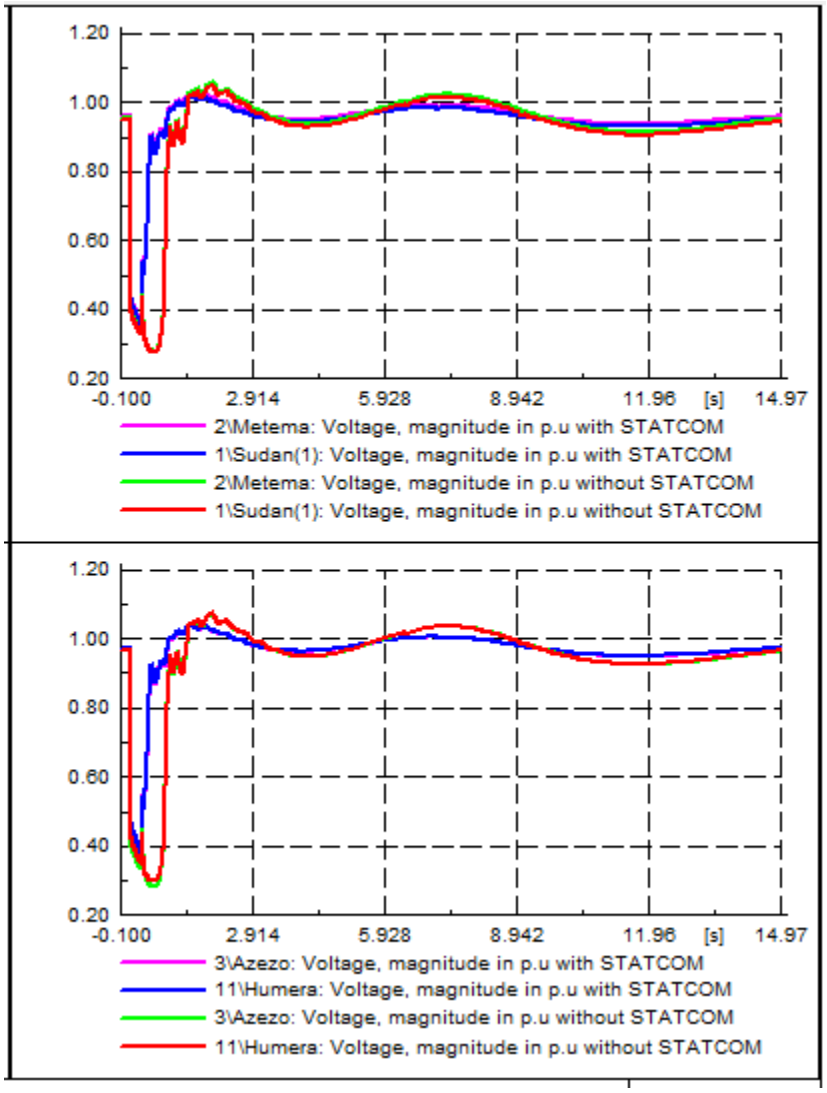

B) Bus voltage response at Humera, Azezo, Metema, and Sudan

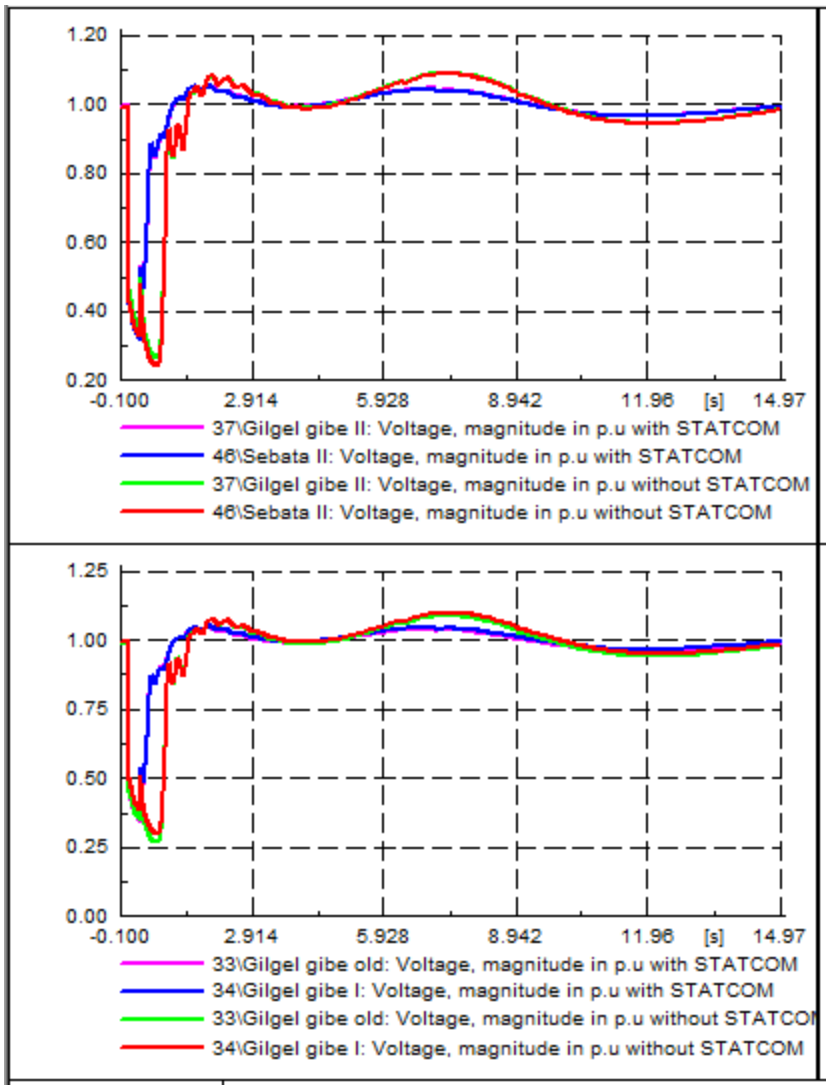

C) Bus voltage response at Gilgel gibe old, Gilgel gibe I, Gilgel gibe II, and Sebeta II

Figure 4.10: A-C bus voltage response with and without STATCOM three phase fault at Kaliti I bus.

In figure 4.11 below shows rotor angle response of generators with and without STATCOM, when three phase faults were occurred at Kaliti I bus.

The rotor angle response of generators shown figure 4.11 below, at the fault clearing time was 367.8 ms. Critical clearing time have been obtained using the same procedure in table 4.4 above. The system critical clearing time was 367.8 ms at without STATCOM. However, when the STATCOM was in operation the critical clearing time increased to 411 ms. Without STATCOM the oscillations were undamped at fault clearing time of 367.8 ms. Figure 4.11 below displays the oscillation damping was better, with STATCOM. Hence, with STATCOM the peak overshoot and the settling time were reduced.

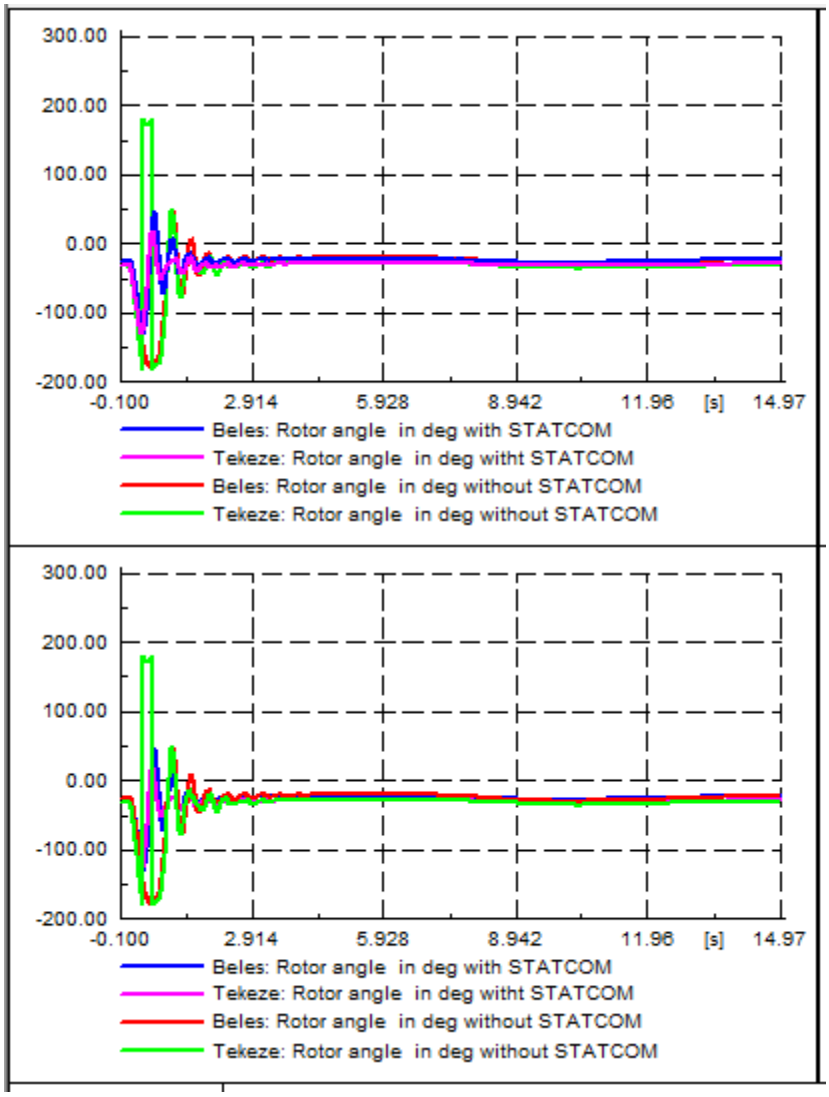

A) Rotor angle response at Beles, Tes Abay II, Tekeze, and Fincha

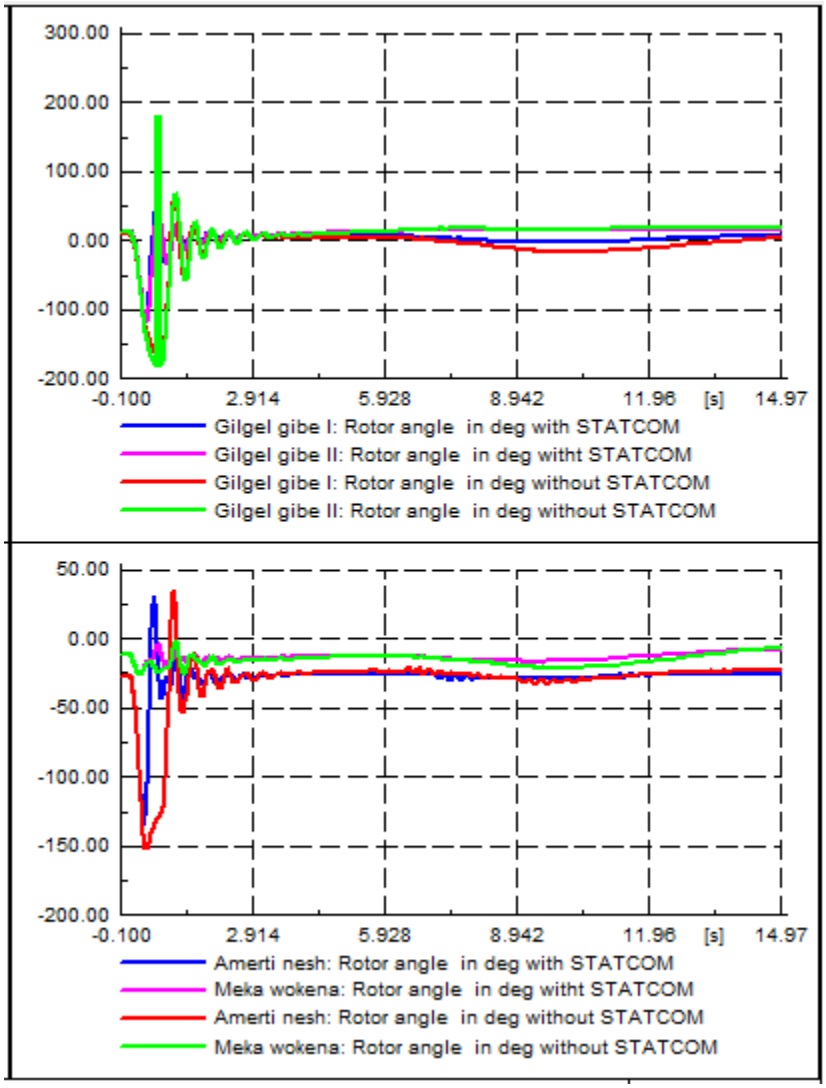

B) Rotor angle response at Gilgel gibe I, Gilgel gibe I, Amerti nesh, and Meka wokena

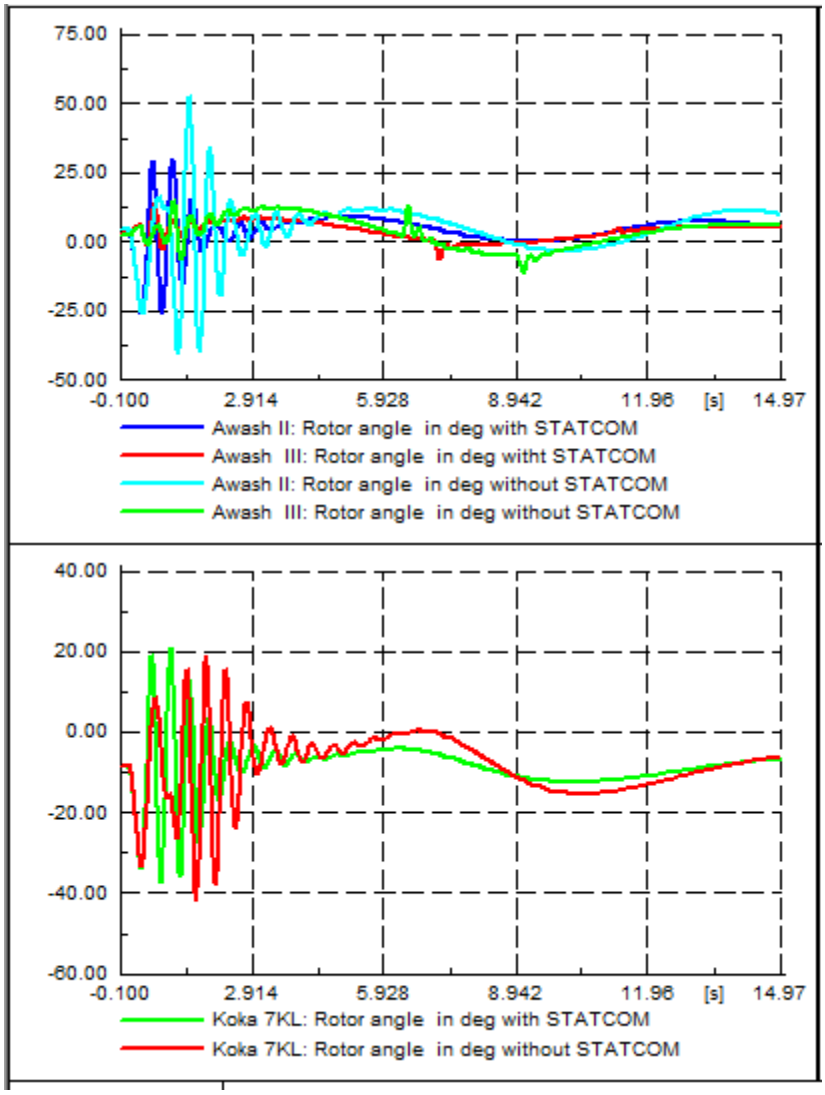

C) Rotor angle response at Koka, and Awash II

Figure 4.11: A-C Rotor angle response of generators with and without STATCOM, when three phase fault was occurred at Kaliti I bus.

The synchronous generators apparent power response shown in figure 4.12 below with and without STATCOM. From the figure 4.12 the power oscillation damping after fault clearing time at 411 ms was instable and go beyond the simulation time 15 second without the STATCOM. However, when STATCOM was in operation the power oscillations were damped to steady state operation.

From figure 4.12 A) displays after the fault was cleared the system regain to their steady state operation of Tana Beles, Tekeze, and Tes Abay II were around 406.4 ms, 368.2 ms,

and 450.8 ms with the corresponding power of 225.865 MVA, 165.536 MVA, and 33.651 MVA respectively.

In figure 4.12 B) shows the apparent power response with and without STATCOM of gibe I, Gilgel gibe II, Amerti nesh, and Meka wokena. After the fault was cleared the system regain to their steady state operation of Gilgel gibe I, Gilgel gibe II, Amerti nesh, and Meka wokena were around 385.8 ms, 493.9 ms, 376.9ms, and 383.3 ms with the corresponding power of 120.695 MVA, 231.405 MVA, 79.827 MVA, and 76.726 MVA respectively with STATCOM.

In figure 4.12 C) Koka, Awash II, Awash III, and Gilgel gibe III were around 514.4 ms, 388.7 ms, 399.9 ms, and 518.5 ms with the corresponding power of 25.073 MVA, 40.068 MVA, 74.202 MVA, and 1764.523 MVA respectively after the fault cleared the system regain to their steady state operation.

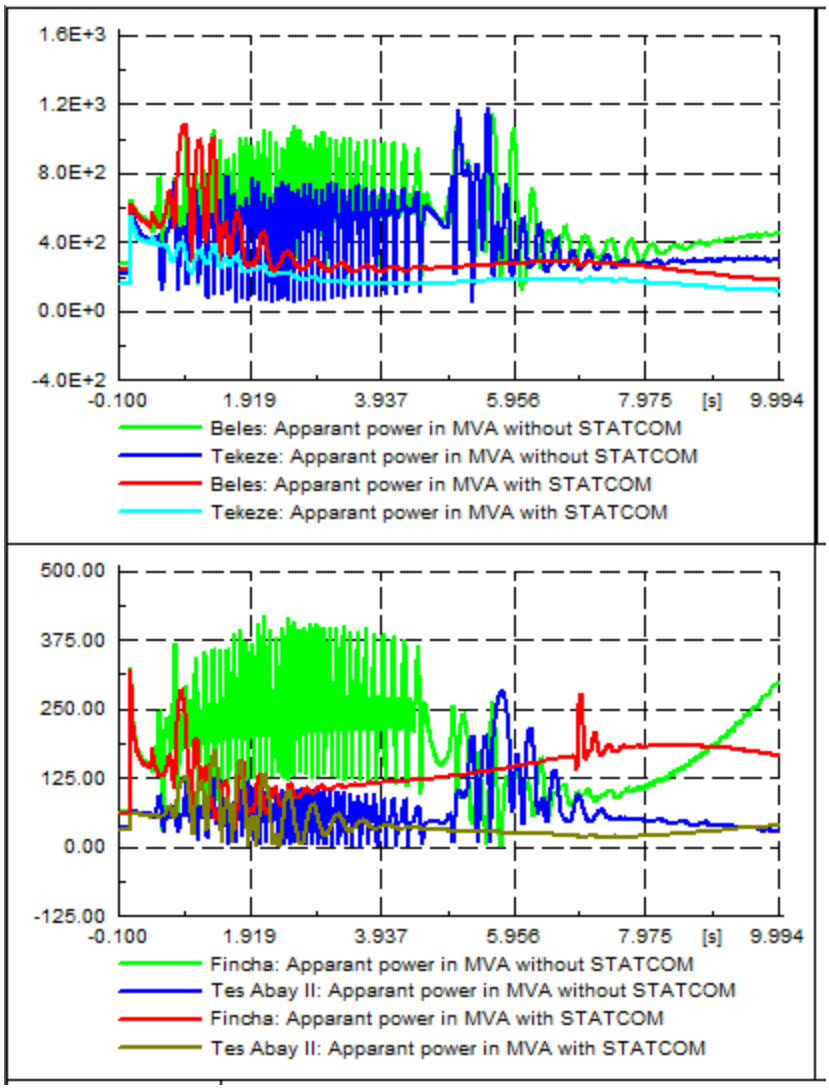

A) Apparent power at Beles, Tekeze, Tes Abay II, and Fincha

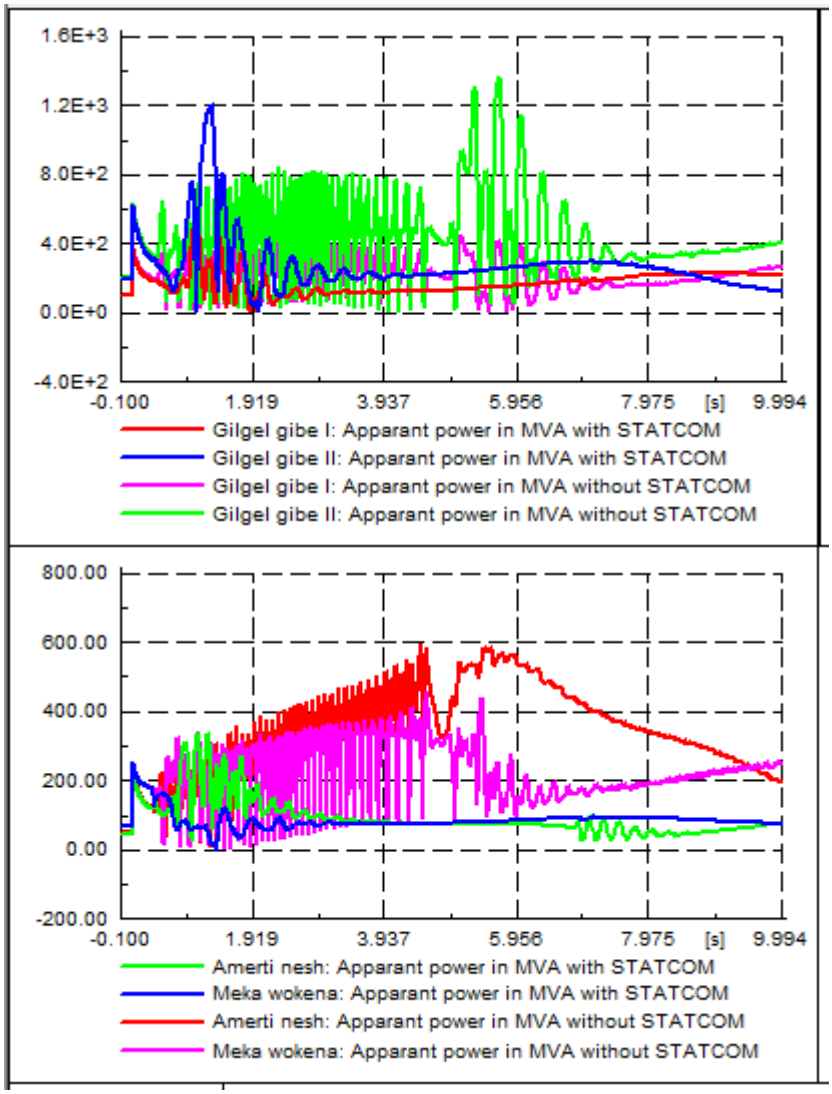

B) Apparent power at Gilgel gibe I, Gilgel gibe II, Amerti nesh, and Meka wokena

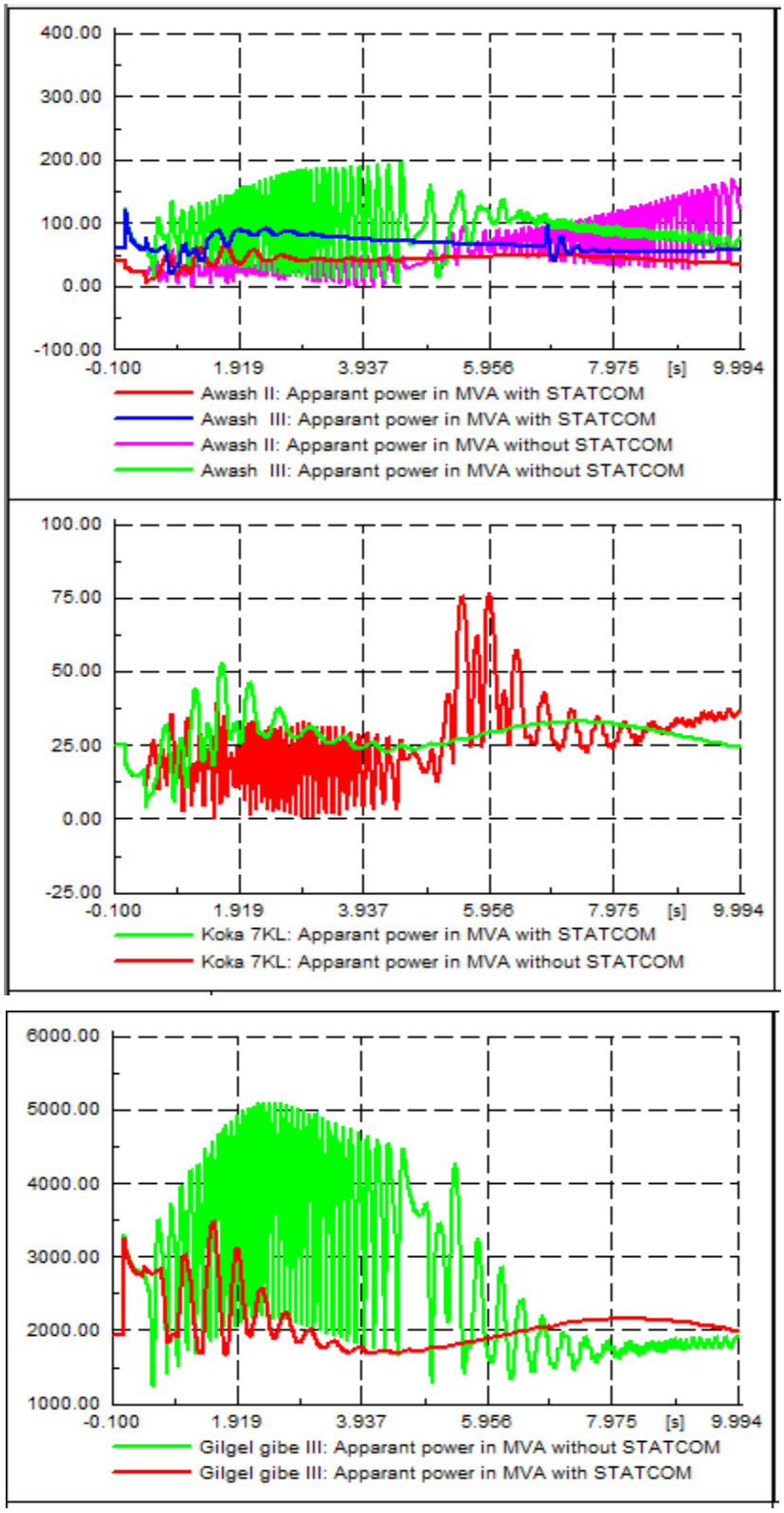

C) Apparent power response of Awash II, Awash III, Koka 7KL, and Gilgel gibe III

Figure 4.12: A-C apparent power response of generators with and without STATCOM, when three phase fault occurred at Kaliti I bus.

CHAPTER FIVE

5. CONCLUSIONS AND RECOMMENDATIONS

5.1. Conclusions

This research is studied the evaluation and enhancement of the critical clearing time and available transfer capability of Ethiopian 230 kV/400 kV transmission system using STATCOM. It is important for power system design, operation and control.

In the vector current controller design active and reactive power is independently control is achieved. The designed control system is stable against the common disturbances that occur in the power. The STATCOM dynamic model was developed using vector current control method.

The placement was obtained using load flow analysis and PV-curve analysis. Based on these methods the device was installed at the weakest bus. The size was obtained based on load flow analysis. From the load flow result and PV-curve analysis the weakest bus was obtained at combolcha. Then the STATCOM was installed at the weakest bus the bus voltage profile improved, the available transfer capability increased, the grid loss reduced and the critical clearing time enhanced. When the device connected, the bus voltage magnitudes were enhanced by 6.3% at the point of connection. The available transfer capability was increased by 235.883 MW (9.377%) with the device in steady state operation.

The transient stability analysis is examined, when three phase faults located at Gilgel gibe III and Kaliti I buses with and without the device. The dynamics of the system were comparing with and without the device, at the occurrence of the fault. In all cases STATCOM had the ability to damp the power oscillation and enhance power system stability by increasing critical clearing time of the system.

When three phase faults considered at different fault clearing time, the system had different operating stability limits. The fault clearing time was small, the system was stable. In contrast, the fault clearing time become large, the system was instable.

The three-phase fault considered at Gilgel gibe III bus terminal, the fault clearing time between 0.1-0.2605 second the system was stable. However, the clearing time beyond 0.2605 second the system become instable/collapse without STATCOM. On the other hand, STATCOM was in operation the clearing time between 0.2605-0.288 second the system was stable. Hence, the critical clearing time was enhanced by 0.0275 second. The three-phase fault considered at Kaliti I bus, the fault clearing time between 0.1-0.3678 second the system was stable. However, the clearing time beyond 0.3678 second the system become instable/collapse without the device. On the other hand, the device was in operation the clearing time between 0.3678-0.411 second the system was stable with device. Hence, the critical clearing time (CCT) was enhanced by 0.0432 second. The simulation result showed that the CCT increases as the fault location farther from the power generation stations.

Therefore, installing STATCOM in a power grid has great advantage in improving the steady state as well as transient stability performance by preventing transient instability and power losses.

5.2. Recommendations

- ✓ It is believed that the Ethiopian power system can benefit significantly from the utilization of STATCOM technologies to solve some of the problems associated with it.
- ✓ It is strongly recommended that EEPCo has to consider the integration of STATCOM FACTS controllers to its upcoming large power system to maintain the system stability thereby improving overall power system power performance in order to maintain power system stability, increase power transfer capability and reduce huge amount of power losses in the system.

5.3. Future work

- ✓ The study of multiple consecutive faults in the network and how the STATCOM responds to such situation.
- ✓ Optimization of STATCOM costs considering converter topologies

REFERENCES

[1] A. Hailemariam, "Power Flow Control and Bus Voltage Enhancement of Power Transmission System Using Unified Power Flow Controller (UPFC) " Degree of Masters, Faculty of Electrical and Computer Engineering Bahir Dar University June , 2017

[2] G. T. Wale, "Critical Clearing Time Evaluation of Ethiopian 230 kV/400 kV Power System," degree of Master of Scienc, Faculty of Electrical and Computer Engineering ,Bahir Dar University December 21, 2017

[3] H. Hashim, I. Abidin, K. S. Yap, I. Musirin, and M. Zulkepali, "Optimization of mechanical input power to synchronous generator based on Transient Stability Center-of-Inertia: COI angle and COI Speed," in Power Engineering and Optimization Conference (PEOCO), 2011 5th International, 2011, pp. 249-254.

[4] M. K. G. Damor, M. V. Agrawal, D. D. M. Patel, and M. H. G. Patel, "Improving Power System Transient Stability by using Facts Devices," International Journal of Engineering Research & Technology (IJERT), vol. 3 issue 7, pp. 2278-0181, July - 2014.

[5] S. O. SANNI, "Assesment of Transient stability Enhancement Capability of unified power flow controller in a multimachine power system " Master of Scince (M.Sc.) Degree in electrical engineering, Electrical and computer engineering, Ahmadu Bello University, Nigeria, AUGUST, 2014

[6] S. O. Sanni, J. O. Haruna, Boyi Jimoh, and U. O. Aliyu, "An Analysis of Transient Stability Enhancement Capability of UPFC in a Multimachine Power System " FUOYE Journal of Engineering and Technology, vol. 1, issue 1, September 2016

[7] M. M. Adibi and N. Martins, "Impact of Power System Blackouts " in IEEE Power & Energy Society General Meeting, ed, 2015, pp. 1-15.

[8] P. Kundur, J. Paserba, V. Ajjarapu, G. Andersson, A. Bose, C. Canizares, et al., "Definition and classification of power system stability IEEE/CIGRE joint task force on stability terms and definitions," IEEE transactions on Power Systems, vol. 19, pp. 1387-1401, 2004.

[9] G. B. Jadhav, D. C. B. Bangal, and D. S. Kanungo, "Transient Stability Analysis with SVC and STATCOM in Multi-Machine Power Systems with and without PSS using Matlab/Simulink " IJEDR, vol. 5, issue 4, pp. ISSN: 2321-9939 2017.

[10] P. Suresh and R. J. Kumar, "Transient Stability Performance Analaysis of an IEEE 9 bus power system using FACTSdevice," International Journal of Computational Research and Development (IJCRD) Impact Factor, vol. 1, pp. 2456 - 3137 2016.

[11] L. Wang and C.-T. Hsiung, "Dynamic Stability Improvement of an Integrated Grid-Connected Offshore Wind Farm and Marine-Current Farm Using a STATCOM," IEEE TRANSACTIONS ON POWER SYSTEMS, vol. 26, NO. 2, pp. 690-698, MAY 2011

[12] M. Molinas, S. Vazquez, M. T. Takaku, J. M. Carrasco, R. Shimada, and T. Undeland, "Improvement of Transient Stability Margin in Power Systems with Integrated Wind Generation Using a STATCOM: An Experimental Verification," IEEE Xplore Conference Paper pp. 1-7, December 2005

[13] P. Khalkho and A. K. Singh, "Transient stability improvement by using PSS and increasing inertia of synchronous machine" American Journal of Electrical Power and Energy Systems vol. 3(2), pp. 45-49, April 20, 2014.

[14] M. S. Rao and L. M. Mohan, "Transient Stability Performance Analysis of Power System Using Facts Devices " Int. Journal of Engineering Research and Applications Vol. , vol. 4, Issue 2(Version 1), February 2014, pp.250-256.

[15] A. Chaudhary and R. A. Jaswa, "Transient Stability Improvement of Multi Machine Power System Using Static VAR compensator " International Journal of Electronic and Electrical Engineering, vol. 7,No.2, pp. 109-114 2014.

[16] B. G. Reddy and K. Sharma, "Improvement of Power System Transient Stability Using Fuzzy Controlled Shunt Facts Device " international journal of science and research (IJSR), vol. 5 Issue 5, May 2016

[17] M.Khan, T. Husain, and M.M.Ansari, "Dynamic Stability Enhancement of Power System network using FACTS Devices Muqueem," international Journal of Advanced Research in Electrical, Electronics and Instrumentation Engineering, vol. 5,issue 5, pp. ISSN (Online): 2278 – 8875 May 2016

[18] L. Mathew and S.Chatterji, "Transient Stability Analysis of Electrical Power Systems by means of LabVIEW based Simulation of STATCOM " International Journal of Advances in Engineering Sciences vol. 1, Issue 2, April, 2011.

[19] P. Bisen and A. Shrivastava, "Comparison between SVC and STATCOM FACTS Devices for Power System Stability Enhancement," International Journal on Emerging Technologies:, vol. 4(2), pp. 101-109, 2013.

[20] J. J. Paserba, "How FACTS controllers benefit AC transmission systems," in Power Engineering Society General Meeting, 2004. IEEE, 2004, pp. 1257-1262.

[21] C. Rambabu, Y. Cbulesu, and C. Saibabu, "Improvement of voltage profile and reduce power system losses by using multi type facts devices," International Journal of Computer Application, vol. 13, 2011.

[22] Mr. Ketan G. Damor , Mr. Vinesh Agrawal , Dr. Dipesh M. Patel, and M. H. G. Patel, "Improving Power System Transient Stability by using Facts Devices," International Journal of Engineering Research & Technology (IJERT), vol. 3, pp. 2278-0181, 2014.

[23] P. Kundur, Power System Stability and Control: McGrawHill, New York, 1994.

[24] H. Saadat, Power System Analysis. New York: WCB McGraw-Hill International Editions, 1999.

[25] J. Wuliam and D. Stevenson, Power System Analysis. North Carolina: McGraw-Hill, 1994.

[26] N. G. Hingorani and L. Gyugyi, "Understanding FACTS: Concepts and Technology of Flexible AC Transmission Systems," IEEE Press, New York, 1999.

[27] S. Patel, "STATCOM & OPERATION," Pandit Deen Dayal Petroleum University, May 2013.

[28] A. Hilawie, "Investigation of VSC-HVDC system for dynamic performance improvement of EEPCO high voltage grid," M.S.c, Addis Ababa University, June 2011.

[29] O. Almutairi, "Fault Current Generation by STATCOM," Master's thesis in Electrical Power Engineering,, Chalmers University of Technology, 2017.

[30] K. Zhou and D. Wang, "Relationship between Space-Vector Modulation and Three-Phase Carrier-Based PWM: A Comprehensive Analysis," IEEE Transactions on Industrial Electronics, vol. 49, pp. 186- 196, 2002.

[31] H. Patel, "Modeling of Voltage Source Converter Based HVDC Transmission System in EMTP-RV," Master of Applied Science thesis, University of Ontario Institute of Technology, , August, 2010.

[32] A. M. Alee, "Comparison of techniques for voltage control and power system stability in the NORTH of IRAQ," M.S.c, Electrical and Electronics Engineering, University of Gaziantep, January 2016.

[33] E. Kabalci, "Converter and Output Filter Topologies for STATCOMs," Springer, 2015.

[34] Oscar Lennerhag and V. Tra¨Ff, "Modelling of VSC-HVDC for Slow Dynamic Studies," M.S.c, Chalmers University of Technology, 2013.

[35] C. Bajracharaya, "Control of VSC-HVDC for Wind Power," M.Sc. thesis, Norwegian University of Science and Technology, June 2008.

[36] L. W, "Control of electrical drives. Springer," New York, 2001.

[37] M. Liserre, "Innovative Control Techniques of Power Converters for Industrial Automation," PhD Thesis, Politecnico di Bari, Italy, Dec, 2001.

[38] Prakash Ji Barnawal and S. M. Tripathi, "A Simple Control of STATCOM for Non-linear Load Compensation," Asian Power Electronics Journal, vol. Vol. 11, pp. 28-32, July, 2017.

[39] E. D. Agüero, J. C. Cepeda, and D. G. Colomé, "FACTS models for stability studies in DIgSILENT Power Factory," August 2014.

APPENDIX

Appendix 1: STATCOM

Appendix 1:1 STATCOM parameters

Components	Value
Transformer	230 kV/30 kV
Converter rating	200 MVA
DC link voltage	61 kV
DC capacitor	537.5 μF
Impedance	0.001+j0.2
Resistance	0.0045 Ω
Inductance	2.866 mH

Appendix 1:2 STATCOM Controller parameters

Inner current controller		DC voltage controller	
Kp	Ti	Kp	Ti
5.76	0.6375	0.5	0.0045

DC voltage set point=1 p.u

Reactive Power Set point=79 MVAr

Appendix 2: STATCOM dynamic model

Appendix 2.1: Composite model frame

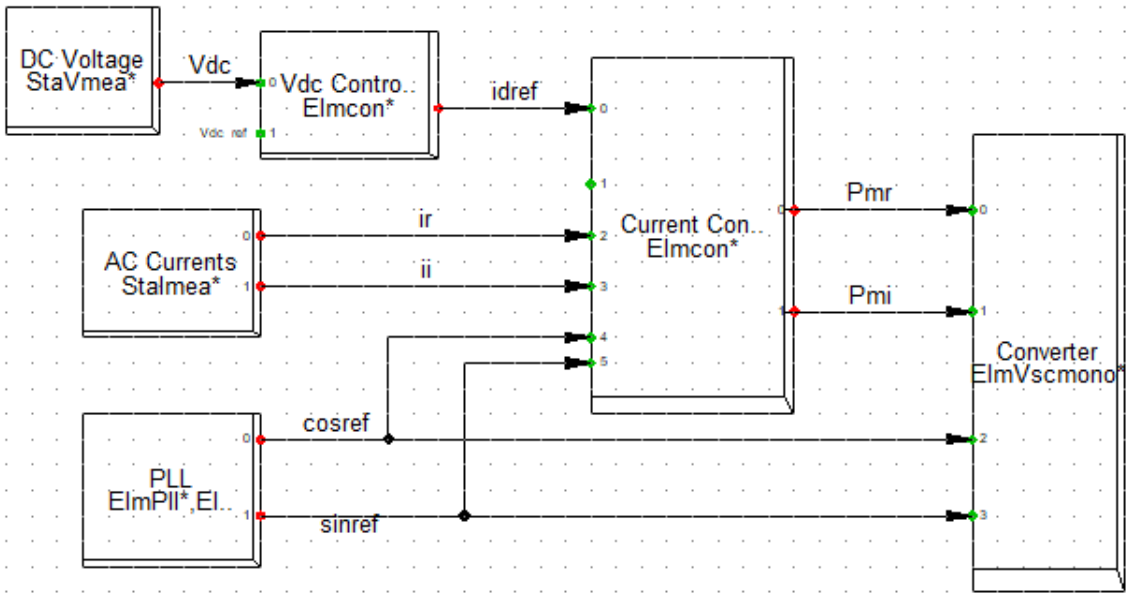

Appendix 2.2: User defined inner current controller

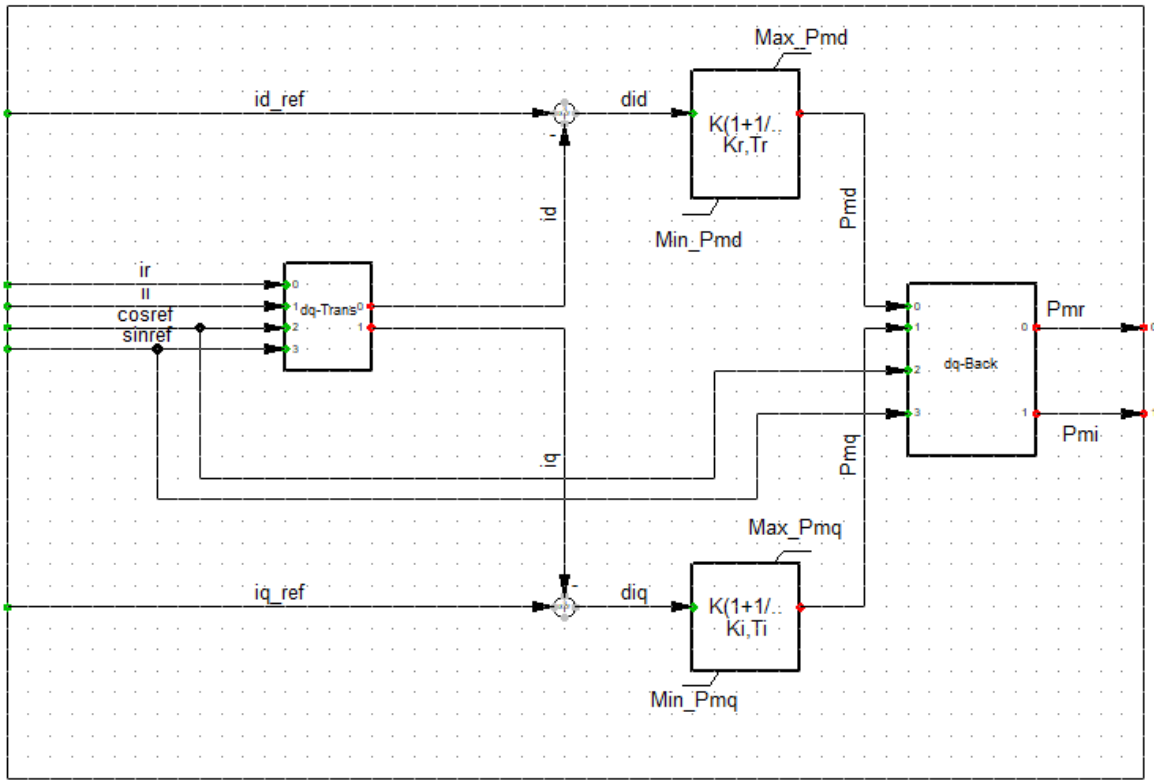

Appendix 2.3: User defined DC-Voltage controller

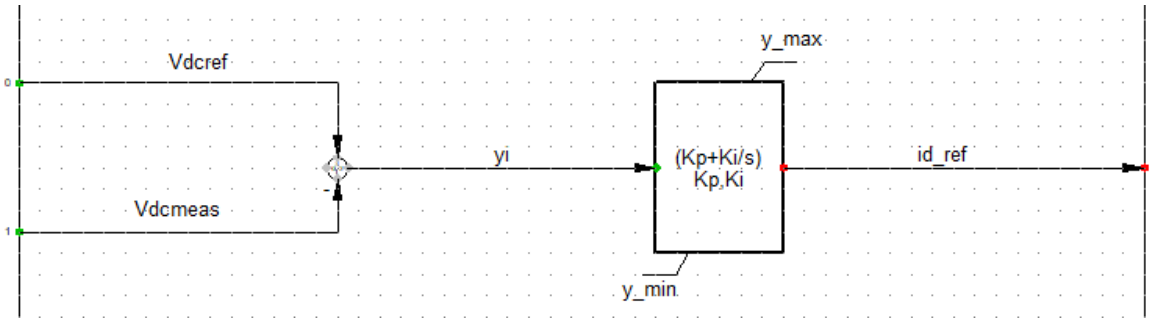

Appendix 2.4: Inner current controller codes

did = id_ref-id

diq = iq_ref-iq

inc(x1)=Pmd*Tr/Kr

inc(x4)=Pmq*Ti/Ki

inc(id_ref)=id

inc(iq_ref)=iq

inc(xid)=id

inc(xiq)=iq

inc(Pmd)=Pmr*cosref+Pmi*sinref

inc(Pmq)=-Pmr*sinref+Pmi*cosref

Appendix 2.4: DC voltage controller codes

model id_ref = 'DC voltage PI'(Vdcref,Vdcmeas;x;Kp,Ki,y_min,y_max;yi) id_ref = '\Library\V14.0 Standard Macros (old).IntFolder\Linear Functions\(Kp+Ki/s).BlkDef'(yi;x;Kp,Ki,y_min,y_max;)

yi = -Vdcmeas+Vdcref

Appendix 3: Voltage profile load flow results

Bus name	Without STATCOM	With STATCOM	Bus name	Without STATCOM	With STATCOM
Hossiana	0.959	0.96	Ramo	1.010	1.011
Adama WF	1.012	1.012	Adama WF1	1.014	1.014
Adigala	0.984	0.984	Sebata II 230 kV	0.989	0.991
Agaro	0.979	0.98	Sebata II 400 kV	0.992	0.994
Assela pp	1.008	1.008	W.Sodow 400 kV	1.041	1.042
Assela ss	1.014	1.015	Wolkite	0.978	0.979
Awash II SS	1.020	1.022	Amerti nesh	0.995	0.997
Awash 7KL	0.996	0.996	Amerti nesh PP	1.001	1.001
Awash III s	1.02	1.022	Ashe 230 kV	0.972	0.984
Awash III	1.015	1.015	Ashe 33 kV	1.00	1.00
Awash II pp	1.	1	B.Dar132 kV	0.991	0.995
Aysha ss	0.984	0.984	B.Dar 400 kV	0.993	0.996
Aysha WF	1	1	Beles pp 15 kV	1.006	1.006
Bedele	0.976	0.977	Beles 400 kV	0.995	0.997
Dirdwa III	0.976	0.976	D.Markos 400 kV	0.990	0.994
Gilgel gibe I	0.992	0.993	D.Markos 230 kV	0.989	0.993
Gilgel gibe II	0.994	0.995	Fincha	0.992	0.995
Gilgel gibe III	1.043	1.044	G.guracha	0.987	0.991
Gilgel gib old	0. 988	0.99	GIS	0.980	0.987
Gilgel gib old	0.993	0.994	Geffersa	0.980	0.987
Gambella	0.971	0.972	Ghedo	0.986	0.99
Gelna1	1.020	1.022	Indeslasie	0.976	0.983
Gelan 400 kV	1.041	1.042	M.Plc	0.973	0.982
Gelan 230 kV	1.027	1.029	Sululta 400	0.985	0.99
Jimma	0.988	0.989	T.Abay SS	0.993	0.996
Gode	1.008	1.008	T.Abay pp	1.00	1.00
Metu	0.974	0.975	Tekeze ss	0.985	0.992
Koka pp	1.000	1.00	Fincha 13.8	1	1
Koka ss	1.020	1.022	Moheni	0.972	0.983
Koka	1.014	1.015	Mota	0.988	0.992
M.wokena	1.011	1.012	Meka Wokena pp	1.007	1.007

Appendix 4: Load demand

Load	Bus Name	Base kV	Load P (MW)	Load Q (MVAr)
1	Sebeta II	230	28.96	14.03
2	Sululta	230	253.68	122.87
3	Geffersa	230	170.83	82.73
4	Legetafo	230	91.86 43.97	43.97
5	Kalti I	230	51.5	24.89
6	Sebeta I	230	85.11	41.22
7	Gelan	230	53	25.81
8	Wolkite	230	13.01	6.3
9	Awash &KL	230	13.44	6.536
10	Didawa III	230	202.8	99.58
11	Adigala	230	3	1.2
12	Gode	230	9	4.36
13	Hurso	230	175.2	78.3
14	Combolcha II	230	302.56 8	87.14
15	Semera	230	10.6	4.15
16	Bahir Dar II	230	63.53	30.762
17	D/Markos	230	16.12	8.22
18	Azezo	230	37	18
19	Mota	230	3.45	1.7
20	Metema	230	4	1.96
21	Humera	230	17.94	8.69
22	Indeslasie	230	13.36	6.46
23	Bekele	230	170.12	82.24

24	Mehoni	230	16.29	7.89
25	Alemata	230	117.85	57.08
26	Mekele PVC	230	34.47	16.69
27	Gilgel Gibe II	230	9.16	4.44
28	Agaro	230	7.1	2.9
29	Bedele	230	6.84	3.31
30	Metu	230	2.35	1.16
31	Gambella II	230	14.66	7.09
32	Jimma II	230	18.54	8.97
33	Ramo	230	2	0.97
34	Meka Wokena	230	42.76	20.72
35	Alaba	230	112.64	54.36
36	Hossana	230	8.75	4.24
37	W/Sodo II	230	456.6	56.57
38	Ghedo	230	18.23	8.83
39	Fincha II	230	3.86	1.87
40	Sudan Gadre	230	200	50

Appendix 5: Transmission lines data in p.u.

From bus	To bus	R (p.u)	X (p.u)	B (p.u)	kA	Km
Fincha	Ghedo	0.010041	0.053852	0.09704	284	67.2
Fincha	Fincha II	0.001673	0.005116	0.01547	318	8.3
Fincha	D.Markos	0.014652	0.076154	0.13763	280	95.2
Ghedo	Geffersa	0.028548	0.079796	0.256275	284	133
Ghedo	GG-old	0.021099	0.102687	0.1886	274	130
Ghedo	Fincha II	0.014923	0.042962	0.129876	318	69.7
Geffersa	Sebeta I	0.0016	0.0045	0.01353	274	11
Sululta	Geffersa	0.003382	0.010038	0.03224	318	16.73
Sebeta I	Kaliti I	0.002314	0.011264	0.02069	274	18.2
Sebeta I	Sebeta II	0.002321	0.011775	0.02228	280	15.02
Sebeta I	Wolkite	0.0069	0.014477	0.002495	280	142
Nesh	Fincha II	0.005897	0.018027	0.0545	318	29.2
GG I	GG old	0.000814	0.003867	0.00744	274	5
Koka	Awash 7KL	0.022453	0.100028	0.192398	274	129.3
Gelan	Kaliti I	0.0077	0.0222	0.0671	318	9
Kaliti I	Legetafo	0.0077	0.0222	0.0671	318	35
Gelan	Koka SS	0.00012	0.0002	0.0004	91	34
Gelan	Koka	0.0077	0.0222	0.0671	318	57
Koka SS	Awash II	0.037911	0.061736	0.01184	91	25.4
Awash II	Awash III	0.002171	0.003512	0.00069	91	2
Combolcha II	Legetafo	0.034	0.1	0.32526	318	287
Adigala	Hurso	0.028047	0.080746	0.2441	274	131
Adigala	Aysha	0.028047	0.080746	0.2441	274	131
M.wokena	M.wokena 1	0.0077	0.0222	0.0671	318	51
Assela	M.wokena	0.0077	0.0222	0.0671	318	51
Awash 7KL	Didawa III	0.035593	0.158565	0.304992	353	205.1
Didawa III	Hurso	0.006117	0.017099	0.054916	402	28.5
Koka	Hurso	0.075556	0.211189	0.678261	402	315
Koka	Adama II	0.0022	0.0065	0.01957	402	1.23
Koka	Meka wokena	0.029689	0.127801	0.24166	257	163.9
D.Markos	Mota	0.017209	0.089447	0.16166	280	111.8
Bahr dar II	Mota	0.012781	0.066429	0.12006	280	83
Bahr dar II	Gondar II	0.029325	0.084425	0.255224	402	137
Gondar II	Metema	0.033358	0.098995	0.31793	318	165
Gondar II	Humera	0.024654	0.071	0.2143	318	217

Alemata	Bahr dar II	0.0207	0.063	0.19063	318	341
Mekele	Tekeze	0.021228	0.062997	0.20232	318	105
Mekele	Mekele PVC	0.0009	0.0024	0.00771	402	4
Mekele	Ashegoda wf	0.0041	0.0117	0.0354	402	7
Alemata	Ashegoda wf	0.0265	0.0762	0.23048	402	123.7
Alemata	Mekele	0.028534	0.084677	0.27195	318	141.1
Alemata	Moheni	0.0077	0.0222	0.06708	402	36
Mekele	Moheni	0.020982	0.060405	0.182609	402	98
Tekeze	Indeslasie	0.032245	0.09569	0.30732	318	159.5
Humera	Indeslasie	0.046434	0.137799	0.44256	318	229.7
Indeslasie	Tekeze	0.032245	0.09569	0.30732	318	159.5
Metema	Ethio-sudan	0.0343	0.096	0.3083	402	165
Alemata	Combo II	0.034126	0.101275	0.32526	318	168.8
Combo II	Semera	0.034276	0.104784	0.31677	318	170
Wolkite	GG old	0.010779	0.056025	0.10125	280	70
Jimma	GG I	0.014081	0.039358	0.126403	402	65.6
Jimma	Agaro	0.008307	0.023219	0.07457	402	38.7
Agaro	Bedele II	0.017494	0.048897	0.157041	402	81.5
Bedele	Metu	0.018245	0.055777	0.16862	402	90.5
Gambella II	Metu	0.029974	0.086293	0.26087	402	140
Hossana	Wolkite	0.019119	0.055043	0.166398	402	89.3
Alaba	Hossana	0.008435	0.024285	0.073416	402	39.4
Ramo	Meka wokena	0.047736	0.133429	0.428524	402	222.4
Ramo	Gode	0.063526	0.177565	0.570273	402	296
Beles	Bahr dar II	0.000958	0.012159	0.37713	1341	62.84
Bahr dar II	Debre Markos	0.002997	0.03986	1.10239	1341	193.7
Debre Markos	G.guracha	0.0014	0.018	0.4979	1341	87.5
Sululta	G.guracha	0.002	0.0271	0.7483	1341	131.5
Sebeta II	GG II	0.002839	0.037756	1.04419	1341	183.5
GG old	GG II	0.000431	0.005737	0.15868	1341	27.89
GG II	Welayta Sodo	0.0025	0.0207	0.79593	1973	119
GG III	Welayta Sodo	0.001	0.0081	0.35653	1973	50
Sebeta II	Gelan	0.000431	0.00574	0.158679	1341	33

Appendix 6: Generator

Appendix 6:1 Generator data

Power plants	Voltage magnitude (kV)	PGen (MW)	Pmax (MW)	Pmin (MW)	Qgen (MVAr)	Qmax (MVAr)	Qmin (MVAr)	Mbase
T-Beles	15	184.038	468	0	-109.21	280.4	-166	532
T-Abay II	10.5	29.5873	60	0	2.976	42.2	-25	80
Fincha	13.8	53.9728	133.2	0	-43.6	73.6	-43.6	140
A.nesh	13.8	39.3046	97	0	-19.2652	79	-46.8	150
Tekeze	13.8	126.4716	312.12	0	-55.7548	84.4	-109.6	350.4
Ashegoda	33	32.67	90	0	-28.1	47.4	-28.1	90
M.wokena	13.8	61.996	153	0	-23.5996	94.8	-56.4	180
G.Gibe I	13.8	85.0923	210	0	-70.2	118.5	-70.2	225
G.Gibe II	15	173.4264	428	0	-127.212	263.2	-156	500
G.Gibe III	13.8	757.728	1870	0	-277.726	1231	-730	2340
Koka	10.5	15.5598	38.4	0	28.5	28.5	-16.8	54
Awash III	10.5	29.1744	72	0	36.1444	42	-24.4	80
Awash II	10.5	29.1744	72	0	36.1444	42	-24.4	80
Adama Wf	33	55.539	153	0	-41.03	100.7	-59.7	191.25
Assela wf	33	108.9	300	0	-19.2488	197.5435	-117.1	375
Aysha Wf	33	108.9	300	0	-23.0418	197.5435	-117.1	375
Ashegoda wf	33	43.56	120	0	-39.8094	66.7543	-39.81	120

Appendix 6:2 Generator dynamic data in PowerFactory model (X" = X"d = X"q)

Power Plant	H in s	Ra in p.u	Xd' in p.u	Xd in p.u	Xq in p.u	Td0' in s	XL in p.u	X'' in p.u	Td0'' in s	Tq0'' in s
Beles	3.14	0	0.31	1.03	0.7	9.2	0.2	0.25	0.13	1
T-AbayII	2.5	0	0.29	1	0.6	7.1	0.14	0.365	0.12	0.12
Fincha	3.04	0	0.230	0.96	0.9	7.393	0.1	0.115	0.045	0.057
A.nesh	2.5	0	0.34	0.7	0.466	5.4	0.15	0.17	0.1	0.2
Tekeze	2.8	0	0.29	1.0	0.6	9.5	0.1	0.173	0.058	0.113
M.wokena	2.63	0	0.17	1	0.25	6	0.1	0.1	6	0.091
G.Gibe I	2.8	0	0.23	1.22	0.7	9.5	0.09	0.164	9.5	0.058
G.Gibe II	3.14	0	0.31	1.03	0.7	9.2	0.1	0.22	9.2	0.13
G.Gibe III	3.14	0	0.31	1.03	0.7		0.1	0.22		
Koka	2.61	0	0.339	0.699	0.66	5.4	0.2	0.24	5.4	0.065
Awash II	2.61	0	0.349	1.04	0.66	5.4	0.1	0.16	5.4	0.075
Awash III	2.61	0	0.349	1.04	0.66	5.4	0.1	0.16	5.4	0.075

Appendix 7: Automatic voltage regulator (AVR)

Appendix 7.1: Exciter type EXST1 data

Model Identifier	TR	VI MAX	VI MIN	TC	TB	KA	TA	VR MAX	VR MIN	KC	KF	TF (> 0)
T-Abay II	0.01	99	-99	0.01	0.01	400	0.02	5	-5	0	0.03	1
Beles	0.01	0.2	-0.3	0.04	0.4	60	0.02	5	-5	0	0.03	1
Tekeze	0.01	0.2	-0.3	0.04	0.4	60	0.02	5	-5	0	0.03	1
GG-II	0.01	0.2	-0.3	0.04	0.4	60	0.02	5	-5	0	0.03	1
GG-III	0.01	0.2	-0.3	0.04	0.4	60	0.02	5	-5	0	0.03	1

Appendix 7:2 Exciter type SCRX data

Model Identifier	TA/TB	TB(>0)	K	TE	Emin	Emax	CSWICH	Rc/rfd
Fincha	0.1	10	100	0.1	0	5	0	0
Awash II	0.1	10	100	0.1	0	5	0	0
GG-I	0.1	10	100	0.1	0	5	0	0
M.wokena	0.1	10	100	0.1	0	5	0	0

Appendix 7:3 Exciter type IEEEX1 data

Model Identifier	TR	KA	TA	TB	TC	VR MAX	VR MIN	KE	TE (>0)	KF	TF1 (> 0)	0. SWICH	E1	SE(E1)	E2	SE(E2)
Koka	0.01	37	0.12	0.01	0.01	2.4	-2.4	0	0.8	0.055	0.3	0	1.73	0.328	2.8	0.687
Awash III	0.01	37	0.12	0.01	0.01	2.4	-2.4	0	0.8	0.055	0.3	0	1.73	0.328	2.8	0.687

Appendix 7:4 Exciter type EXDC2 data

Model Identifier	TR	KA	TA	TB	TC	VR MAX	VR MIN	KE	TE (>0)	KF	TF1 (> 0)	0. SWICH	E1	SE(E1)	E2	SE(E2)
Nesh	0.01	20	0.055	0	0	3.5	-2.5	-0.1	0.4	0.125	1.4	0	4.5	0.15	6	0.5

Appendix 8: Control parameters for generators with governor type HYGOV

Model Identifier	R, Permanent Droop	r, Temporary Droop	Tr (> 0) Governor Time Constant	Tf (> 0) Filter Time Constant	Tg (> 0) Servo Time Constant	VELM, Gate Velocity Limit	GMAX/ GMIN Maximum/ Minimum Gate Limit	TW (> 0) Water Time Constant	At, Turbine Gain	Dturb, Turbine Damping	qNL, No Load Flow
Beles	0.04	0.5	6	0.05	0.5	0.167	1 / 0	2	1.2	0.3	0.1
T-AbayII	0.04	0.5	6	0.05	0.5	0.167	1.2 / 0	2	1.2	0.3	0.1
Fincha	0.04	0.5	6	0.05	0.5	0.167	1 / 0	2	1.2	0.3	0.1
A.nesh	0.04	0.5	6	0.05	0.5	0.167	1 / 0	2	1.2	0.4	0.1
Tekeze	0.04	0.5	6	0.05	0.5	0.167	1 / 0	2	1.2	0.4	0.1
M.wokena	0.04	0.5	6	0.05	0.5	0.167	1 / 0	2	1.2	0.4	0.1
G.Gibe I	0.04	0.5	6	0.05	0.5	0.167	1 / 0	2	1.2	0.4	0.1
G.Gibe II	0.04	0.5	6	0.05	0.5	0.167	1 / 0	2	1.2	0.4	0.1
G.Gibe III	0.04	0.5	6	0.05	0.5	0.167	1 / 0	2	1.2	0.4	0.1
Koka	0.04	0.5	6	0.05	0.5	0.167	1 / 0	2	1.2	0.4	0.1
Awash II	0.04	0.5	6	0.05	0.5	0.167	1 / 0	2	1.2	0.3	0.1
Awash III	0.04	0.5	6	0.05	0.5	0.167	1 / 0	2	1.2	0.3	0.1